ESA Climate Change Initiative (CCI)
Sea Level Budget Closure (SLBC_cci)

Final Report
ESA_SLBC_cci_D4.7

(Version 1.1, issued 14 February 2020)

Prime & Science Lead: Martin Horwath

Technische Universität Dresden (TUDr)

Martin.Horwath@tu-dresden.de

Technical Officer: Jérôme Benveniste

ESA ESRIN, Frascati, Italy

Jerome.Benveniste@esa.int

Contract No.:   4000 11 9910/17/I-NB

Consortium: Technische Universität Dresden (TUDr)

Laboratoire d'Etudes en Géophysique et Océanographie Spatiales (LEGOS)

Universität Bremen (UB)

Universität Zürich (UZH)

University of Leeds (UoL)

Goethe-Universität Frankfurt (GUF)

Danmarks Tekniske Universitet, DTU Space, Geodynamics (DTU-GDK)

Danmarks Tekniske Universitet, DTU Space, Geodesy (DTU-GEK)

Nansen Environmental and Remote Sensing Center (NERSC)

University of Reading (UoR)

Mercator Ocean, Toulouse (MerO)

CCI Sea Level Budget Closure
ESA/ESRIN contract 4000119910/17/I-NB
Reference: ESA_SLBC_cci_D4.7
Version: v1.1
Date: 14.02.2020
Page: 2 of 101

		CCI Sea Level Budget Closure
		ESA/ESRIN contract 4000119910/17/I-NB
esa		Reference: ESA_SLBC_cci_D4.7
		Version: v1.1
		Date: 14.02.2020
		Page: 3 of 101

Signatures page

Prepared by	Christoph Knöfel Deputy project manager, TUDr Martin Horwath Science Leader, TUDr Anny Cazenave, Hindumathi Palanisamy, LEGOS; Ben Marzeion, UB; Frank Paul, UZH; Petra Döll, Denise Cáceres, GUF; Anna Hogg, Inés Otosaka, Andrew Shepherd, UoL; Valentina Barletta, Rene Forsberg, DTU-GDK; Ole B. Andersen, Stine K. Rose, DTU-GEK; Johnny Johannessen, Roshin P. Raj, NERSC; Benjamin D. Gutknecht, TUDr; Christopher John Merchant, Claire Rachel MacIntosh, UoR; Karina von Schuckmann, MerO	Date: 2020-02-14
Checked by	Martin Horwath Science Leader, TUDr	Date: 2020-02-14
Approved by	Jérôme Benveniste Technical Officer, ESA	Date:

		CCI Sea Level Budget Closure
		ESA/ESRIN contract 4000119910/17/I-NB
		Reference: ESA_SLBC_cci_D4.7
		Version: v1.1
		Date: 14.02.2020
		Page: 4 of 101

Change Log

Issue	Author, Org.	Affected Section	Reason/Description	Status
1.0	M. Horwath / TUDr	All	Document Creation	Released to ESA 2019-12-04
1.1	M. Horwath / TUDr	1, 4, 5, 6, 7	Revision in reply to Review of v1.0 document by ESA	Released to ESA 2020-02-14

Distribution List

Organization	Consortium Member
TUDr	Martin Horwath
LEGOS	Anny Cazenave
UB	Ben Marzeion
UZH	Frank Paul
UoL	Andrew Shepherd, Anna Hogg
DTU- GDK	Rene Forsberg
GUF	Petra Döll
NERSC	Johnny Johannessen
DTU-GEK	Ole B. Andersen
UoR	Christopher Merchant
MerO	Karina von Schuckmann
ESA	Jérôme Benveniste Marco Restano Américo Ambrózio

		CCI Sea Level Budget Closure
		ESA/ESRIN contract 4000119910/17/I-NB
		Reference: ESA_SLBC_cci_D4.7
		Version: v1.1
		Date: 14.02.2020
		Page: 5 of 101

Table of contents

		CCI Sea Level Budget Closure
		ESA/ESRIN contract 4000119910/17/I-NB
		Reference: ESA_SLBC_cci_D4.7
		Version: v1.1
		Date: 14.02.2020
		Page: 6 of 101

		CCI Sea Level Budget Closure
		ESA/ESRIN contract 4000119910/17/I-NB
		Reference: ESA_SLBC_cci_D4.7
		Version: v1.1
		Date: 14.02.2020
		Page: 7 of 101

Acronyms and Abbreviations

Acronym	Explanation
20CRv2	Twentieth Century Reanalysis (V2) (NOAA)
AIS	Antarctic Ice Sheet
ALES, ALES+	Adaptive Leading Edge Subwaveform retracker
AOD	atmospheric and oceanic de-aliasing
AP	Antarctic Peninsula
Argo	global array of temperature/salinity profiling floats
ASCII	American Standard Code for Information Interchange
ATBD	Algorithm Theoretical Baseline Document
AVISO	Archiving, Validation and Interpretation of Satellite Oceanographic data
BISICLES	Berkeley Ice Sheet Initiative for Climate Extremes
CCI, cci	Climate Change Initiative (initiated by ESA)
CECR	Comprehensive Error Characterisation Report
CF	Climate and Forecast
CFSR	NCEP Climate Forecast System Reanalysis
C-GLORS	CMCC Global Ocean Reanalysis System
CMC	Continental Mass Change
CMCC	Centro Euro-Mediterraneo sui Cambiamenti Climatici (Euro-Mediterranean Center on Climate Change)
CMEMS	Copernicus Marine Environment Monitoring Service
CPOM	Centre for Polar Observation and Modelling
CRU	Climatic Research Unit (University of East Anglia, Norwich, UK)
CRU CL, CRU TS	CRU Timeseries (grids of observed climate)
CSIRO	Australia's Commonwealth Scientific and Industrial Research Organisation
CSR	Center for Space Research (University of Texas at Austin)
CTD	conductivity, temperature, and depth
CSV, csv	Comma-separated values
DAC	Dynamic Atmospheric Correction
DTU	Danmarks Tekniske Universitet
DTU18MSS	MSS model by DTU Space
EAIS	East Antarctic Ice Sheet
ECMWF	European Centre for Medium-Range Weather Forecasts
ECV	Essential Climate Variables
ELA	Equilibrium Line Altitude
EN4	version 4 of the Met Office Hadley Centre ''EN'' series of data sets of global quality controlled ocean temperature and salinity profiles
ENSO	El Niño-Southern Oscillation
Envisat	"Environmental Satellite", Earth-observing satellite operated by ESA
EOF	End Of Header
EOS-80	1980 International Equation of State for Seawater
EPSG	European Petroleum Survey Group

		CCI Sea Level Budget Closure
		ESA/ESRIN contract 4000119910/17/I-NB
		Reference: ESA_SLBC_cci_D4.7
		Version: v1.1
		Date: 14.02.2020
		Page: 8 of 101

EPSG3031	EPSG Projection 3031 - WGS 84 / Antarctic Polar Stereographic
EPSG3413	EPSG Projection 3413 - WGS 84 / NSIDC Sea Ice Polar Stereographic North
ERA	Earth system ReAnalysis
ERS-1/2	European Remote Sensing Satellite -1/2
ESA	European Space Agency
ESM	ESA Earth System Model
ETOPO5	global 5-minute gridded elevations/bathymetry NOAA product
EWH	equivalent water height
FES2014	Finite Element Solution) tide model
GAA, GAB, GAC, GAD	Names of data products related to GRACE atmospheric and oceanic background models (refer to section 3.2.2)
GFO	GRACE Follow-On mission
GFZ	GeoForschungsZentrum Potsdam
GGM	Global Glacier Model
GIA	Glacial Isostatic Adjustment
GIS	Greenland Ice Sheet
GMB	Gravimetric Mass Balance / GRACE Mass Balance
GMSL	Global Mean Sea Level
GMSSLA	Global Mean Steric Sea Level Anomaly (SSLA)
GPCC	Global Precipitation Climatology Centre
GPS / GNSS	Global Positioning System / Global Navigation Satellite System
GRACE	Gravity Recovery and Climate Experiment
GRACE-FO	GRACE-Follow On
GrIS	Greenland Ice Sheet
GSFC	Goddard Space Flight Center
GSSL	Global mean Steric Sea Level
GSSLA	Global Steric Sea Level Anomaly
Gt	Gigatons
GUF	Goethe University Frankfurt
HYCOM	Hybrid Coordinate Ocean Model
IB	Inverse Barometer
ICE-4, ICE-5G, ICE-6G_C	models of postglacial relative sea-level history
ICESat	Ice, Cloud, and land Elevation Satellite, part of NASA's Earth Observing System
IPRC	International Pacific Research Center
ITSG	Institute of Geodesy, Theoretical Geodesy and Satellite Geodesy (TU Graz)
JAMSTEC	Japan Agency for Marine-earth Science and Technology
JPL	Jet Propulsion Laboratory
JRA-25	Japanese 25-year ReAnalysis
JRA-55	Japanese 55-year ReAnalysis
LARS	Lars Advanced Retracking System
LEGOS	Laboratoire d'Etudes en Géophysique et Océanographie Spatiales
LRM	Low Rate Mode (CryoSat-2)
LWS	Land Water Storage

		CCI Sea Level Budget Closure
		ESA/ESRIN contract 4000119910/17/I-NB
		Reference: ESA_SLBC_cci_D4.7
		Version: v1.1
		Date: 14.02.2020
		Page: 9 of 101

MERRA-2	Modern-Era Retrospective analysis for Research and Applications, Version 2
MOG2D	Modèle d'Onde de Gravité à 2 Dimensions
MSS	Mean Sea Surface
NASA	National Aeronautics and Space Administration
NERSC	Nansen Environmental and Remote Sensing Center
netCDF	Network Common Data Form (to support the creation, access, and sharing of array-oriented scientific data)
NOAA	National Oceanic and Atmospheric Administration
NSE	Nash-Sutcliffe efficiency
OBP	Ocean Bottom Pressure
OMC	Ocean Mass Change
OMCT	Ocean Model for Circulation and Tides
PGR	post-glacial rebound
PP	Pulse Peakiness
PSD	Product Specification Document
PUG	Product User Guide
RADS	Radar Altimetry Database System
RGI	Randolph Glacier Inventory
RL05, RL06	(GRACE) solution Release 05/06
RMS	Root Mean Square
RMSE	Root Mean Square Error
RSS	Root Square Sum
SAR	Synthetic Aperture Radar
SARAL	Satellite with ARgos and ALtiKa, cooperative altimetry technology mission of Indian Space Research Organisation (ISRO) and CNES (Space Agency of France)
SARIn	SAR Interferometric mode (CryoSat-2)
SCRIPPS	Scripps Institution of Oceanography (University of California)
SEC	Surface Elevation Change
SH	spherical harmonic
SLA	sea level anomaly
SLBC	Sea Level Budget Closure
SL_cci	ESA CCI_Sea Level Project
SLE	Sea Level Equivalent
SLR	Satellite Laser Ranging
SMOS	Soil Moisture and Ocean Salinity mission
SSH, ssh	Sea Surface Height
SSL	Steric Sea Level
SSLA	Steric Sea Level Anomaly
SSL4SLBC	Steric Sea Level for Sea Level Budget Closure
SST	Sea Surface Temperature
STD	Standard Deviation
TOPAZ	(Towards) an Operational Prediction system for the North Atlantic European coastal Zones
TOPEX	TOPography EXperiment, part of the TOPEX/Poseidon satellite(joint radar altimetry project, NASA and CNES)

		CCI Sea Level Budget Closure
		ESA/ESRIN contract 4000119910/17/I-NB
		Reference: ESA_SLBC_cci_D4.7
		Version: v1.1
		Date: 14.02.2020
		Page: 10 of 101

T&S	Temperature and Salinity
TOPAZ	(Towards) an Operational Prediction system for the North Atlantic European coastal Zones
TS	Time Series
TU	Technische Universität / Technical University
TWS	Total Water Storage
TWSA	Total Water Storage Anomaly
UB	University of Bremen
UK	United Kingdom
UNF	WaterGAP-defined binary data format
UoL	University of Leeds
UoR	University of Reading
UZH	University of Zurich
v0, v1	version 0/1 data set within SLBC_cci project
v2	version 2 data set (final data set) within SLBC_cci project
VM	model of the radial viscoelastic structure of the Earth (used fo ICE-5G)
WCRP	World Climate Research Programme
w.e.	water equivalent
WAIS	West Antarctic Ice Sheet
WATCH	The WATer and global CHange project
WFDEI	Watch Forcing Data based on ERA-Interim reanalysis
WGHM	Water GAP Global Hydrology Model
wg22d_gl	non-standard version of WaterGAP2.2d global hydrology model, including glaciers
wg22d_std	WaterGAP2.2d standard global hydrology model
WGMS	World Glacier Monitoring Service
WP	Work Package
XBT	Expendable Bathythermograph
XCTD	Expendable Conductivity/Temperature and Depth

		CCI Sea Level Budget Closure
		ESA/ESRIN contract 4000119910/17/I-NB
		Reference: ESA_SLBC_cci_D4.7
		Version: v1.1
		Date: 14.02.2020
		Page: 11 of 101

1. Introduction

The Sea Level Budget Closure (SLBC_cci) project was funded within ESA's Climate Change Initiative (CCI) programme. As the sea level integrates a variety of essential climate variables (ECVs), this project represents a cross-ECV initiative.

This document describes the work done within the SLBC_cci, presents its results and highlights the most important findings of the SLBC_cci project.

The document is structured as follows. Chapter 2 outlines the scientific context. Chapter 3 describes the SLBC_cci project approach. Chapter 4 reports on the work for the provision of individual sea level budget components. Chapter 5 reports on the ocean mass budget and sea level budget analyses. Chapter 6 draws the conclusions, including the outline of the roadmap towards follow-on activities.

More details about the conducted work are reported in the project deliverable reports on the science requirements and the roadmap (Novotny et al. 2017a, 2018a, Horwath et al. 2019a), on the data product description (Novotny et al. 2017b, 2018b, Horwath et al. 2019b), and on the budget assessment (Novotny et al. 2018c. Horwath et al. 2019c, 2019d).

		CCI Sea Level Budget Closure
		ESA/ESRIN contract 4000119910/17/I-NB
		Reference: ESA_SLBC_cci_D4.7
		Version: v1.1
		Date: 14.02.2020
		Page: 12 of 101

2. Scientific context

Sea level is one of the best indicators of climate change. In effect, sea level integrates changes of several components of the climate system in response to anthropogenic forcing as well as natural forcing factors. The Earth is currently in a state of thermal imbalance because of anthropogenic greenhouse gas emissions. 93% of this heat excess is accumulated in the ocean, the remaining 7% being used to warm the atmosphere and continents and melt sea and land ice (von Schuckmann et al., 2016). Global mean sea level (GMSL) rise is a direct consequence. Present-day GMSL rise primarily reflects ocean warming (through thermal expansion of sea waters) and land ice melt, two processes resulting from anthropogenic global warming (Church et al., 2013). Anthropogenic changes in land water storage constitute an additional contribution (Cazenave et al., 2014; Dieng et al. 2015), modulated by effects of climate variability (Reager et al., 2016). Precisely monitoring the related essential climate variables (ECVs) is crucial to understand processes at work under current climate change and to validate the climate models used for future projections. Therefore, ESA's Climate Change Initiative (CCI) programme includes ECVs related to sea-level variations, in particular sea level, glaciers and ice sheets.

For processes as complex as sea-level change it is of utmost importance to regularly assess the accuracy and reliability of our knowledge about this process and its causes. Assessments of the sea-level budget are indispensable in this context. Closure of the sea-level budget implies that we have:

$$\Delta SL(t) = \Delta SL_{Mass}(t) + \Delta SL_{Steric}(t), \qquad (2.1)$$

where Δ means change of a given variable with time t; $\Delta SL(t)$ is time-variable sea level, $\Delta SL_{Mass}(t)$ and $\Delta SL_{Steric}(t)$ are the effects of time variable ocean mass and the steric sea-level, respectively (e.g. Cazenave et al, 2009; Leuliette and Miller, 2009). Steric sea level can be further separated into volume changes through ocean salinity (halosteric) and ocean temperature (thermosteric) effects, from which the latter is known to play a dominant role in observed contemporary rise of global mean steric sea level (GSSL).

Water mass conservation in the climate system implies closure of the ocean mass budget:

$$\Delta M_{Ocean}(t) = - [\Delta M_{Glaciers}(t) + \Delta M_{ice\ sheets}(t) + \Delta M_{LWS}(t) + \Delta M_{Atm}(t) + missing\ mass\ terms], \qquad (2.2)$$

where the $\Delta M(t)$ terms refer to ocean mass change, glacier and ice sheet mass balances, changes in land water storage (LWS, including seasonal snow cover), and atmospheric water vapour and clouds.

The difference between the left side and the right side of Equation 2.1 and 2.2 is called the sea level budget misclosure or ocean mass budget misclosure, respectively.

Over the course of its five assessments, the IPCC has reported a significant improvement in our understanding of the sources and impacts of global sea-level rise, and today, the sea-level

		CCI Sea Level Budget Closure
		ESA/ESRIN contract 4000119910/17/I-NB
		Reference: ESA_SLBC_cci_D4.7
		Version: v1.1
		Date: 14.02.2020
		Page: 13 of 101

budget is often considered closed, within uncertainties (Church et al., 2013). However, significant challenges remain. IPCC Fifth Assessment Report (AR5) identified a 0.4 mm/yr difference between the observed GMSL rate and the sum of contributions over 1993-2010 (Church et al., 2013).

Moreover, uncertainties of sea-level rise on the one hand and the sum of components on the other hand were large. Church et al. (2013, Tab. 13.1) report 90% confidence intervals spanning over 0.8 mm/yr and 1.1 mm/yr, respectively, which still exclude certain sources of uncertainties, such as climate variability effects on land water storage.

Since the IPCC AR5, several studies have reassessed the sea-level budget over different time spans and using different data sets (e.g., Chambers et al., 2017; Dieng et al., 2017; Chen et al., 2017; Nerem et al. 2018 for the most recent ones). Recently, in the context of the Grand Challenge entitled "Regional Sea Level and Coastal Impacts" of the World Climate Research Programme (WCRP), an international effort involving the sea level community worldwide has been carried out with the objective of assessing the various data sets used to estimate components of the sea-level budget during the altimetry era (1993 to present) (WCRP Sea Level Budget Group, led by A. Cazenave, 2018). Almost all available quality data sets have been used for each component, resulting in a large number of considered datasets. Ensemble means for each component were used for the budget assessment.

ESA's CCI Sea-Level Budget Closure project (SLBC_cci) aimed at exercising sea-level budget analyses by taking advantage of the improved quality of related EO datasets produced within the CCI programme. It is specific to the SLBC_cci project to concentrate on datasets generated by the consortium members so that they have first-hand insights into their genesis and uncertainty characteristics. This approach is complementary to projects like the WCRP initiative described above, to which it contributed essentially.

The SLBC_cci project aimed at assessing the global budget of the sea level. In addition, the Arctic Ocean was chosen for a dedicated regional sea-level budget study. the specific focus on the Arctic sea level budget is due to the fact that the region has warmed at a rate about twice the rest of the globe during the recent decades. The sea level of the region may therefore be influenced by the oceanic thermal expansion, as well as the melting of the high latitude glaciers and the Greenland Ice Sheet associated with the warming of the Arctic region in recent decades.

		CCI Sea Level Budget Closure
		ESA/ESRIN contract 4000119910/17/I-NB
		Reference: ESA_SLBC_cci_D4.7
		Version: v1.1
		Date: 14.02.2020
		Page: 14 of 101

3. The SLBC_cci approach

3.1 Programme of conducted work

The work of SLBC_cci was structured into four generic parts, which defined the Work Packages (WPs) 100, 200, 300, 400. Figure 3.1.1 shows a scheme of the time line and interactions of these WPs. Figure 3.1.2 shows a more general flowchart.

WP 100 consisted in the consolidation and update of the **science requirements**. This activity also resulted in a **roadmap for future work**.

WP200 consisted in the provision of datasets on **individual components of the sea level budget** and in the provision of respective uncertainty assessments.

The considered components were

- Total sea level change
- Steric component of sea level change
- Ocean mass component of sea level change
- Glaciers contribution to ocean mass change
- Ice sheet contribution to ocean mass change
- Land water contribution to ocean mass change.

The datasets built, as much as possible, on existing CCI products. For example, products on total sea level change had been developed by the CCI sea level project. These products needed to be further assessed and updated. For other components, new data products needed to be generated. These data products used data sources from existing CCI projects (Glaciers, Ice Sheets, Sea Surface Temperature) along with non-CCI data. The incorporation of CCI products
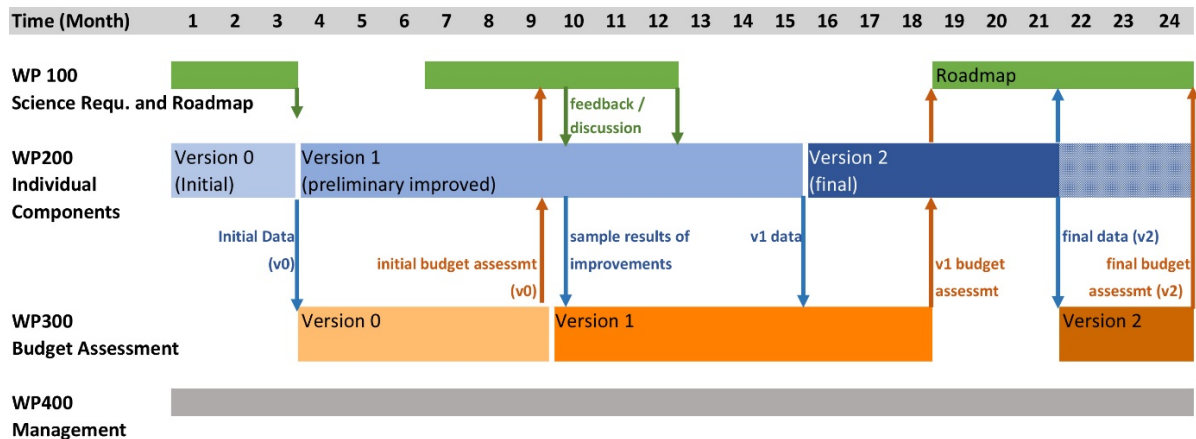
Figure 3.1.1: time line of the SLBC project

		CCI Sea Level Budget Closure
		ESA/ESRIN contract 4000119910/17/I-NB
		Reference: ESA_SLBC_cci_D4.7
		Version: v1.1
		Date: 14.02.2020
		Page: 15 of 101

enabled the assessment and full exploitation of these CCI products for the purpose of sea level-related investigations.

The coordinated provision of the whole set of sea level budget components followed a common framework in terms of product definition, spatial coverage, temporal resolution, and data formats. The task of treating uncertainties consistently over the involved groups and disciplines was tackled with particular attention.

Therefore, all components were managed in the single work package WP 200, with common documents and common data packages.

WP 300 concerned the **assessment of the budget closure or misclosure**. The assessment was done on three levels:

- Assessment of the ocean mass budget,
- assessment of the total sea level budget,
- assessment of mass and total sea level budget for the Arctic Ocean.

The analyses included feedback between the three levels as well as to WP 200 and WP 100.

Iteration of the tasks of WP 100, 200 and 300 was an essential element of the project. This iteration allowed

- feedback from the integrated budget assessment to the development of datasets for the budget components
- feedback from the integrated budget assessment to the prioritization of science requirements and of elements of a future science roadmap
- evaluation of the benefit from improved datasets, especially from CCI products.

Work started with an initial (**Version 0**) compilation of data sets of the budget components, which was available by the start of the project, prior to any further improvement. Assessing the
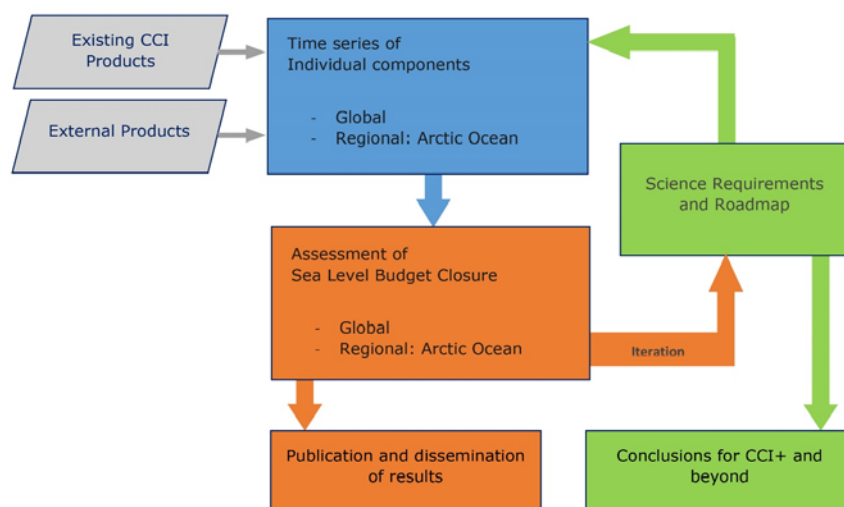
Figure 3.1.2: Project flowchart

		CCI Sea Level Budget Closure
		ESA/ESRIN contract 4000119910/17/I-NB
		Reference: ESA_SLBC_cci_D4.7
		Version: v1.1
		Date: 14.02.2020
		Page: 16 of 101

sea level budget based on these initial datasets helped to consolidate science requirements and requirements on the improvement of the individual components. Two improved versions of the budget components (**Version 1** and **Version 2**) were developed during the project within WP 200.

The effects on the budget closure was subsequently assessed within WP 300. Interaction and feedback between the improvement of budget components and the budget assessment was exercised throughout the project. For example, an additional **exchange on sample improvements** was done in the middle of the version 1 product improvement process.

Finally, **WP 400** concerned the **scientific lead and project management.**

3.2 Framework for the budget assessment

3.2.1 Concept of time series

The budget closure assessment is based on time series of changes of state parameters, such as sea level, glacier mass, etc., in the form

$$z(t). \hspace{5cm} (3.2.1)$$

In our case *z(t)* refers to a mean value over a time interval (e.g., one calendar month). We identify the time interval with a single time *t* where *t* is the interval midpoint. Moreover, *z(t)* does not denote the state parameter in an absolute sense but the *difference* between the state at time *t* and a reference state Z_0. The reference state Z_0 needs to be well defined but it does not need to be quantified explicitly. In SLBC_cci, Z_0 is defined as the mean state over the 10 calendar years from 2006 to 2015. This choice (as opposed to alternative choices such as the state at the start time of the time series) affects plots of *z(t)* by a simple shift along the ordinate axis. However, it has a more complicated impact on uncertainties of *z(t)* if errors are correlated in time. To avoid inconsistencies and misinterpretation of uncertainties it is important to define the reference states explicitly and consistently.

An alternative way of thinking about temporal changes is by the rates of change

$$\frac{\Delta z}{\Delta t}(t) \hspace{5cm} (3.2.2)$$

In practice, again, *t* refers to a time interval with length Δt (e.g. a month or a year) and Δz refers to the change of the state parameter *z* during that interval. Cumulation of *(Δz/dΔ)(t)* gives *z(t)*:

$$z(t) = \sum_{\tau=t_0}^{t} \frac{\Delta z}{\Delta t}(\tau)\,\Delta t, \hspace{3cm} (3.2.3)$$

where the summation is over the discrete time steps from t_0 to *t*.

Glaciological modelling and hydrological modelling have $\Delta z / \Delta t$ as their primary product, from which *z(t)* is derived as a secondary product. In contrast, for satellite altimetry and satellite

		CCI Sea Level Budget Closure
		ESA/ESRIN contract 4000119910/17/I-NB
		Reference: ESA_SLBC_cci_D4.7
		Version: v1.1
		Date: 14.02.2020
		Page: 17 of 101

gravimetry $z(t)$ is usually considered as their primary product and temporal changes arise as derived products.

Based on the time series we analyse the closure of the different budgets on different levels. First, we analyse budget closure on a time series level. That is, we evaluate the budget equations 2.1, 2.2 for every time step t.

Second, we perform an un-weighted least squares regression to estimate a linear trend (together with seasonal parameters, where appropriate), according to

$$z(t) = a_1 + a_2 t + a_3 \cos(\omega_1 t) + a_4 \sin(\omega_1 t) + a_5 \cos(2\omega_1 t) + a_6 \sin(2\omega_1 t) + \varepsilon(t) \qquad (3.2.4)$$

with $\omega_1 = 2\pi$ / year. We then analyse the budget of the parameters a_2 fitted to every budget element. The seasonal parameters $a_3,..., a_6$ are co-estimated only in cases where the underlying time series contain the seasonal signal owing to their temporal resolution and the absence of a prior correction for a seasonal signal. Then, we also analyse the budget of the seasonal parameters a_3 and a_4.

For the analysis on time series level, time series had to be brought to an identical temporal sampling, which implied some reduction of the temporal sampling to epochs where data was available for all involved time series, unless small data gaps could be filled by interpolation.

For the analysis of fitted trends, each time series was used with its original temporal sampling and reduced to a common overall time interval. This interval was defined

- Jan 1993 - Dec 2016
- Jan 2003 - Dec 2016.

In cases where GRACE-based time series were involved, the last month of which was August 2016, the intervals were defined to end in August (instead of December) 2016.

3.2.2 Concept of uncertainties

Following the ISO "Guide to the expression of uncertainty in measurement" (JCGM 2008), uncertainties of a measurement (including its corrections) are quantified in terms of the second moments of a probability distribution that "characterizes the dispersion of the values that could reasonably be attributed to the measurand". Specifically, the standard uncertainty (i.e. standard deviation) should be always specified.

This quantification of uncertainty is transferable: The uncertainty evaluated for one result can be used as a component in evaluating the uncertainty of another measurement in which the first result is used. The law of uncertainty propagation is to be used. In the simple case of a summation of results with uncorrelated errors, the combined standard uncertainty is the root sum square od the standard uncertainties of the individual components. Error covariances have to be accounted for if errors are correlated.

ISO (1995) discusses in its Appendix E4.4: "It has been argued that, whereas the uncertainties associated with the application of a particular method of measurement are statistical parameters characterizing random variables, there are instances of a "truly systematic effect"

whose uncertainty must be treated differently. [...] But if the possibility of such an offset is acknowledged to exist and its magnitude is believed to be possibly significant, then it can be described by a probability distribution, however simply constructed, based on the knowledge that led to the conclusion that it could exist and be significant." This argument is adopted also for the GIA correction. The *concept* of uncertainty quantification should obey to standard uncertainties and the law of uncertainty propagation, irrespective of the imperfection in the *realisation* of this concept.

Uncertainties refer to the estimation of a well-defined measurand. The elementary measurand in the sea level budget assessment is the time-dependent state parameter *z(t)* or the time-dependent rate of change *($\Delta z/\Delta t$)(t)*. Information on temporal correlations need to be included if applicable. Likewise, information on temporal correlations of monthly errors need to be applied when aggregating monthly values to annual values. The uncertainty of corrections that are linear in time, such as the GIA correction, is an example for such temporal correlations, which can just be stated as an uncertainty on the linear trend.

		CCI Sea Level Budget Closure
		ESA/ESRIN contract 4000119910/17/I-NB
		Reference: ESA_SLBC_cci_D4.7
		Version: v1.1
		Date: 14.02.2020
		Page: 19 of 101

4. Provision of individual sea level budget components and associated uncertainties

This chapter reports the developments and the results conducted under WP200 for the provision of individual sea level budget components and associated uncertainties. Three versions v0, v1, and v2 of data products were provided, each version involving further developments upon the previous versions. This report concentrates on the final version v2. More details on all product versions are given by Novotny et al. (2017b) and Horwath et al. (2018b, 2019b) and in the cited publications.

4.1 Global mean sea level change

4.1.1 Methods

The time series of Global Mean Sea Level (GMSL) change are derived from satellite altimetry observations.

The SLBC_cci v2 time series uses version 2.0 of the European Space Agency/ESA Climate Change Initiative/CCI 'Sea Level' project. It combines data from the TOPEX/Poseidon, Jason-1/2, GFO, ERS-1/2, Envisat, CryoSat-2 and SARAL/Altika missions and is based on a new processing system with dedicated algorithms and adapted data processing strategies (Ablain et al., 2015, 2017b; Quartly et al., 2017; Legeais et al., 2018). It is available as a global gridded 1°x1° resolution data over 82°N and 82°S latitudinal range. The CCI sea level product has been validated using different approaches including a comparison with tide gauge records as well as to ocean re-analyses and climate model outputs.

The CCI gridded sea level data has been averaged over 65°N and 65°S latitudinal range to obtain the SLBC_cci version 2 GMSL time series. Furthermore, TOPEX A instrumental drift due to aging of the TOPEX A altimeter placed in the TOPEX/Poseidon mission from January 1993 to early 1999 has also been corrected from the CCI GMSL time series based on Ablain et al. (2017a). The TOPEX A drift value based on this methodology corresponds to (1.0 ± 1.0) mm/yr over January 1993 to July 1995 and (3 ± 1.0) mm/yr over August 1995 to February 1999.

The Glacial Isostatic Adjustment (GIA) correction of -0.3 mm/yr (Peltier, 2004) has been applied to the CCI GMSL time series. Annual and semi-annual signals were removed from the time series through a least square fit of 12 month and 6 month period sinusoids. A 60 day smoothing has also been applied on the GMSL time series.

|		**CCI Sea Level Budget Closure**
		ESA/ESRIN contract 4000119910/17/I-NB
		Reference: ESA_SLBC_cci_D4.7
		Version: v1.1
		Date: 14.02.2020
		Page: 20 of 101

4.1.2 Products

The final v2 altimetry based GMSL data file consists of a monthly GMSL time series from the ESA CCI project, averaged over 65°N and 65°S latitudinal range. Figure 4.1.1 displays the evolution of this GMSL time series.

4.1.3 Uncertainty assessment

Over the recent years, several articles (Ablain et al., 2015, 2017b; Dieng et al, 2017; Quartly et al., 2017; Legeais et al., 2018) have discussed sources of errors in GMSL trend estimation. Ablain et al. (2019) extends this work by considering new altimeter missions (Jason-2, Jason-3) and recent findings on altimetry error estimates.

The uncertainty data for GMSL time series provided here for SLBC_cci version 2 are obtained from Ablain et al. (2019). This manuscript provides a very detailed explanation for the methodology adapted for the GMSL uncertainty assessment.

Three major types of errors are considered in the uncertainty estimation of altimetric GMSL: (a) biases in GMSL between successive altimetry missions characterized by bias uncertainties at any given time; (b) drifts in GMSL due to onboard instrumental drifts or long-terms drifts such as GIA, orbit etc. characterized by trend uncertainty, and (c) other measurement errors such as due to geophysical corrections (wet tropospheric, orbital, etc.) which exhibit time-
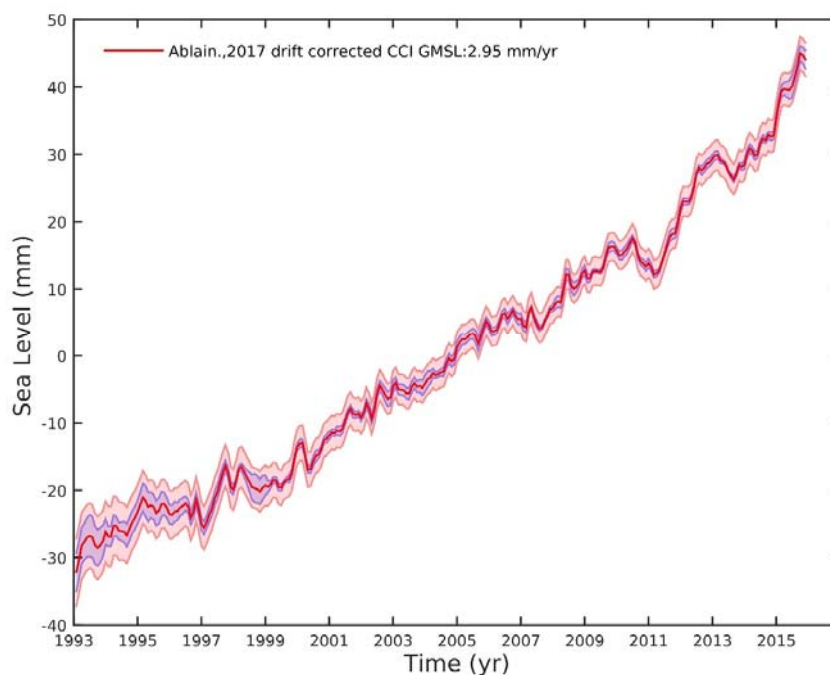
Figure 4.1.1: CCI based GMSL averaged over 65°N and 65°S latitudes, TOPEX A drift correction over Jan. 1993-Feb. 1999 applied. Red envelope: uncertainty band from the comprehensive uncertainty assessment by Ablain et al. (2019). Blue envelope: uncertainty band based on the RMS of the dispersion of available GMSL time series.

		CCI Sea Level Budget Closure
		ESA/ESRIN contract 4000119910/17/I-NB
		Reference: ESA_SLBC_cci_D4.7
		Version: v1.1
		Date: 14.02.2020
		Page: 21 of 101

correlation and are characterized by their standard deviation. All the error sources are assumed to be independent from each other. The individual variance-covariance matrix of each of the error sources is calculated from a large number of random draws (>1000) of simulated error using fed with a standard normal distribution. Thus, the total error variance-covariance matrix (Σ) is the sum of the individual variance-covariance matrix of each error source in the error budget. The dominating error terms are in the diagonal of the total matrix. The GMSL uncertainty envelope is estimated from the square root of the diagonal terms of the total matrix. The different terms of the altimeter GMSL error are based on the current knowledge of altimetry measurement errors. As the altimetry record increases in length with new altimeter missions, the knowledge of the altimetry measurement also increases, and the description of the errors improves. This implies that the error variance-covariance matrix is expected to improve and change in the future (Ablain et al. 2019).

Figure 4.1.1 displays the uncertainty envelope based on Ablain et al. (2019) in red. We can observe that the GMSL time series shows a larger uncertainty during the TOPEX/Poseidon period (5 mm to 8 mm) than during the Jason period (close to 4 mm) mainly due to the TOPEX A instrumental drift issue. The blue shaded uncertainty envelope is the uncertainty estimate based on the root mean square of the dispersion of each of the available GMSL time series from different processing groups such as NASA, AVISO, University of Colorado, CSIRO from the ensemble mean. This uncertainty envelope based on the dispersion from their ensemble mean is due to the use of different processing technique, different versions of auxiliary data and different interpolation methods applied by the different groups (Henry et al., 2014; Masters et al., 2012). We can observe that this blue envelope is smaller than the real uncertainty envelope (in red) in GMSL because all groups use similar methods and corrections to process the raw data and thus several sources of systematic uncertainty is not accounted for in the spread.

In terms of trend uncertainty, Ablain et al. (2019) estimates the GMSL trend uncertainty to be ± 0.4 mm/yr (90% confidence level, after correcting the TOPEX A drift) which means that at 1 sigma the uncertainty is ± 0.24 mm/yr.

4.2 Steric sea level change

4.2.1 Methods

Scientific background

Several global mean steric sea level (GSSL) variations from Argo and other in situ observations have been derived over the past couple of years (e.g. Willis et al., 2008; Cazenave et al, 2009; Leuliette and Miller, 2009; von Schuckmann et al., 2009). There are substantial differences in these global statistical analyses, which have been related to instrumental biases, quality control and processing issues, role of salinity and influence of the reference depth.

A given heat uptake can produce different steric height changes depending on the initial conditions. Density of sea water is a function of temperature and salinity at any given pressure, and is described through the Thermodynamic Equation of Seawater.

Overview of method

The basic approach is to estimate steric sea level anomaly (SSLA) fields in a grid, and average across the ocean to determine the global mean steric sea level anomaly (GMSSLA) that contributes to global mean sea level rise.

For this approach we use grid cells at 5°x5°, monthly resolution, a grid defined collectively within the SLBC_cci project, and compatible with the resolution of gravity-based mass change estimates. Our calculation method is updated from that of von Schuckmann and Le Traon (2011), and adopts the common vertical grid used therein for profile calculations, but here the horizontal resolution is refined. This vertical grid extends to 2000 m depth, and the SSLAs are therefore effectively assuming no steric contribution from depths below 2000 m.

Cells that are partially comprised by ocean are included in proportion to their ocean area at the sea surface. Where bathymetry within the cell is shallower than 2000 m, the steric thickness anomaly is estimated for a given profile to a depth no deeper than the sea floor using the mean bathymetry at a spatial resolution of 1°x1°. In this way, shelf seas are included, although Argo profiles are generally absent for such areas.

Using Sea Surface Temperature (SST) to condition the climatology

The way in which SST data have been introduced is by conditioning the climatology. This idea can be expressed as replacing the climatology and its variability, with the profile best estimate given the climatology, its variability and the SST observation, and the error covariance matrix of that best estimate.

The effect of conditioning the climatology is illustrated in Figure 4.2.1. For this particular month (August), year (2003) and location (30.5°N, -9.5°E), the SST is about 2°C below the climatology value. The conditioning is strong for the upper ~50 m of the ocean, which is a modest depth range, and the conditioned profile is clearly more realistic given the SST (approximately isothermal over a mixed layer). The uncertainty is reduced at the surface, where the cell-month SST is well known from the satellite data. Below about 150 m, the effect of conditioning decays towards zero (conditioned and unconditioned profiles converge).

The GMSSLA time series obtained is shown in Figure 4.2.2. Note how the uncertainty is larger in the earlier years, reflecting the low numbers of Argo profiles at that time. Also note that the uncertainty calculation here uses the approximation of independence of error between cells, which is a good approximation later in the record (when the results are dominated by Argo), and an optimistic approximation earlier in the record (when the results depend more on the conditioned climatology, because the Argo profiles are so few). Therefore, the contrast in uncertainty between 2002 and 2018 is probably underestimated, with uncertainties attributed to 2002 being smaller than they should.

		CCI Sea Level Budget Closure
		ESA/ESRIN contract 4000119910/17/I-NB
esa	TECHNISCHE UNIVERSITÄT DRESDEN / Universität Zürich / UNIVERSITY OF LEEDS / LEGOS / Universität Bremen / GOETHE UNIVERSITÄT FRANKFURT AM MAIN / DTU Space National Space Institute / University of Reading / MERCATOR OCEAN INTERNATIONAL	Reference: ESA_SLBC_cci_D4.7
		Version: v1.1
		Date: 14.02.2020
		Page: 23 of 101

The global mean SSLA time series contains substantial regional variability. Whilst this product is intended primarily as an estimator of global or basin-scale studies, it is reassuring that spatial patterns of change are broadly in agreement with spatially resolved estimates in the literature. Comparing 2005 to 2015, there is a clear tendency towards increased SSLA (Figure 4.2.3 a and b). Positive anomalies in the gulf stream, Kuroshio currents and Indian Ocean are associated with rapid warming, while the warming / cooling dipole in the tropical Pacific is the classic pattern associated with ENSO (von Schuckmann, et al., 2014). In the North Atlantic, subpolar gyre negative anomalies are associated with a cooling of the mixed layer, although they are somewhat offset by increased freshwater in the region (Robson, et al., 2018).
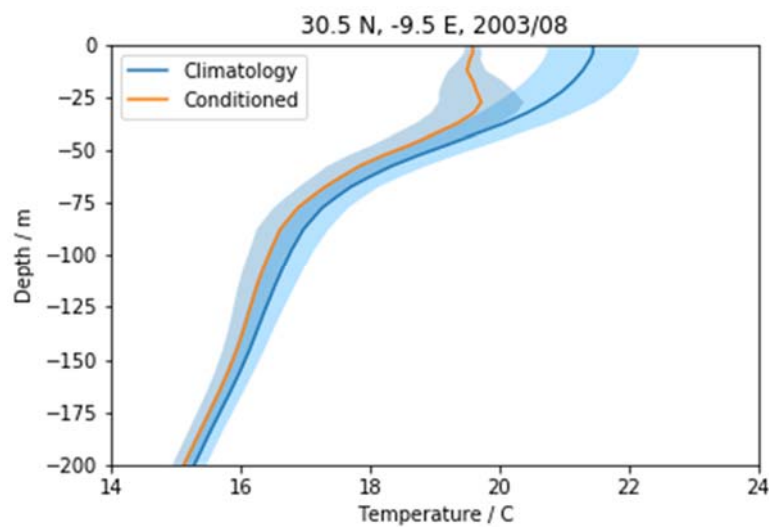
Figure 4.2.1: Example of conditioned climatology in comparison with unconditioned case.
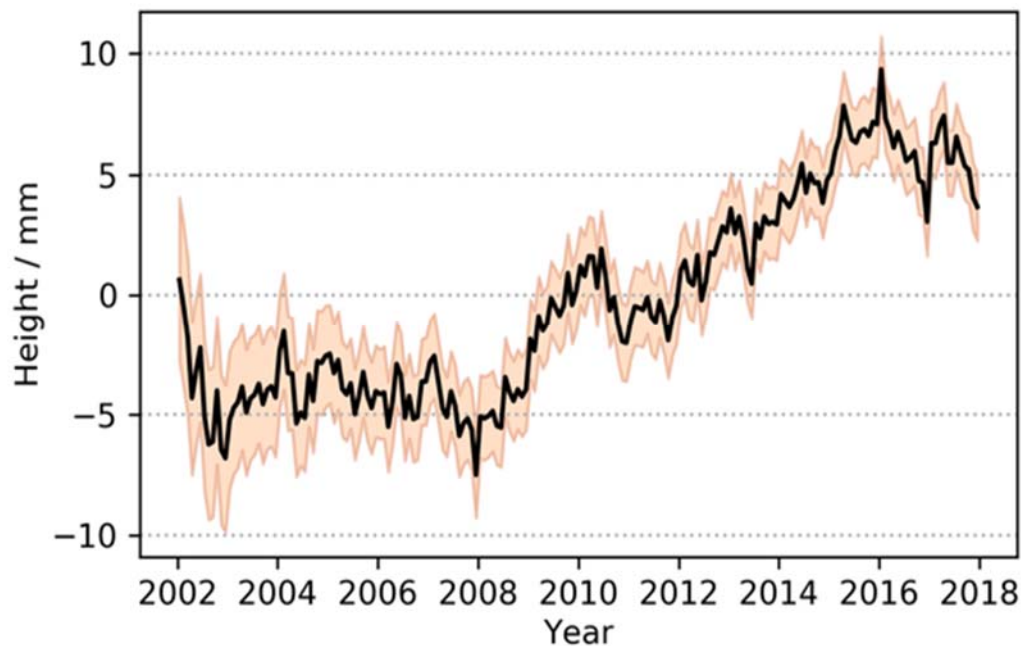
Figure 4.2.2: Global steric sea level anomaly, monthly, 2002-2017. Shading denotes standard (1σ) uncertainty

		CCI Sea Level Budget Closure
	TECHNISCHE UNIVERSITÄT DRESDEN · Universität Zürich · UNIVERSITY OF LEEDS · LEGOS · Universität Bremen · GOETHE UNIVERSITÄT FRANKFURT AM MAIN · DTU Space National Space Institute · University of Reading · MERCATOR OCEAN INTERNATIONAL	**ESA/ESRIN contract 4000119910/17/I-NB**
eesa		Reference: ESA_SLBC_cci_D4.7
		Version: v1.1
		Date: 14.02.2020
		Page: 24 of 101

In general, the uncertainty associated with a single cell (Figure 4.2.3 e, f) is the same order of magnitude as the SSLA estimate itself (Figure 4.2.3 a, b). Cells which are not sampled by Argo (Figure 4.2.3 c, d), use the conditioned climatology only to estimate SSLA; they therefore appear to have small height anomalies, but large associated uncertainty. This effect is particularly noticeable in coastal waters, where shallow seas limit the penetration of Argo platforms.
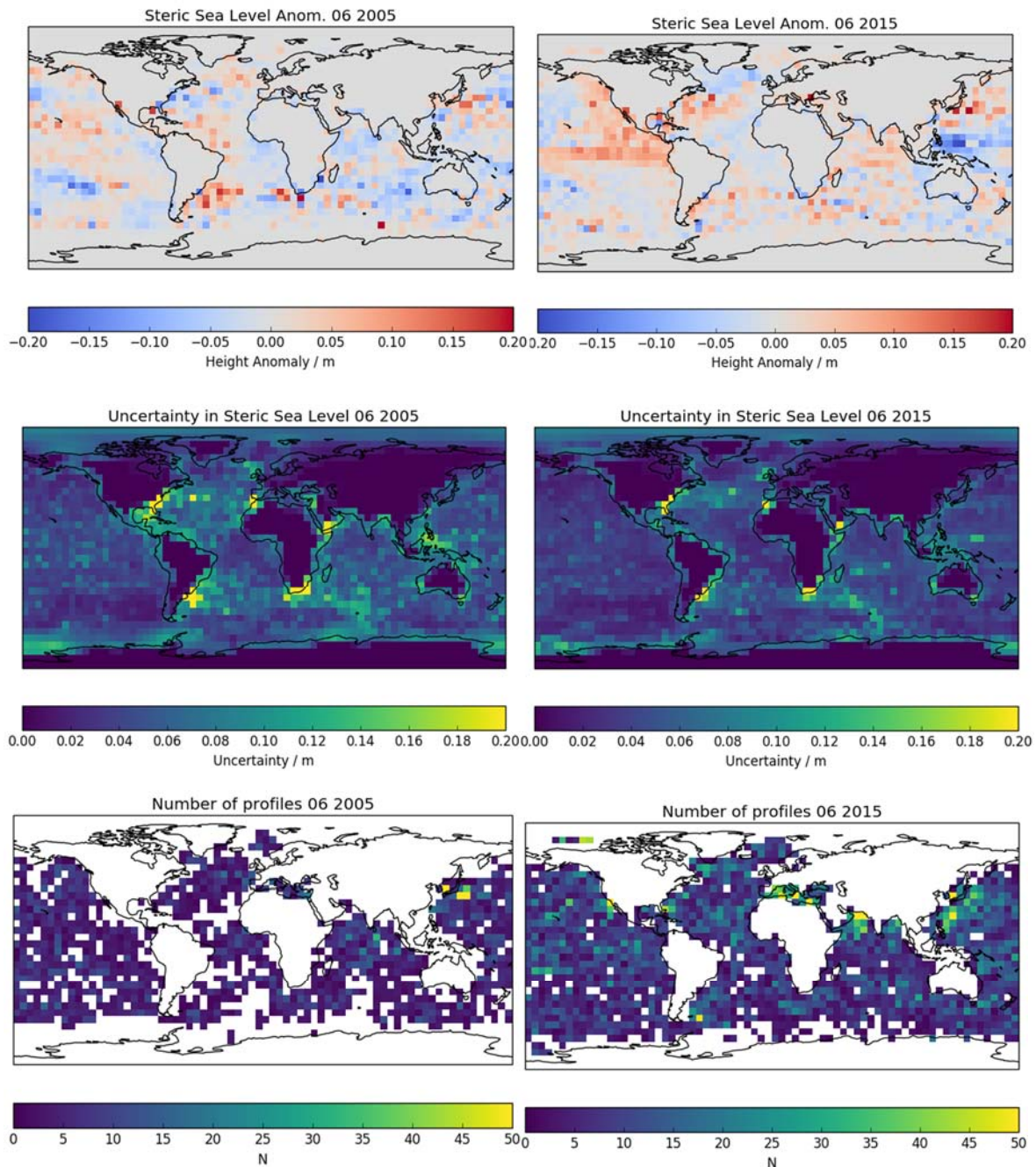
Figure 4.2.3: Steric sea level (a, b), uncertainty (e, f), and number of contributing Argo profiles (c, d) early in the time series (2005, a, c, e) and late in the time series (2015, b, d, f).

		CCI Sea Level Budget Closure
		ESA/ESRIN contract 4000119910/17/I-NB
eesa	TECHNISCHE UNIVERSITÄT DRESDEN · Universität Zürich · UNIVERSITY OF LEEDS · LEGOS · Universität Bremen · GOETHE UNIVERSITÄT FRANKFURT AM MAIN · DTU Space National Space Institute · University of Reading · MERCATOR OCEAN INTERNATIONAL	Reference: ESA_SLBC_cci_D4.7
		Version: v1.1
		Date: 14.02.2020
		Page: 25 of 101

Regions which have large interannual variability have a larger uncertainty for a given sampling density, since representativity error is reasonably expected to be larger in these regions. Between 2005 and 2015 the effect of increased Argo coverage is particularly noticeable in current regions such as the Gulf Stream, and in the Southern Ocean; such improvements are noticeably smaller or entirely absent from coastal waters.

Effect of conditioning

The addition of SST via a conditioned climatology both constrains the mixed layer and forms a product that is spatially complete.

These effects reduce uncertainty and stabilise the final product and can be separated as shown in Figure 4.2.4. Here, we compare the final product (red; includes SST in the mixed layer and is spatially complete), with an estimate derived only from cells that contain Argo information (blue; includes SST in the mixed layer, does not include cells that are not sampled by Argo). The difference between the red and blue lines is therefore the impact of making the product spatially complete using the climatology which is conditioned on SST. A further estimate
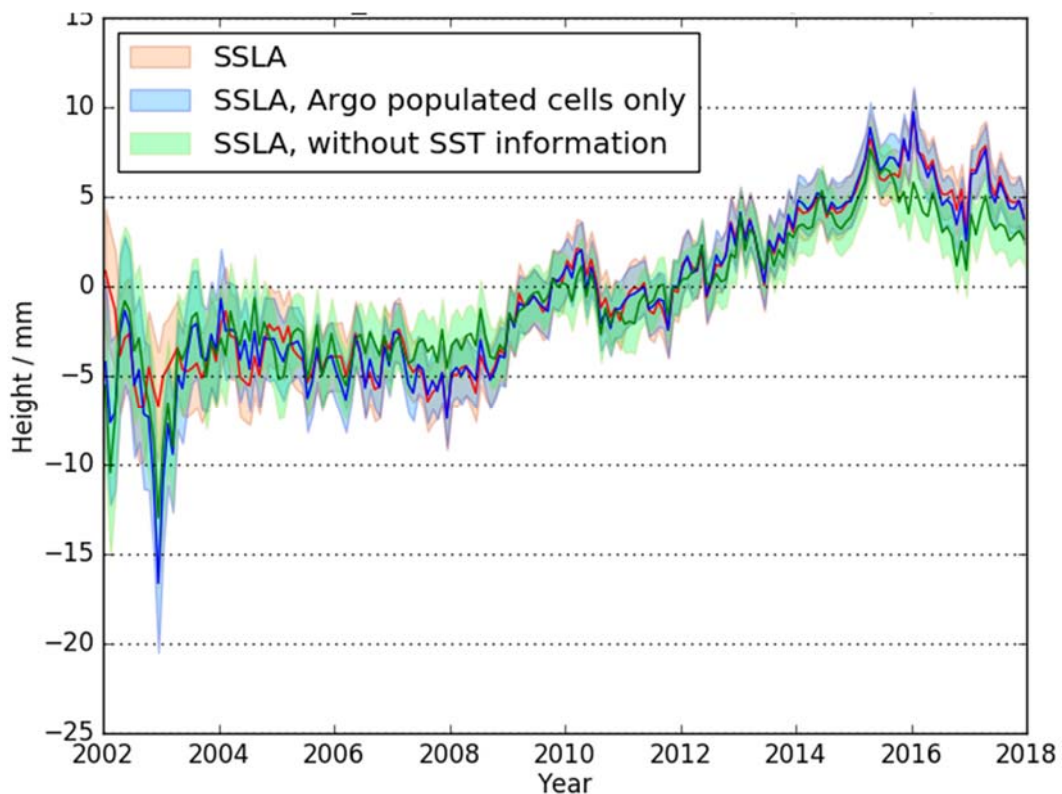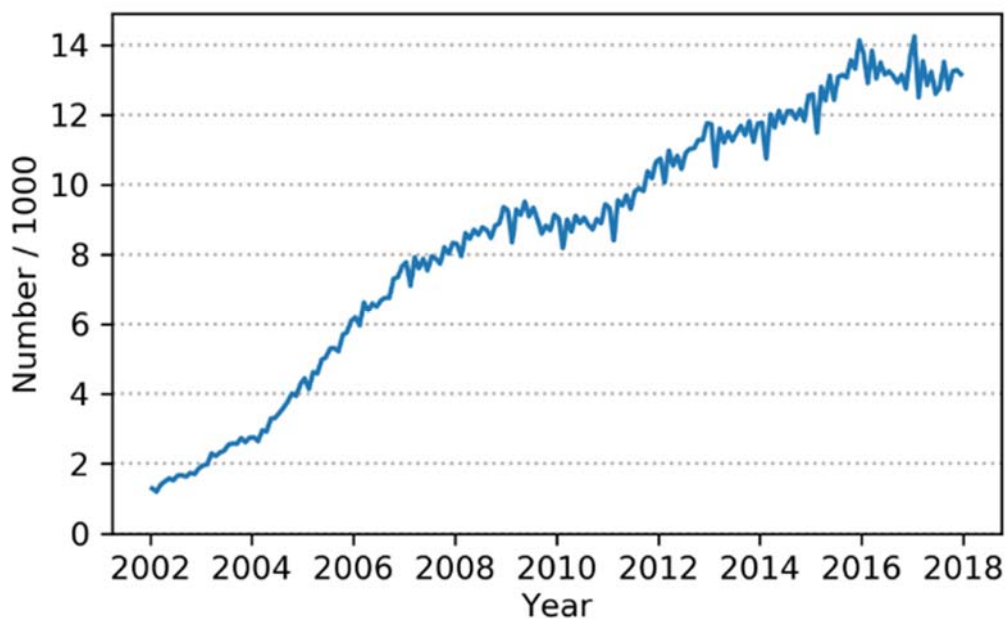

Figure 4.2.4: Steric Sea Level Anomaly, monthly, between 65° and -65° lat. Effect of removing the spatial completeness constraint (blue), removing the SST conditioning (green) with the full SSSLHA timeseries (red).

		CCI Sea Level Budget Closure
		ESA/ESRIN contract 4000119910/17/I-NB
esa	[university logos]	Reference: ESA_SLBC_cci_D4.7
		Version: v1.1
		Date: 14.02.2020
		Page: 26 of 101

(green) is derived only from Argo data and climatology, i.e. no estimate is made in cells which are not sampled by Argo; and additionally, in sampled cells SST conditioning of the climatology is removed. The unconditioned climatology itself still informs each cell estimate, however.

An important consideration is to make a judgement regarding when the GMSSLA time series is adequately constrained by Argo profile data to constitute useful data for time series analysis. At the start of 2002, the number of profiles is a tenth of the number available by 2015, and so the earliest years are therefore not adequately constrained. This is clear in Figure 4.2.4, in that the time series without the additional SST constraint (green line) in the annual mean exhibits larger than expected inter-annual variability over the first three years in particular. These are stabilised by use of the conditioned climatology (red line).

By the end of 2004, the number of profiles per month is a quarter of the 2015 number (Figure 4.2.5). The relatively shallower slope of our product before about 2004, is a result of the stabilising effect of the climatology in the limit of very sparse Argo sampling. As a result, the apparent anomaly is reduced beyond what is physically reasonable. Taken together, these observations indicate it is reasonable to use v2.0 from 2004 onwards for time series analysis, in common with other analyses of Argo profiles (von Schuckmann and Le Traon, 2011; Good, et al., 2013; Cazenave, et al., 2009).

The much smaller uncertainty estimate in the conditioned, spatially complete product before 2005 is the result of the much larger number of populated cells From 2005 onwards, Argo coverage is dense enough (Figure 4.2.5) that the effect of adding SST has a larger effect on the global mean than does spatial completeness. Beyond 2012, as most cells contain at least one Argo profile each month, there is little difference between including or ignoring cells which contain no Argo profiles.

Figure 4.2.5: Number of profiles used in the record by month.

		CCI Sea Level Budget Closure
		ESA/ESRIN contract 4000119910/17/I-NB
		Reference: ESA_SLBC_cci_D4.7
		Version: v1.1
		Date: 14.02.2020
		Page: 27 of 101

Including conditioned SST reduces GMSSLA in 2008, and increases it from 2016 onwards. Both observed SSTs and the baseline climatology are cooler than a static climatology early in the time series, and warmer late in the time series. Therefore, including SST in the mixed layer increases the overall change in steric height. This leads to an apparently increased trend in GMSSLA between 2006-2018 in the conditioned product relative to unconditioned. The size of the effect varies substantially by region.

Improvements to the methodology

Including SST information has been shown to reduce uncertainty and to affect steric height in the mixed layer enough to have a visible effect in the global mean. Over the period 2005-2018 the trend in steric height is larger when including SST via a conditioned climatological profile than when using a static climatology as the prior. That is, the addition of SST mitigates the over-stabilising effect of the climatology.

The implication is that there remains an effect due to the use of static climatology below the mixed layer, which will cause the estimated trend to be smaller than the true value.

The use of static climatology to fill gaps in Argo profiles has been shown to cause systematic underestimates of trends in the literature (e.g. Ishii and Kimoto, 2009). In our framework, it is possible that the use of a static climatology as a first guess – a sort of prior – exacerbates our sensitivity to this issue.

Two main improvements can be made to address this issue. The first is the choice of prior itself, and the second is how the prior is weighted relative to observations.

Ideally, we would choose a prior that does not cause a bias in the derived trend. One possibility might be to use a "time-varying" climatology, separating the long-term trend and the interannual variability, and use a climatology that is the sum of the mean state and the long term trend for each year (e.g. Ishii et al., 2017; Hirahara et al., 2014). Uncertainty associated with the climatology would then in principle be the interannual variability from the residual, but some consideration would need to be given to the effect on the uncertainty model, to avoid simply re-distributing uncertainty explicit evaluation in the current model to implicit in the method.

Weighting of the climatology relative to each Argo profile is a question of representativity uncertainty. Currently, a 1:1 correspondence is assumed between interannual and intra-cell variability. Interannnual variability is calculated from 10 years of Argo data, and a scaling factor applied to account for the shortness of the record.

An alternative observation-based approach might be to calculate inter-annual and intra-cell variability from the ~40-year SST record, plus an empirical, vertical scaling factor to account for changing variability at depth, produced from the decade of Argo observations.

A model-based approach would be to use a high-resolution model to calculate interannual and intra-cell variability. Both approaches will be developed and evaluated in future iterations of the product.

		CCI Sea Level Budget Closure
		ESA/ESRIN contract 4000119910/17/I-NB
		Reference: ESA_SLBC_cci_D4.7
		Version: v1.1
		Date: 14.02.2020
		Page: 28 of 101

4.2.2 Products

The gridded v2.0 product is available at 5° x 5° monthly resolution, from January 2002 to December 2017. Note that the gridded product is not spatially complete The global average over the latitude range from 65°N to 65°S covers the same period.

4.2.3 Uncertainty assessment

The uncertainty estimate of the GMSSLA is done by uncertainty propagation from the individual sources of uncertainty. We assume that errors are independent between cells. This is an approximate model for the error correlation, because (i) SST errors may be correlated on scales greater than the cell size, and (ii) some cells have the same Argo profilers contributing data to them in a given month (when the profilers move from one cell to the next within the month).

Overall, three aspects of the uncertainty model are recognized to be potentially optimistic: the modelling of measurement errors as independent between profiles rather than platforms; the use of only 10 years for assessing inter-annual variability; and the assumption of full independence of errors between cells when forming the global average. On the other hand, two assumptions are potentially conservative: measurement errors in salinity and temperature were combined in their worst-case combination; representativity errors in profiles are assumed to be fully correlated vertically, whereas in reality they are likely to decorrelate over large vertical separations. Furthermore, three parameters in the uncertainty model are presently based on expert judgement: the scale factor of 1 between intra-cell and cell-mean inter-annual variability; and the scale parameters for time and space. Lastly, note that uncertainty in the evaluation of vertical correlations from Argo data in order to condition the climatology are not included in the uncertainty model. In summary, the uncertainty modelling and propagation are largely comprehensive and rigorous, but nonetheless need further development to fully ensure their quantitative realism.

4.3 Ocean mass change

4.3.1 Methods

The mass change of the global ocean can be determined through its effect on the gravity field. Within SLBC_cci, time series of ocean mass change (OMC) were generated from monthly gravity field solutions from the GRACE missions. The GRACE mission has two identical space crafts flying about 220 km apart in a near-polar orbit originally at 480 km above the Earth. GRACE maps the Earth's gravity field by making accurate measurements of the distance between the two satellites, using GPS and a microwave ranging system. Under the assumption that mass

		CCI Sea Level Budget Closure
		ESA/ESRIN contract 4000119910/17/I-NB
		Reference: ESA_SLBC_cci_D4.7
		Version: v1.1
		Date: 14.02.2020
		Page: 29 of 101

redistribution occurs in a "thin" layer on the Earth's surface, comprising the hydrosphere, atmosphere and cryosphere, these changes are expressed in terms of of mass per surface area in kg/m² , or equivalent water height (EWH) in mm w.e.

Within SLBC_cci OMC time series were generated based on spherical harmonic (SH) GRACE solutions. This allowed full control on the methodology and a full uncertainty assessment. Extensive analyses within SLBC_cci and the adoption of developments within the larger scientific community (Johnson and Chambers 2013, WCRP 2018, Uebbing et al. 2019) led to significant improvements and refinements from v0 to v2 products. This report concentrates on the v2 products.

The following GRACE monthly gravity field solutions series were used:

- ITSG-Grace2018, with maximum spherical harmonic degree 60 (Mayer-Gürr et al. 2018a,b) (data source ftp://ftp.tugraz.at/outgoing/ITSG/GRACE/ITSG-Grace2018/monthly/ monthly_n60)
- CSR_RL06, GFZ_RL06, JPL_RL06, with maximum spherical harmonic degree 60 (Data source: https://podaac.jpl.nasa.gov/GRACE)

We chose ITSG_2018 as the preferred input SH solution because it showed the lowest noise level among all releases, with no indication for differences in the contained signal (Groh et al. 2019).

Based on EWH grids generated by involving the corrections mentioned further below, the total mass change over an area like the global ocean is derived by spatial integration. The reduced spatial resolution causes leakage effects: Mass changes in coastal regions cannot be uniquely assigned to either the land side or the ocean side of the coastline. Since hydrological (or glaciological) changes on the land side tend to have larger amplitudes than oceanic mass changes on the ocean side, a buffer zone is typically masked out from the ocean integration kernel (Chambers, 2009). Conversely, for estimating continental water or ice mass changes, a respective buffer zone may be added to the integration kernel.

In the SLBC_cci v2 OMC processing, we use an un-smoothed ocean kernel in order to avoid damping effects from filtering. A 300 km buffer is applied along the ocean margins. Around islands, the buffer is generally active when their surface area is greater than 20,000 km² (2,000 km² for near-polar latitudes >±50°). The integral is subsequently scaled by the ratio between total ocean area (361 million km²) and the integrated area (i.e. total ocean area minus buffer area). The same applies to OMC over the ocean restricted to ±65° in latitude, where we re-scale mass change to the area of the un-buffered ocean between ±65°. For the Arctic Ocean, we re-scale mass change to the un-buffered Arctic Ocean area. Surface areas are given in the OMC files, respectively.

We have rescaled the obtained mass changes from a 300 km leakage-buffered ocean onto a common global ocean area of 3.61e+14 m² .

For comparison, we also include:

		CCI Sea Level Budget Closure
		ESA/ESRIN contract 4000119910/17/I-NB
		Reference: ESA_SLBC_cci_D4.7
		Version: v1.1
		Date: 14.02.2020
		Page: 30 of 101

- Don Chambers' OMC time-series series (Johnson and Chambers 2013, updated) based on CSR, GFZ and JPL spherical-harmonic solutions.

- Goddard Space Flight Center (GSFC) Mascons solutions v02.4 (Luthcke et al. 2013), dedicated for ocean mass research; data source: https://earth.gsfc.nasa.gov/geo/data/grace-mascons. Time series of total ocean mass change were derived within SLBC_cci by the weighted integral over all oceanic points using the ocean-land point-set mask provided with the GSFC Mascon solutions. We strictly used the area information provided with the GSFC data set and rescaled the resulting mass change to a standard ocean surface as used within SLBC_cci.

AOD Restore issues. Modelled short-term atmospheric and oceanic mass variations (AOD products) are accounted for within the gravity field estimation procedure (Flechtner et al., 2014; Dobslaw et al., 2013) and are not included in the monthly solutions. To retain the full mass variation effect, the respective monthly averages of the AOD fields need to be added back to the monthly solutions. The GAD products (Flechtner et al., 2014) contain the sum of atmospheric surface pressure effects and ocean mass effects over the ocean domain and are advised for use for comparisons with ocean bottom pressure observations. Different options of restoring mass variations in the oceanic domain exist for different oceanic applications of GRACE (compare section "De-aliasing products and ocean-only mascons" in the GSFC mascon description at https://earth.gsfc.nasa.gov/geo/data/grace-mascons). The SLBC_cci v2 OMC time-series processed from CSR-, GFZ-, JPL- and ITSG-data have the GAD product restored and the spatial mean of atmospheric surface pressure over the full ocean removed. Our investigations showed that calculating the GAD averages only over the buffered area (that is, excluding the 300 km zone) would lead to OMC trends that are on the order of 0.3 mm/yr higher than for our preferred approach. Similar findings are reported by Uebbing et al. (2019).

Degree 1 and C20. GRACE is insensitive to surface mass displacement components of SH degree one (mass exchange between hemispheres). We implemented the approach proposed by Swenson et al. (2008) and further developed by Bergmann-Wolf et al. (2014) and calculated the degree-one components by combining the GRACE solutions for degree n≥2 with assumptions on the ocean mass redistribution. GRACE has also a reduced sensitivity to the C_{20} component of the gravity field (dynamic flattening term). Therefore, GRACE-based C_{20} components are commonly replaced by results from satellite laser ranging (Cheng et al. 2013, https://podaac-tools.jpl.nasa.gov/drive/files/allData/grace/docs/TN-11_C20_SLR.txt) and this approach was adopted within SLBC_cci.

GIA correction. Mass redistribution processes in the Earth interior, such as glacial isostatic adjustment (GIA) cannot be subsumed in the concept of surface load changes. Therefore, they need to be corrected prior to the conversion of gravity field changes to surface mass changes. This is usually done by using results from geophysical modelling. We corrected for GIA using three different GIA modelling results:

   a) A et al. (2013), based on ICE-5Gv2 glaciation history from Peltier (2004),

		CCI Sea Level Budget Closure
		ESA/ESRIN contract 4000119910/17/I-NB
		Reference: ESA_SLBC_cci_D4.7
		Version: v1.1
		Date: 14.02.2020
		Page: 31 of 101

b) Peltier et al. (2015, ICE-6G_C, VM5a) and

c) Caron et al. (2018).

We also provide OMC time-series without GIA effect correction applied as a supplementary product. The preferred GIA correction for our GRACE-based OMC is the one according to Caron et al. (2018). It is based on the ICE-6G deglaciation history (Peltier et al. 2015), while the model by A et al. (2013) is based on its predecessor model ICE-5G. Furthermore, while the models by A et al. (2013) and Peltier et al. (2015) are single GIA models, the solution by Caron et al. (2018) arises from a large ensemble of models, where the glaciation history and the solid Earth rheology have been varied and tested against independent geodetic data to provide probabilistic information. Using this probabilistic information, Caron et al. (2018) calculated a weighted mean of the individual GIA models.

4.3.2 Products

Ocean mass change

Integrated OMC time series were generated within SLBC_cci for the 4 series of SH GRACE solutions, 3 GIA corrections (and the option of no GIA correction), and 3 different integration domains as specified above. For comparison, the integrated GSFC Mascon-based OMC time series and the time series according to Johnson and Chambers (2013, updated) were also used.

Table 4.3.1 shows global OMC trends for different choices of input SH GRACE solutions and GIA corrections and compares them with the trends from external OMC products. Figure 4.3.1 shows respective time series of OMC.

Supplementary gridded products were generated based on the ITSG-Grace2018 SH solutions, including unfiltered and filtered versions. However, the preferred products in a gridded representation were those based on the GSFC-Mascons solutions.

Continental mass change

By adaptation of the methodology outlined in Section 4.3.1, integrated mass changes over all land areas (excluding Antarctica and Greenland) were derived from GRACE SH solutions and provided as monthly time series.

		CCI Sea Level Budget Closure
		ESA/ESRIN contract 4000119910/17/I-NB
		Reference: ESA_SLBC_cci_D4.7
		Version: v1.1
		Date: 14.02.2020
		Page: 32 of 101

Table 4.3.1: OMC trends over 01/2003–08/2016 [mm/yr w.e.] from different GRACE solutions and different GIA corrections. The first four lines of data show results from different SH solution series generated within SLBC_cci. The last two lines show external products, namely the ensemble mean from Chambers' OMC time series and the GSFC mascon solution. Each column uses different GIA corrections as indicated in the header line. The preferred solution is printed in bold font.

	GIA from A et al. (2013)	GIA from Peltier et al. (2015)	**GIA from Caron et al. (2018)**
ITSG-Grace2018	1.99 ±0.22	1.93 ±0.22	**2.19 ±0.22**
CSR RL06 sh60	1.97 ±0.22	1.91 ±0.22	2.17 ±0.22
GFZ RL06 sh60	1.90 ±0.22	1.84 ±0.22	2.10 ±0.22
JPL RL06 sh60	1.99 ±0.22	1.93 ±0.22	2.19 ±0.22
Chambers ensemble	2.17 ± n/a	n/a	n/a
GSFC v2.4 SLA mascons	2.25 ± n/a	n/a	n/a
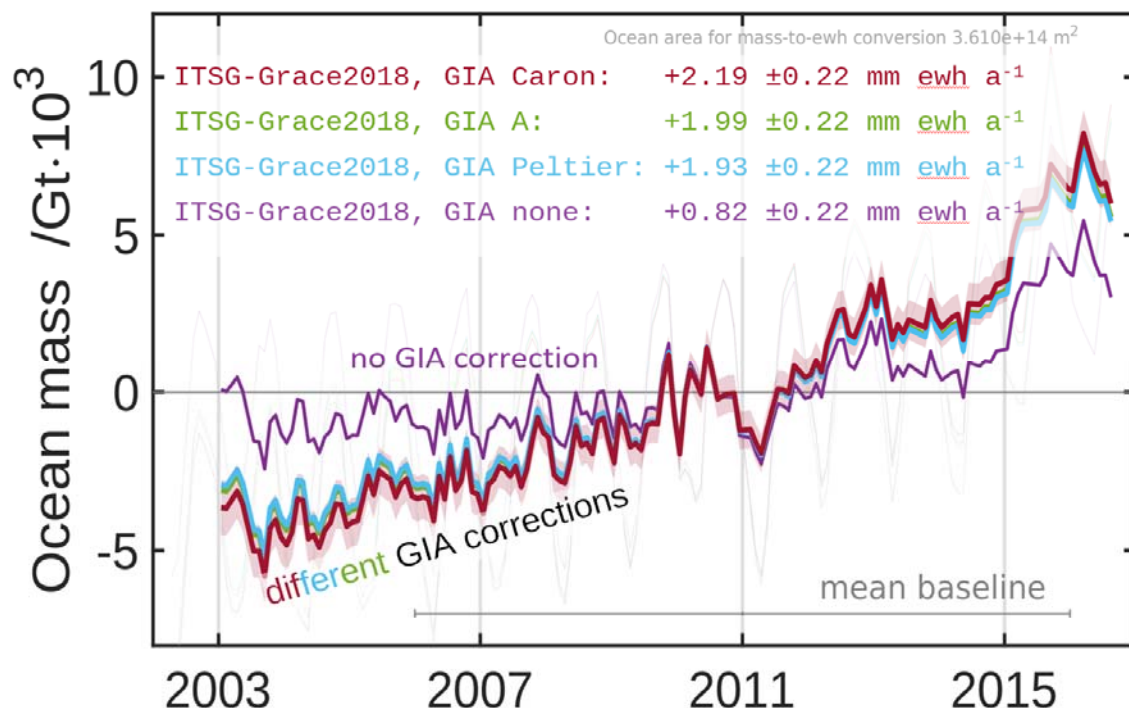
Figure 4.3.1: GRACE global ocean mass change (OMC) derived from the ITSG-Grace2018 solution with different GIA corrections applied. The 1-sigma uncertainty band is shown in red shade for the solution with GIA correction after Caron et al. (2018). All curves are plotted with respect to the Jan 2006 to Dec 2015 mean ('baseline'). For the bold curves we removed the annual and semi-annual cycle by subtracting the respective sine and cosine content of a multi-parameter adjustment from the original data (shown in faint colours in the background).

		CCI Sea Level Budget Closure
		ESA/ESRIN contract 4000119910/17/I-NB
esa	(university logos)	Reference: ESA_SLBC_cci_D4.7
		Version: v1.1
		Date: 14.02.2020
		Page: 33 of 101

4.3.3 Uncertainty assessment

The following sources of uncertainty are important

- GRACE errors: Errors in the GRACE observations as well as in the modelling assumptions applied during GRACE processing propagate into GRACE results.

- Errors in C_{20} and Degree-1 terms: Errors in these components, due to their very large scale nature and possible systematic effects are particularly important for global ocean mass change applications (cf. Quinn and Ponte, 2010; Blazquez et al. 2018).

- GIA is a significant source of signal and error for mass change estimates. Current models show strong discrepancies, and errors may be correlated to GIA-based errors of altimetric GMSL changes and GRACE based ice sheet mass changes (Quinn and Ponte, 2010; Chambers et al., 2010; Tamisiea, 2011; Rietbroek et al., 2016; , Blazquez et al. 2018).

- Leakage errors arise from the vanishing sensitivity of GRACE to small spatial scales (high SH degrees). In SLBC_cci, GRACE data were therefore used only up to a degree 60 (~333 km half-wavelength). Then, signal from the continents (e.g. ice-mass loss) leaks into areas over the ocean. Differences in methods to avoid (or repair) leakage effects can amount to a several tenths of mm w.e./yr in regional OMC estimates (e.g. Kusche et al., 2016). To mitigate such leakage, we apply an ocean kernel that 'buffers' out the closest 300 km surrounding continents. However, the buffering does not fully avoid leakage and requires a subsequent upscaling of the integrated mass changes to the full ocean area, based on the assumption that the mean EWH change in the buffer is equal to the mean EWH change in the buffered ocean area.

- Other sources of uncertainties include the correction for rotational feedback effects (polar tides) to long-term mass re-distributions, and corrections for atmospheric mass variations.

We separate the error into two components distinguished by their temporal characteristics:

- noise, considered temporally uncorrelated, with equal variance for each month
- systematic errors of the linear trend.

We note that this treatment simplifies the situation by not considering autocorrelated errors other than errors that evolve linearly with time.

The uncertainty per epoch in a time series of mass change $m(t)-m(t_0)$ with respect to a reference time t_0 then arises from the combination of the two components of uncertainties in the form

$$\sigma^2_{total}(t) = \sigma^2_{noise}(t) + (\sigma_{trend}*(t-t_0))^2. \qquad (4.3.1)$$

The noise is assumed to be temporally uncorrelated and of same variance for every month. It is assessed from the GRACE OMC time series themselves. The de-trended and de-seasonalized

		CCI Sea Level Budget Closure
		ESA/ESRIN contract 4000119910/17/I-NB
		Reference: ESA_SLBC_cci_D4.7
		Version: v1.1
		Date: 14.02.2020
		Page: 34 of 101

Table 4.3.2: Assessed uncertainty components for the SH-based OMC solutions.

Uncertainty component	global ocean domain	ocean domain 65°S -- 65^N	Ocean domain North of 65°N
Noise	**1.65 mm**	**1.77mm**	**20.91mm**
Trend uncertainty Degree 1	0.14 mm/yr	0.14 mm/yr	1.23 mm/yr
Trend uncertainty C20	0.05 mm/yr	0.07 mm/yr	0.67 mm/yr
Trend uncertainty GIA	0.14 mm/yr	0.17 mm/yr	0.49 mm/yr
Trend uncertainty leakage	0.10 mm/yr	0.09 mm/yr	0.48 mm/yr
Trend uncertainty combined	**0.22 mm/yr**	**0.25 mm/yr**	**1.56 mm/yr**

time series are high-pass filtered in the temporal domain. The variance of the filtered time series is assumed to be dominated by noise. This variance is scaled by a factor that accounts for the dampening of uncorrelated noise variance imposed by the high-pass filtering. The assessed noise component of the uncertainty comprises uncorrelated errors from all sources listed above, except for GIA which is considered purely linear in time.

The systematic errors of the linear trends are assumed to originate from the sources Degree-1, C20, GIA, and leakage. The related uncertainties are assessed for each source individually. They are then summed in quadrature. The analysis of systematic errors of the linear trends follows the approach as described by Nagler et al. (2018b) for the ESA CCI Antarctica project with GRACE Mass Balance derived changes over Antarctica.

For example, our GIA correction choses one GIA model out of a small sample of possible GIA model options. The uncertainty assessment is based on this small sample of GIA correction options. The standard deviation of the sample of options is taken as the standard uncertainty of the GIA correction. Note that this is not the same as trying to determine the uncertainty of the mean value, or expectation value, of all GIA correction options. We do not assume such an expectation value to represent the truth. The same approach as described for GIA is applied for the Degree-one uncertainty and for the C20 uncertainty.

To estimate the error that arises from leakage, in conjunction with buffering and rescaling, we performed a simulation study based on synthetic mass change data from the ESA Earth System Model (ESM; Dobslaw et al., 2015). The ESM data was processed according to the settings of the SLBC_cci OMC analysis (pseudo-observed) and compared with the full-resolution ESM data (pseudo-true) over the identical target area and time. The weighted RMS of misfits between pseudo-observed and pseudo-true OMC trends for a set of different 9–12 years long time frames was taken as the estimate of the leakage error uncertainty.

Results of the trend uncertainty assessment for the ITSG-2018-based OMC solutions are summarized in Table 4.3.2.

		CCI Sea Level Budget Closure
		ESA/ESRIN contract 4000119910/17/I-NB
		Reference: ESA_SLBC_cci_D4.7
		Version: v1.1
		Date: 14.02.2020
		Page: 35 of 101

4.4 Glacier contribution

4.4.1 Methods

The objective of model-based estimates of glacier mass change is to complement observations of glaciers with observations of the state of the atmosphere and physical understanding of glacier mass balance. While there is a growing number of glacier models being developed and used for projecting future glacier change, there is currently only one that allows to reconstruct past and reproduce current glacier change on the global scale, while also accounting for glacier geometry change (Marzeion et al., 2012). We used this model for all calculations. Special constraints such as storage of water in endorheic basins or potential future lakes forming in overdeepenings (e.g. Haeberli and Linsbauer 2013) of currently still ice-covered glacier beds have to be considered separately.

The global glacier model (GGM, Marzeion et al. 2012) requires (1) global glacier outlines, (2) atmospheric boundary conditions, and (3) measured mass balances (for calibration and validation) as an input. These datasets are freely available from the following sites: Glacier outlines are taken from the Randolph Glacier Inventory (RGI) version 6.0 (updated from Pfeffer et al. 2014). Atmospheric boundary conditions were obtained from 7 different global reanalysis products/gridded observational data sets. The model was calibrated and validated using observations of glacier mass balance from the collections of the World Glacier Monitoring Service (WGMS, 2016).

The model uses global fields of temperature and precipitation rates to estimate the glacier mass balance. Changes in glacier geometry are modeled following an area-volume-time scaling approach, enabling the model to account for various feedbacks between glacier geometry and mass balance. Glacier geometries obtained through remote sensing (from the RGI) are used to initialize the model, as well as validate results and obtain uncertainty characteristics. From the time of initialization, the model is run forward by using volume changes obtained from the mass balance module to calculate changes in glacier area, length, and terminus altitude. Glacier changes prior to the time of initialization are obtained using an iterative process: the model is also run forward during the time preceding the initialization. However, to find the correct starting conditions, the model iteratively searches for that state of the glacier at the beginning of the model run, which results in the observed state of the glacier at the time of glacier observation (i.e., at the time the glacier outlines were obtained). A detailed description of the model is found in Marzeion et al. (2012).

The procedure described above was repeated for all seven forcing data sets, as well as their mean, in order to obtain an ensemble estimate of the glacier mass change. Local (i.e., glacier-specific) parameters were re-calibrated and cross-validated following the procedure described in Marzeion et al. (2012). Global parameters were optimized following a multi-objective optimization routine as described below.

		CCI Sea Level Budget Closure
		ESA/ESRIN contract 4000119910/17/I-NB
		Reference: ESA_SLBC_cci_D4.7
		Version: v1.1
		Date: 14.02.2020
		Page: 36 of 101

For each of the eight forcing data sets described above, 900 calibration/cross-validation runs of the model were performed, varying the following global parameters:

1. the air temperature above which melt of the ice surface is assumed to occur;

2. the temperature threshold below which precipitation is assumed to be solid;

3. the vertical precipitation gradient used in the model to capture local precipitation patterns not resolved in the forcing data set;

4. a precipitation multiplication factor used in the model to account for effects from (among other things) wind-blown snow and avalanching, not resolved in the forcing data set.

The model performance of each of these in total 7200 model runs was validated employing a leave-one-glacier-out cross validation routine. The optimal model configuration (i.e., forcing data set and global parameter set) was then chosen based on the assessment of three criteria:

1. the temporal correlation between modeled and observed mass balances, with a higher correlation indicating a generally higher ability of the model to represent observed glacier mass change;

2. the ratio of the temporal variance of modeled and observed mass balances, with a ratio close to one indicating a realistic sensitivity of the model to climate variability and change;

3. the bias (or mean absolute error) of the model, with a bias close to zero indicating a negligible artificial trend in the modeled glacier mass change.

Figure 4.4.1 shows the optimal model run (i.e., results obtained using the optimal parameter set) for each of the eight different atmospheric forcings. It turned out that the model forced by the mean of the seven atmospheric data sets performed best. All the results presented below are thus based on the optimal model run forced by the ensemble mean.

Figure 4.4.2 shows the resulting v2 time series of monthly accumulated glacier contribution in comparison with former v1 and v1 time series.

		CCI Sea Level Budget Closure
		ESA/ESRIN contract 4000119910/17/I-NB
		Reference: ESA_SLBC_cci_D4.7
		Version: v1.1
		Date: 14.02.2020
		Page: 37 of 101
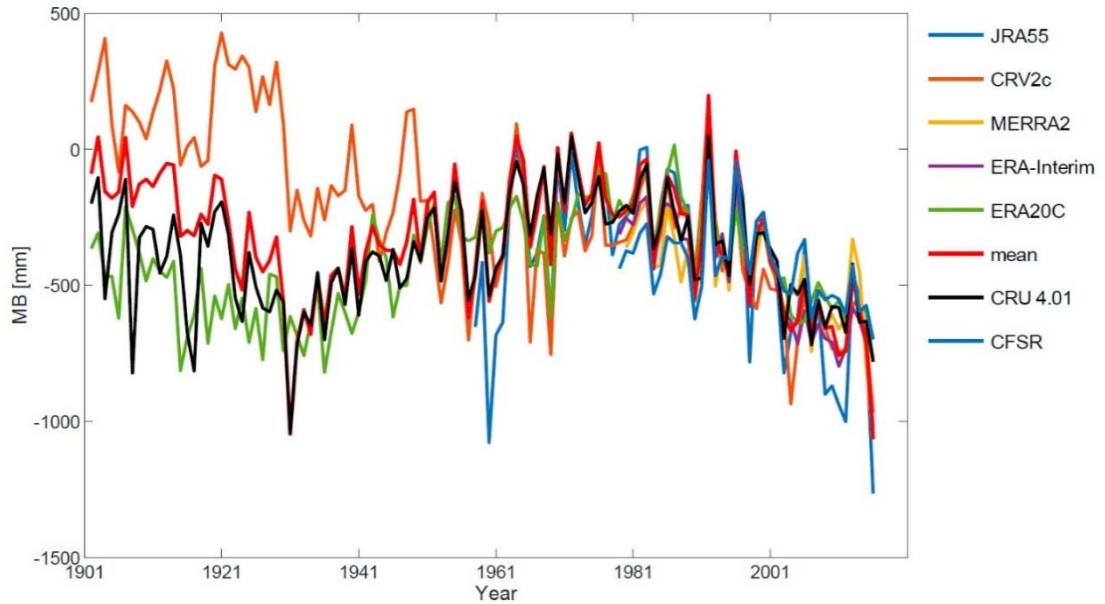
Figure 4.4.1: Ensemble of reconstructed annual global mean glacier mass balance showing the entire period for each of the eight atmospheric forcing data sets. For each atmospheric data set, the results using the optimal parameter set are shown. The mean forcing (red line) corresponds to the v2 data product.
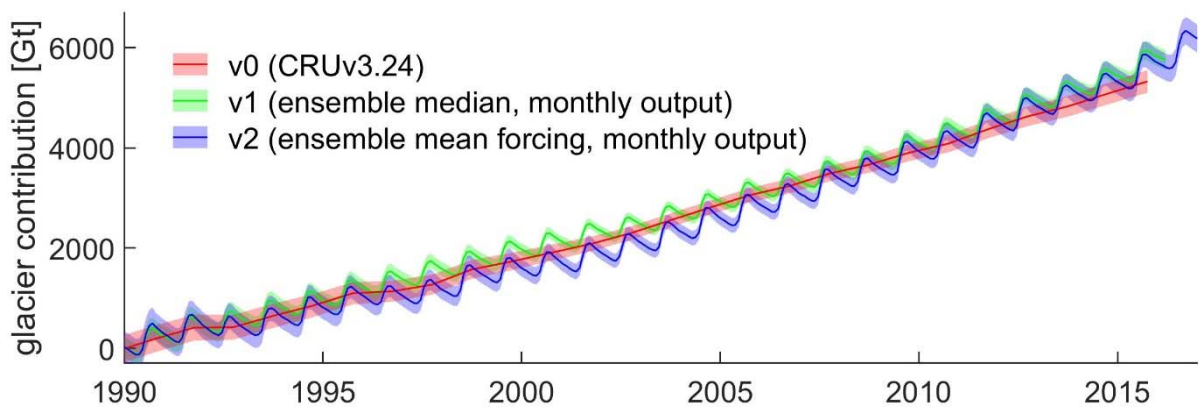
Figure 4.4.2: Comparison of the temporally accumulated contribution of glaciers to sea-level change of data product version 0, version 1, and final version 2.

		CCI Sea Level Budget Closure
		ESA/ESRIN contract 4000119910/17/I-NB
		Reference: ESA_SLBC_cci_D4.7
		Version: v1.1
		Date: 14.02.2020
		Page: 38 of 101

4.4.2 Products

Glacier mass change is calculated in the unit m water equivalent (w.e.) and multiplied with glacier area (in m²) and water density (1000 kg m⁻³) to obtain the mass of water in Gt. This is the temporally accumulated mass contribution of glaciers within each grid cell to sea-level change. Regional or global values of glacier mass change can be obtained by summing over the region of interest.

While the global datasets exclude the Greenland peripheral glaciers, separate datasets for these glaciers are also given. In this way, Greenland peripheral glaciers can be excluded or included in the glacier model assessment, depending on whether they are included or excluded within the Greenland Ice Sheet assessment.

4.4.3 Uncertainty assessment

Uncertainties of glacier mass change are obtained from the cross-validation of the model using annual values. To obtain the monthly values, it is assumed that each month of the mass balance year contributes equally to the annual uncertainty. The uncertainties are accumulated temporally forward and backward from the initialization year of each glacier, and then accumulated spatially for all glaciers contained within each grid cell. The mass change estimate ± this uncertainty indicates the 5th to 95th percentile of the uncertainty band. Regional or global values of the uncertainty are obtained by taking the square root of the sum of the squares of these uncertainties over the region of interest. To convert the given uncertainties to standard uncertainties, the numbers are divided by 1.645. The underlying assumption of a normal distribution of errors is supported by the uncertainty assessment.

The most relevant sources of error are:

1. uncertainty in the initialization data set (i.e., errors in glacier outlines);
2. simplification of physics in the model (concerning both the mass balance module and the simple representation of ice dynamics);
3. uncertainty in the forcing data (i.e., scarce observations of temperature and precipitation near glaciers that impact the aggregated climate data as well as the reanalysis data used),
4. uncertainty in the observations of glacier mass balance used to calibrate the model,
5. uncertainty in the model calibration.

Uncertainties increase forward and backward in time relative to the year of model initialization, which is typically around the year 2000 (but differs for glaciers individually), since then the model's results depend on the modeled rather than observed glacier geometries, which become more uncertain. This increasing uncertainty is included in the error propagation.

The total uncertainty of the resulting glacier mass change estimates is determined using a leave-one-glacier-out cross validation of the glacier model. In this procedure, the out-of-sample uncertainties of the model are measured by:

		CCI Sea Level Budget Closure
		ESA/ESRIN contract 4000119910/17/I-NB
		Reference: ESA_SLBC_cci_D4.7
		Version: v1.1
		Date: 14.02.2020
		Page: 39 of 101

1. calibrating the model based on glacier observations, but withholding from the calibration all observations from one glacier;
2. running the model for that glacier and determine model uncertainty;
3. repeat the above two steps for all glaciers with available mass balance observations.

A total of 255 glaciers with 3997 observed mass balance years were used in this procedure.

As uncertainties in the estimated mass balance feed back to the modeled glacier geometry, these uncertainty estimates were then propagated through the entire model chain, forward and backward in time relative to the year of model initialization. The obtained uncertainty estimates of temporally integrated glacier area and volume change were then validated once more using observations of glacier area and volume change.

Compared to version 0 and the preliminary version 1 of the data product, the final version 2 uses an ensemble approach, particularly to reduce – as far as possible – error source 3 listed above. The glacier-specific model parameters were recalibrated for each of the ensemble members in each of the 7200 optimization runs.

The multi-objective optimization lead to the following changes in uncertainty measures:

1. the temporal correlation between observed and modeled mass balances was increased from 0.60 (v1) to 0.64 (v2);

2. the ratio of the temporal variance of modeled and observed mass balances was improved from 0.83 (v1) to 1.00 (v2);

3. the model bias was changed from 5 mm w.e. (v1) to -4 mm w.e. (v2, both values statistically indistinguishable from zero).

As a result, our confidence in the model results has grown, most critically by the improved capability of the model to accurately represent the observed variability of mass balance of individual glaciers. The model errors are spatially and temporally uncorrelated. While the model results for any given individual glacier are therefore quite uncertain (RMSE of a similar order of magnitude as the typical annual mass balance), the relative error becomes smaller for ensembles of glaciers (e.g. all glaciers within a grid cell, on a mountain range, or globally).

4.5 Ice sheets contribution: Greenland

4.5.1 Methods

GRACE-based estimates

GRACE satellite gravimetry is used to estimate the Greenland Ice Sheet (GIS) mass changes for the interval 2003-2016. The principles of GRACE satellite gravimetry are introduced in

		CCI Sea Level Budget Closure
		ESA/ESRIN contract 4000119910/17/I-NB
		Reference: ESA_SLBC_cci_D4.7
		Version: v1.1
		Date: 14.02.2020
		Page: 40 of 101

Section 4.3. We use the method developed within the Greenland Ice Sheet CCI project and described in the related documents (Khvorostovski et al. 2018, Nagler et al. 2018d).

In brief, the Gravimetric Mass Balance (GMB) product used here applies the direct point mass inversion method for determining the monthly mass changes from the monthly GRACE data. The method is based on Forsberg and Reeh (2007), Sørensen and Forsberg (2010) and Barletta et al. (2013). Prior to the inversion, corrections (prescribed GIA, C20 and degree one) and filtering (KK3 from Kusche et al., 2009) are applied to the GRACE data.

Altimetry-based estimates

Satellite radar altimetry is used to derive elevation changes of the GIS for the given time period. The elevation changes are interpolated to cover the entire ice sheet. The elevation changes are corrected for any elevation change signal that is not associated with ice mass loss (GIA, elastic uplift and changes in firn compaction), by calibrating the radar mass change series by the observations from ICESat.

The v2 data set described here is the annual mean mass loss for the GIS in the period of ESA radar altimetry (1992-2017). The data are calibrated using the 2003-2009 data from ICESat laser altimetry and snow/firn modelling to both account for firn changes and radar penetration. The combined radar volume change data-series is published in Simonsen and Sørensen (2017) and Sørensen et al. (2018).

The mass change estimate is derived in a three-step procedure:

1) The coverage of the radar altimetry is limited to ice sheets slopes less than 1.5 degrees. To estimate the volume change of the entire GIS, the volume change is extrapolated using nearest-neighbor interpolation. This will underestimate the volume change in the fast losing areas for GIS and is in need of calibration.

2) Following the methodology of Sørensen et al. (2011) the volume change is converted into mass change by the appropriate density.

3) As the radar volume shown in Figure 4.5.1, is not accounting for the correction terms given above and the radar also are biased by changing scattering horizon in the firn column (Nilsson et al., 2015) it was decided to account for all of the terms at once by calibrating the mass change rate during the ICESat era.

4.5.2 Products

GRACE-based estimates

The v2 data set is the time series of mass changes of the GIS derived from GRACE data. The product is publicly available as one of the ECVs of the Greenland Ice Sheet CCI, and hence is described in depth in the various documents (deliverables) of this programme. The summary here is based on the reference documents from the Greenland Ice Sheet CCI.

		CCI Sea Level Budget Closure
		ESA/ESRIN contract 4000119910/17/I-NB
ESA logo	University logos	Reference: ESA_SLBC_cci_D4.7
		Version: v1.1
		Date: 14.02.2020
		Page: 41 of 101

The GRACE-derived time series for Greenland is available for free download at http://products.esa-icesheets-cci.org/products/downloadlist/GMB/ (Sørensen et al., 2017).

The v2 data makes use of the CSR_RL06 SH GRACE solutions.

Ice mass changes for the entire ice sheet and for the single basins are estimated and provided. The drainage basins used are an aggregation of those described by Zwally et al. (2012). The mass change is the mass anomaly in Gt (relative to a chosen zero level) with the associated errors (see Forsberg et al., 2013).

The time series for the entire ice sheet is constructed so that the estimate also includes the signal from outlying Glaciers and ice caps, while the individual basin estimates are derived in a way that aims at leaving those out of the solution. Therefore, there is a difference between the mass balance derived from the total time series and the sum of the individual basins. For further information on how ice sheet and the surrounding glaciers and ice caps are separated see Khvorostovsky et al. (2016).

Altimetry-based estimates

The v2 product consists in a grid of mass change rates at 100x100 km² resolution. Figure 4.5.1 shows the resulting mass change estimate for the main Greenland Ice Sheet, excluding weakly-connected ice and peripheral glaciers.

The spatial coverage for the yearly mass change rates is the entire ice sheet with a resolution of 100x100 km². The temporal coverage is from 1992 to 2017.
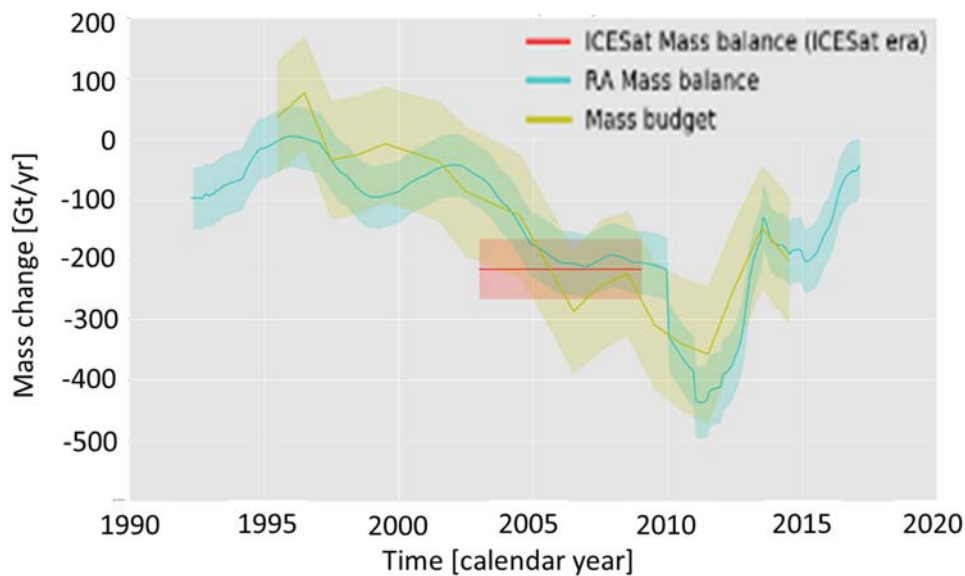
Figure 4.5.1: GrIS volume change estimates from radar altimetry have been converted into mass by scaling to a known mass change field. Here, the "known" field is based on the laser altimetry mass change (Sørensen et al., 2011) (in red). The yellow line indicates an independent mass balance estimate from the bass budget method (Colgan et al., 2019).

		CCI Sea Level Budget Closure
		ESA/ESRIN contract 4000119910/17/I-NB
		Reference: ESA_SLBC_cci_D4.7
		Version: v1.1
		Date: 14.02.2020
		Page: 42 of 101

4.5.3 Uncertainty assessment

GRACE-based estimates

The error characterization of the GRACE product is provided in detail in Forsberg et al. (2013). Errors in GRACE-derived mass changes have several origins. The three major contributions arise from:

1. GRACE errors in the monthly solutions,
2. Leakage errors due to the limited spatial resolution achieved by GRACE,
3. Errors in models used to reduce superimposed mass signals.

We derive the uncertainties which are related to the data errors provided directly with the GRACE monthly models by using a Monte-Carlo-like approach in which 200 simulations are performed. The simulations are created from Stokes coefficients drawn from normal distributions with zero mean, and the standard deviation provided with the GRACE level-2 data.

In order to give an estimate at basin scale of the effect of the outer glaciers leakage effect, we compute two solutions which represent an upper and lower bound for the mass loss and find that this leakage error is between 4% and 10% of the mass trend.

The GIA error is meaningful only for the linear trends in mass changes. For the entire GIS we used the value in Barletta et al. (2013). For our best value we chose to use the A et al. (2013) model, which is an ICE5g-VM2 compressible model with rotational feedback. This GIA contribution for Greenland is -5.4 Gt/yr and the uncertainty is up to ± 7.2 Gt/yr. Note that the GIA contribution is not included in the submitted v1 and final version.

Altimetry-based estimates

The sources of errors are

1. Uncertainty in the interpolation of elevation change point estimates into volume change,
2. error in the firn compaction,
3. error in bedrock movement,
4. error from neglecting basal melt and possible ice build-up above the Equilibrium Line Altitude (ELA).
(5.) Radar altimetry has in addition an error source from changing radar penetration of the firn column.

Following the error sources above the uncertainty is given as a conservative estimate based on converting the radar altimetry volume error into mass by ascribing ice densities to all grid cells. This estimate is assumed to be slightly overestimating the combined error of the five error sources, however as seen in Figure 4.5.1, the estimated uncertainty reconciles the radar altimetry mass balance with the GRACE estimate.

		CCI Sea Level Budget Closure
		ESA/ESRIN contract 4000119910/17/I-NB
		Reference: ESA_SLBC_cci_D4.7
		Version: v1.1
		Date: 14.02.2020
		Page: 43 of 101

4.5.4 Global sea level fingerprints based on mass contributions from continental ice mass change and land water change

As part of the Greenland Ice Sheet sub-WP, prototype calculations of global sea level fingerprints were calculated from the linear trends of all ocean mass contributions, namely glaciers, the two ice sheets, and land water storage. The initial results shown here are relevant for possible follow-on studies with more focus on the geographic patterns of sea level change.

Mass redistribution between continents and the global ocean lead to (a) vertical deformations of the ocean bottom and (b) changes of the geoid. In result of the two effects, changes of the height of the ocean water column (that is, of relative sea level) are not uniform. Their geographic patterns are called sea level fingerprints. Here, only the effect of present-day mass redistributions (that is, no GIA) was considered. The calculation of these patterns do not account for changes in ocean dynamics or steric changes, which are an additional source of non-uniformity of relative sea level change.

Figure 4.5.2 shows the relative sea level fingerprints calculated from the four different sources of land ice / land water change.

4.6 Ice sheets contribution: Antarctica

4.6.1 Methods

GRACE-based estimates

GRACE satellite gravimetry is used to estimate the Antarctic Ice Sheet (AIS) mass changes for the interval 2003-2016. The principles of GRACE satellite gravimetry are introduced in Section 4.3. We use the method developed within the Antarctic Ice Sheet CCI project and described in the related documents (Nagler et al. 2018a,b, Thorvaldsen et al. 2018).

The AIS GMB products are derived from the spherical harmonic monthly solution series by ITSG-Grace2016 by TU Graz (Klinger et al., 2016; Mayer-Gürr et al., 2016) following a regional integration approach with tailored integration kernels that account for both the GRACE error structure and the information on different signal variance levels on the ice sheet and on the ocean (Horwath and Groh, 2016).

Altimetry-based estimates

The data set described here is the time series of ice mass loss for the East Antarctic Ice Sheet (EAIS), the West Antarctic Ice Sheet (WAIS) and the Antarctic Peninsula (AP) for the time period 1992-2016 derived from radar altimetry and a time evolving ice density mask. Details are published in the Antarctic Ice Sheet CCI documents (Nagler et al. 2018a,b, Thorvaldsen et al. 2018) and in the journal publications by Shepherd et al. (2019) and McMillan et al. (2014).

		CCI Sea Level Budget Closure
		ESA/ESRIN contract 4000119910/17/I-NB
esa	TECHNISCHE UNIVERSITÄT DRESDEN / Universität Zürich / UNIVERSITY OF LEEDS / LEGOS / Universität Bremen / GOETHE UNIVERSITÄT FRANKFURT AM MAIN / DTU Space National Space Institute / University of Reading / MERCATOR OCEAN INTERNATIONAL	Reference: ESA_SLBC_cci_D4.7
		Version: v1.1
		Date: 14.02.2020
		Page: 44 of 101

Figure 4.5.2: Relative sea level fingerprints calculated from the geographic patterns of mass trend in (a) the global glaciers without Greenland and Antarctica, (b) Greenland ice masses, (b) Antarctic ice masses, (d) Land water storage changes.

	CCI Sea Level Budget Closure
	ESA/ESRIN contract 4000119910/17/I-NB
	Reference: ESA_SLBC_cci_D4.7
	Version: v1.1
	Date: 14.02.2020
	Page: 45 of 101

The mass change time series is derived from surface elevation change generated by processing Level 2 elevation measurements provided by ESA, and acquired by multiple radar altimetry satellite missions, ERS-1, ERS-2, ENVISAT and CryoSat-2.

The algorithm for elevation changes is described in the Antarctic Ice Sheet Climate Change Initiative (AIS_CCI) Algorithm Theoretical Basis Document (ATBD) (Nagler et al., 2018a) and is summarized here.

Elevation change method. Several methods for deriving elevation changes from repeat radar altimetry exist. Here, we have employed the plane fit method (McMillan et al., 2014). The plane fit method is an adaption of the along track method which can be applied to satellites which operate in both short 27-35 day orbit repeat periods (such as the main operational periods of Envisat, ERS-1,2 and Sentinel-3A,B) and long 369 day repeat periods where measurements do not exactly repeat within monthly time scales such as CryoSat-2.

The plane fit method grids both ascending and descending measurements in a regular polar stereographic grid instead of gridding separately along track. It derives a surface elevation change estimate at the center of each grid cell by applying a surface model to the measurements within that cell and has been shown in the CCI round robin experiments to perform as well or better than other along track methods for all missions (except Envisat's drifting phase from Oct 2010- Apr 2012, where special techniques are required for all methods) and hence is the primary along track method chosen for the Antarctic CCI. Another advantage of the plane fit method is that surface elevation change (SEC) results are produced on the same grid as the SEC output product and hence do not require re-gridding which can introduce an additional error and reduce accuracy.

Correction for Glacial Isostatic Adjustment. A post-glacial rebound (PGR) correction was applied to all the residual heights in each selected cell. The correction used was the IJ05_R2 correction, from Ivins et al (2013).

Treatment of unobserved areas. New methods of estimating the SEC of the unobserved regions of the ice sheets have been developed, both between satellite's ground tracks and beyond the latitude limits of the satellite's orbit.

- Polar hole filling: beyond the orbit limits, SEC is estimated from an annular region, 80°S-81°S. Most drainage basins within that region are treated together but Zwally basin 18 is a special case: its snow area is treated separately, and its ice area, which includes the Kamb Ice Stream, is used to estimate all unobserved ice, since the unobserved ice area is continuous.

- Between-tracks: the between-track estimates are based on spatially-limited triangulation, followed by a velocity-guided interpolation (using BISICLES) on the ice sheet margins, i.e. within 100km of the coast, and mean estimates elsewhere

Derivation of Height Time Series. Time series calculations used the *dz* and *dt* values retained after the model-fitting stage and aggregated in 140-day epochs, which were only calculated for

		CCI Sea Level Budget Closure
		ESA/ESRIN contract 4000119910/17/I-NB
		Reference: ESA_SLBC_cci_D4.7
		Version: v1.1
		Date: 14.02.2020
		Page: 46 of 101

grid cells that were observed by satellite. Time series can be calculated over any region. In each case, unobserved grid cells had to be filled.

Inter-Mission Cross Calibration. The previous calculations produced a time series of changes in height per mission. To produce a continuous dataset, biases had to be added between missions. The biasing method used is applied to each grid cell individually, which is known as pixel cross-calibration. In each case, the biasing aimed to bring ERS1, ERS2 and CryoSat-2 data onto the same baseline as the Envisat data.

Conversion from Volume to Mass. As radar altimeters penetrate some (unknown) depth into the snow surface, direct application of a firn correction to the elevation change measurement, and then derivation of mass at the density of ice from the residual signal, has known issues in Antarctica. Therefore, we use a time-evolving density mask to delimit the region where we convert volume to mass at the density of snow (350kg/m³) and ice (917kg/m³). To derive mass change, grid cells are identified as containing changing amounts of either snow or ice, using a time-dependent density mask. In this study, the density mask was derived from the pixel cross-calibrated time series and the Berkeley Ice Sheet Initiative for Climate Extremes (BISICLES) ice velocity map (Cornford et al, 2013).

Down sampling of mass change time series at annual temporal resolution. The mass change time series is provided with an epoch of 140 day and we additionally provide the mass change time series at annual temporal resolution. The annual estimates are computed by taking the total accumulation at the end of each year from the 140 day time series.

4.6.2 Products

GRACE-based estimates

The v2 data set is the time series of mass changes of the AIS derived from GRACE data. The product is publicly available as one of the ECVs of the Antarctic Ice Sheet CCI, and hence is described in depth in the various documents of this project (Nagler et al. 2018a,b). Mass change time series are provided for a number of drainage basins, based on the boundary definitions by Zwally et al. (2012). They describe the evolution of ice mass relative to a modelled reference value. This reference value is defined to be the GRACE-derived mass as of 2009-01-01. Respective time series are also derived for the total areas of the WAIS, the EAIS, the AP and the AIS as a whole.

The gridded changes are given in millimetres of equivalent water height (mm w.e., or kg/m²). The applied algorithm is consistent with the one used for the GMB Basin Product.

Altimetry-based estimates

We provide mass change time series for the WAIS, the EAIS, the AP, and for the AIS as a whole. The data product contains information on time, cumulative mass balance, and the measurement uncertainty respectively. Figure 4.6.1 shows the resulting mass change estimate

		CCI Sea Level Budget Closure
	TECHNISCHE UNIVERSITÄT DRESDEN · Universität Zürich · UNIVERSITY OF LEEDS · LEGOS · Universität Bremen · GOETHE UNIVERSITÄT FRANKFURT AM MAIN · DTU Space National Space Institute · University of Reading · MERCATOR OCEAN INTERNATIONAL	**ESA/ESRIN contract 4000119910/17/I-NB**
		Reference: ESA_SLBC_cci_D4.7
		Version: v1.1
		Date: 14.02.2020
		Page: 47 of 101

for the Antarctic ice sheet. The time series span the interval 1992 to 2017. They are provided with two temporal resolutions, namely with an epoch of 140 days and with annual values.

### 4.6.3 Uncertainty assessment

GRACE-based estimates

The uncertainty assessment follows a strategy similar to the one outlined in Section 4.3.3. It is described in detail in the Antarctic Ice Sheet CCI CECR (Nagler et al., 2018b). Dominant sources of uncertainty are the GIA uncertainty and the uncertainty associated to the degree-one components and the C_{20} component of the gravity field. The combined trend uncertainty amounts to 38 Gt/yr.

Altimetry-based estimates

In the datasets delivered (140-day epoch and 1-yr epoch), the error estimates are cumulative estimates referenced at the start of the time series in 1992. We also provide estimates of the non-cumulative error for both the 140-day and 1-yr epoch datasets.

The uncertainty in mass change is estimated by summing in quadrature the uncertainty associated with our elevation change measurements (taking into account systematic errors, time-varying errors and errors associated with the calculation of inter-satellite biases) and the snowfall variability uncertainty to account for the additional error associated to the identification of ice dynamical imbalance. The total uncertainty is then converted to an equivalent mass change with the density of ice (917 kg m^{-3}) or snow (250 kg m^{-3}) based on our map of ice dynamic imbalance areas.

The uncertainty is provided in the data product per epoch as the standard uncertainty of cumulated mass change and as the standard uncertainty of uncumulated mass change.
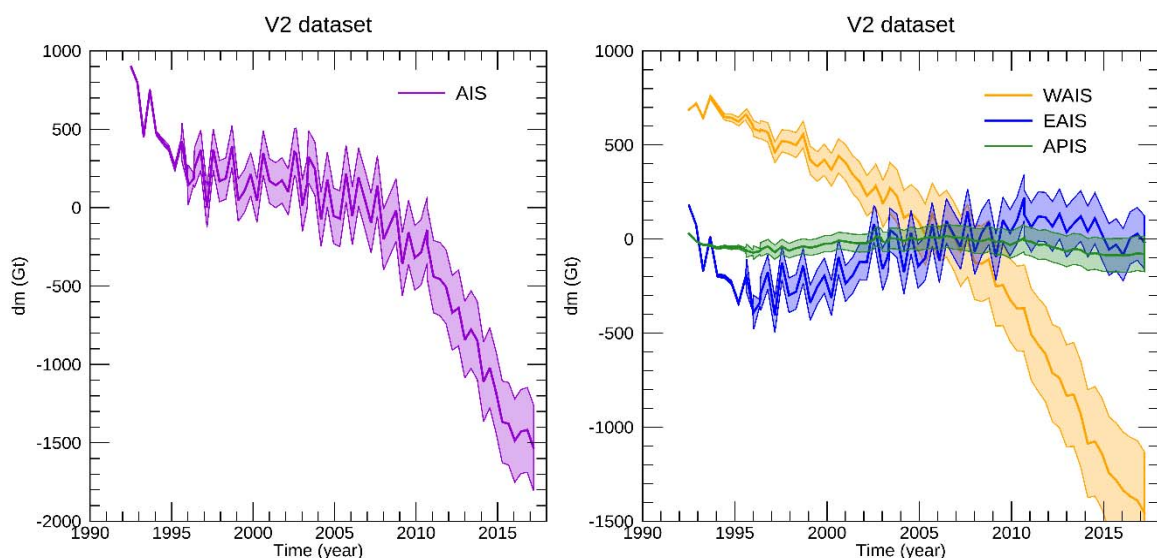
Figure 4.6.1: Antarctic Ice sheet mass change time series derived from radar altimetry by CPOM Leeds

		CCI Sea Level Budget Closure
		ESA/ESRIN contract 4000119910/17/I-NB
		Reference: ESA_SLBC_cci_D4.7
		Version: v1.1
		Date: 14.02.2020
		Page: 48 of 101

4.7 Land water contribution

4.7.1 Methods

Global and gridded time series of total land water storage (TWS) were obtained with the WaterGAP Global Hydrology Model (WGHM), which is applied and developed at the Institute of Physical Geography of the Goethe-University of Frankfurt (GUF). Within the SLBC_cci project, several model enhancements were implemented, which lead from the WaterGAP2.2b version used for SLBC_cci v0 through the WaterGAP2.2c version used for SLBC_cci v1 to the final WaterGAP2.2d version used for SLBC_cci v2.

WGHM (Müller Schmied et al., 2014) computes total land water storage by accounting for the water in the canopy, snow , soil , groundwater and surface water body (wetlands, rivers, lakes and man-made reservoirs) storage compartments. Regarding human water use, initially time series of water abstraction and consumptive water use are computed by separate water use models for five water use sectors (irrigation, livestock farming, domestic use, manufacturing industries and cooling of thermal power plants). Subsequently, these time series are translated into net abstraction (total abstraction minus return flow) by the sub-model GWSWUSE, which distinguishes the source of abstracted water (surface water or groundwater). The net abstraction time series are then subtracted from the surface water and groundwater storage compartments of WGHM, respectively (Müller Schmied et al. 2014; Döll et al. 2014). From SLBC_cci v0 to SLBC_cci v1, model enhancements related to the reservoir operation algorithm and to the estimation of groundwater depletion were implemented.

In WaterGAP2.2b, the commissioning year of each reservoir had not yet been included; this means that all reservoirs were assumed to always have existed, which did not allow for the model to simulate the filling phase upon reservoir construction. For v1, the information on the first operational year was included for each individual reservoir. This model enhancement also led to the revision of the assumptions previously underlying the treatment of reservoirs (Döll et al. 2009).

Groundwater depletion (GWD) is often observed in regions with a very high water demand that is mainly satisfied by groundwater water withdrawals. Globally, irrigation is by far the most consumptive water use sector. Assumptions regarding irrigation water use are an important source of uncertainty when estimating GWD in these regions. Using WaterGAP 2.2a, Döll et al. (2014) concluded that assuming that farmers irrigate at approximately 70% of the optimal rate resulted in improved results as compared to independent estimates in GWD regions.

WaterGAP 2.2c was run under the two following irrigation assumptions with three climate forcings, in order to assess the impact of irrigation water use on groundwater storage (GWS) variations:

		CCI Sea Level Budget Closure
	TECHNISCHE UNIVERSITÄT DRESDEN / Universität Zürich / UNIVERSITY OF LEEDS / LEGOS / Universität Bremen / GOETHE UNIVERSITÄT FRANKFURT AM MAIN / DTU Space National Space Institute / University of Reading / MERCATOR OCEAN INTERNATIONAL	**ESA/ESRIN contract 4000119910/17/I-NB**
esa		Reference: ESA_SLBC_cci_D4.7
		Version: v1.1
		Date: 14.02.2020
		Page: 49 of 101

- Farmers irrigate at 70% of the optimal rate in GWD regions and at optimal rate (100%) in non-GWD regions (hereafter "70% deficit irrigation" variant) (for more details, see Döll et al., 2014)

- Farmers irrigate at optimal rate worldwide (hereafter "optimal irrigation" variant) (for more details, see Döll et al., 2014)

Global GWD trends are considerably stronger under optimal irrigation for all forcings. This reflects larger irrigation abstractions under this variant, which results in higher groundwater mass losses. Differences in global trends due to different forcings are smaller, except during 2003-2013. On the other hand, these differences can be considerable in terms of inter-annual variability.

The results of comparisons with independent observational data were not conclusive as to which irrigation variant provides better results for WaterGAP 2.2c at regional scale. For instance, in the High Plains aquifer, simulated GWD is closer to independent estimates under 70% deficit irrigation, whereas in the Central Valley a better fit is found for all three forcings under optimal irrigation. Concerning the impact of using different climate forcings at regional scale, the conclusions differ depending on the case considered. For example, in the North China Plain (NCP), the impact is low, whereas in the Gulf coastal plain it is rather large.

Comparisons with independent data also indicated that the WaterGap 2.2b version highly overestimates GWD trends in the NCP and underestimates GWD in the Gulf coastal plain, which is mainly due to an underestimation (and overestimation, respectively) of groundwater recharge in these regions. Based on these results, two parameters, namely the runoff coefficient and the fraction of runoff recharging the aquifer, were optimized at regional scale in order to improve the model's performance. Despite the adjustments performed for the NCP and the Gulf coastal plain, there remain several regions for which the model still performs poorly (e.g. Atlantic coastal plain).

From v1 to v2 (WaterGAP2.2c to WaterGAP2.2d), a series of model enhancements were conducted:

- Integration of historic development of irrigated grid cells (1900-2005)
- New standard semi-arid/arid mask
- Modification of groundwater recharge algorithm in semi-arid regions; in case of precipitation below the critical value, the water that does not become groundwater recharge now remains in the soil instead of running off, which increases the soil water content and evapotranspiration
- New consistent river velocity algorithm based on river storage, with adjustment of roughness coefficient to avoid overestimation of velocity
- Elimination of inconsistent (too high) values of domestic and manufacturing water use in coastal areas as defined by the WATCH-CRU ocean land mask

		CCI Sea Level Budget Closure
		ESA/ESRIN contract 4000119910/17/I-NB
		Reference: ESA_SLBC_cci_D4.7
		Version: v1.1
		Date: 14.02.2020
		Page: 50 of 101

– Elimination of inconsistent negative values of actual consumptive water use; net groundwater abstraction is adjusted when not all net surface water abstraction can be satisfied, and thus return flows from irrigation with surface water are smaller (and net groundwater abstraction therefore larger)
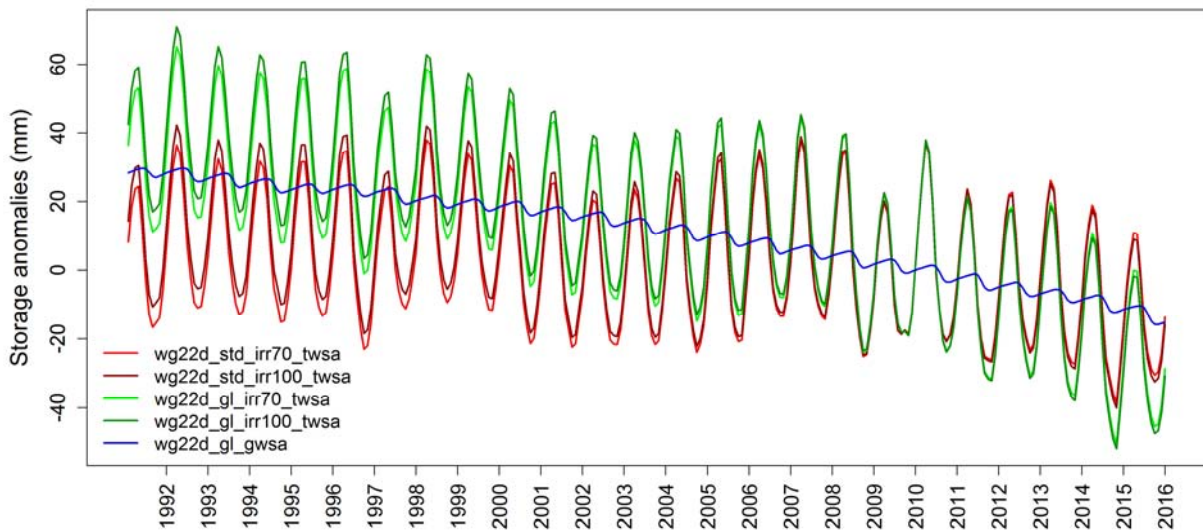
In terms of globally-averaged TWSA over the altimetry era (1992-2016), WaterGAP2.2c standard and WaterGAP2.2d standard (hereafter "wg22d_std") only vary slightly for both the 70% deficit irrigation and the optimal irrigation variants.

Moreover, a non-standard version of WaterGAP2.2d (hereafter "wg22d_gl") that includes a glacier water storage compartment, and thus explicitly simulates the effect of glacier mass variations on the continental water balance was developed. This was achieved by integrating annual time series of glacier area, as well as monthly time series of precipitation on glacier area and glacier mass loss from the GGM model (provided by WP230) as an input to WaterGAP. Even though GGM is conceived to simulate each individual glacier, these time series were provided as a 0.5° by 0.5° grid covering the entire globe for consistency with the spatial resolution of WaterGAP. Note that in the gridded GGM time series, the mass loss of a glacier that in reality may be spread over several grid cells is assigned to the grid cell where the center of the glacier is located. This also applies to the gridded glacier area and precipitation on glacier area time series.

A number of code adaptations were required to develop wg22d_gl. A glacier water storage compartment, assumed to increase with incoming precipitation on glacier area and decrease with outgoing glacier runoff, was included. Moreover, the land area of each WaterGAP grid cell was reduced by the glacier area. Furthermore, the grid cell precipitation was adapted by adding the precipitation on glacier area (from WP230) to the precipitation from the input forcing corresponding to the fraction of continental area without glacier(s). Glacier runoff was added to the grid cell fast runoff, which partly flows directly into the river, the rest flowing to the surface water bodies. It was assumed that glacier runoff does not recharge the soil and groundwater storages.

Figure 4.7.1 shows the difference between global TWSA from wg22d_std and from wg22d_gl (for two irrigation variants). Due to introducing the strongly decreasing glacier storage volume into WaterGAP, the TWSA of the two wg22d_gl variants shows a much stronger decreasing trend over time than wg22d_std, which does not include simulation of glacier mass variations.

Figure 4.7.2 compares global TWSA as observed by GRACE (Section 4.3) and as simulated by different WaterGAP variants. Inclusion of glacier water storage anomalies into WaterGAP strongly improves the fit to GRACE TWSA, with the seasonality fitting very well. Performance indicator values (Nash-Sutcliffe Efficiency and correlation coefficient) increase significantly with wg22d_gl (Table 4.7.1).

		CCI Sea Level Budget Closure
		ESA/ESRIN contract 4000119910/17/I-NB
		Reference: ESA_SLBC_cci_D4.7
		Version: v1.1
		Date: 14.02.2020
		Page: 51 of 101

Figure 4.7.1: Effect of adding a glacier water storage compartment on global TWSA in mm with respect to the global continental area (except Greenland and Antarctica) from WaterGAP2.2d forced with WFDEI-GPCC for two irrigation variants (70% deficit and optimal irrigation variants). Red curves: TWSA from WaterGAP2.2d standard, green curves: TWSA from WaterGAP2.2d variant including glaciers explicitly, blue curve: glacier water storage anomalies from WaterGAP2.2d variant including glaciers explicitly. All anomalies are relative to the mean of 2006-2015.
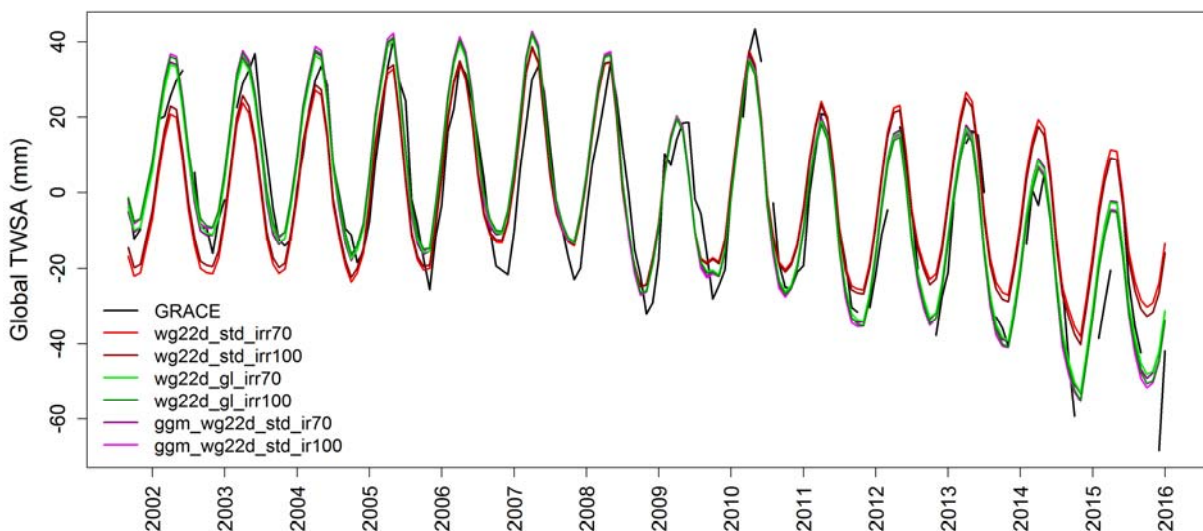
Figure 4.7.2: Comparison between global TWSA in mm with respect to the global continental area (except Greenland and Antarctica) from GRACE (solution provided by WP220 version 1) and from modeling (WFDEI-GPCC) for two irrigation variants (70% deficit and optimal irrigation variants). Black curve: GRACE, red curves: WaterGAP2.2d standard, green curves: WaterGAP2.2d variant including glaciers explicitly. The magenta curves were obtained by summing TWS from WaterGAP2.2d standard and glacier water storage from GGM, and deriving anomalies. All anomalies are relative to the mean of January 2003 – January 2016.

		CCI Sea Level Budget Closure
		ESA/ESRIN contract 4000119910/17/I-NB
		Reference: ESA_SLBC_cci_D4.7
		Version: v1.1
		Date: 14.02.2020
		Page: 52 of 101

Table 4.7.1: Performance indicators values derived from comparison between GRACE-derived (solution provided by WP220 version 1) and modeled TWSA for global land area (except Greenland and Antarctica). The first two rows correspond to WaterGAP2.2d standard, rows 3 and 4 correspond to the WaterGAP2.2d variant including glaciers. Rows 5 and 6 correspond to the TWSA derived from the sum of TWS from WaterGAP2.2d standard and glacier water storage from GGM. All modeling solutions are given for the 70% deficit and the optimal irrigation variants. NSE: Nash-Sutcliffe efficiency, r: Pearson product-moment correlation coefficient.

WFDEI-GPCC	NSE	r	WFDEI-CRU	NSE	r
wg_std_ir70	0.7208	0.8522	wg_std_ir70	0.7703	0.8837
wg_std_ir100	0.7611	0.8762	wg_std_ir100	0.8025	0.9023
wg_gl_ir70	**0.8715**	0.9379	wg_gl_ir70	**0.8777**	**0.9417**
wg_gl_ir100	0.8685	**0.9382**	wg_gl_ir100	0.8687	0.9392
ggm_wg22d_std_ir70	0.8627	0.9345	ggm_wg22d_std_ir70	0.8706	0.9392
ggm_wg22d_std_ir100	0.8594	0.9354	ggm_wg22d_std_ir100	0.8606	0.9371

4.7.2 Products

Two versions of WaterGAP2.2d (wg22d_std and wg22d_gl) were run with two irrigation variants (70% deficit irrigation variant and optimal irrigation variant) and two state-of-the-art climate forcings:

- daily WFDEI ("WATCH Forcing Data methodology applied to ERA-Interim data") dataset (Weedon et al. 2014) with precipitation bias corrected using GPCC monthly precipitation sums (Schneider et al. 2015) (WFDEI-GPCC)
- daily WFDEI dataset with precipitation bias corrected using CRU TS 3.23 monthly precipitation sums (Harris et al. 2014) (WFDEI-CRU)

Eight gridded datasets (2 model versions x 2 climate forcings x 2 irrigation variants) of TWSA are provided.

4.7.3 Uncertainty assessment

For v2 data products, the uncertainty in simulated TWSA due to spatially distributed climate input data and to the modeling approach with respect to, on the one hand, the explicit simulation of glaciers and, on the other hand, irrigation water use in groundwater depletion regions (choice between two irrigation variants) was considered by running different model variants.

In order to assess the uncertainty due to the three sources of error mentioned above, the following model variants were used to compute monthly time series of TWS and derive TWSA relative to the mean over the period January 2006 - December 2015:

- – Wg22d_std, 70% deficit irrigation, WFDEI-GPCC forcing
- – Wg22d_std, 70% deficit irrigation, WFDEI-CRU forcing
- – Wg22d_std, optimal irrigation, WFDEI-GPCC forcing
- – Wg22d_std, optimal irrigation, WFDEI-CRU forcing

		CCI Sea Level Budget Closure
		ESA/ESRIN contract 4000119910/17/I-NB
		Reference: ESA_SLBC_cci_D4.7
		Version: v1.1
		Date: 14.02.2020
		Page: 53 of 101

–   Wg22d_gl , 70% deficit irrigation, WFDEI-GPCC forcing
–   Wg22d_gl, 70% deficit irrigation, WFDEI-CRU forcing
–   Wg22d_gl, optimal irrigation, WFDEI-GPCC forcing
–   Wg22d_gl, optimal irrigation, WFDEI-CRU forcing.

Uncertainties are characterized by the spread between the model runs. For each epoch, the standard deviation of the values from the time series was taken as the standard uncertainty. The resulting uncertainties are presented further below in Section 5.1.1.

4.8 Arctic Ocean focus for all components

4.8.1 Methods

For the Arctic, sea level heights from satellite altimetry as well as sea level heights and steric sea level from the TOPAZ4 model are provided and described in the following sections.

Altimetry

The altimetric sea level anomaly (SLA) record is obtained from ERS-2, Envisat, and CryoSat-2 vdata north of 65°N to 81.2°N. Large parts of the Arctic Ocean have a permanent or seasonal sea ice cover, which makes accurate range estimation difficult.

To obtain the altimetric SLA record, ERS-2 and Envisat data have been retracked using the Adaptive Leading Edge Subwaveform (ALES+) retracker. The ALES+ (Passaro et al., 2018) retracker is similar to the original ALES retracker (Passaro et al., 2014), but has been adjusted to fit waveform returns from all types of water surfaces, i.e. not only open ocean, but also coastal areas, lakes and rivers, and sea ice covered areas. 1 Hz CryoSat-2 data in LRM and SAR mode were taken from the Radar Altimetry Database System (RADS, Scharoo et al., 2013). However, 20 Hz CryoSat-2 SAR and SARIn data have been retracked by the Lars Advanced Retracking System (LARS) system (Stenseng, 2011), since RADS is not able to handle 20 Hz data, which is necessary in order to retrieve height estimates from leads in-between sea ice.

The retracking methods used for the v2 data have been chosen due to the need for a better height retrieval in the Arctic Ocean, where traditional retrackers are not sufficient for extracting accurate height estimates in sea ice leads. In addition, not only a higher quality of data is needed, but definitely also a higher quantity of data. At the moment, most data are acquired during the late summer season, where peaky waveforms from melt ponds on top of sea ice might be mistaken for the desired waveforms stemming from sea ice leads.

Using the ALES+ retracker as well as utilizing the retracking of CryoSat-2 SAR and SARIn data in the LARS system at DTU Space will provide a higher quality and quantity of data compared to standard ocean retracking.

		CCI Sea Level Budget Closure
		ESA/ESRIN contract 4000119910/17/I-NB
esa	TECHNISCHE UNIVERSITÄT DRESDEN · Universität Zürich · UNIVERSITY OF LEEDS · LEGOS · Universität Bremen · GOETHE UNIVERSITÄT FRANKFURT AM MAIN · DTU Space National Space Institute · University of Reading · MERCATOR OCEAN INTERNATIONAL	Reference: ESA_SLBC_cci_D4.7
		Version: v1.1
		Date: 14.02.2020
		Page: 54 of 101

ALES+ is a subwaveform retracking algorithm that takes into account the sea state and the slope of the trailing edge. The retracking algorithm itself is based on the Brown-Hayne model (Brown, 1977; Hayne, 1980) and contains a preliminary step in order to estimate the most appropriate length of the trailing edge contained by the subwaveform. For very specular waveforms, the trailing edge is much shorter, which is taken into account during the fitting of the procedure if the waveform is found to be a "non-standard" ocean waveform. Non-standard ocean waveforms are detected by identifying waveforms with a pulse peakiness (PP) higher than 1

For 20 Hz SAR and SARIn data from LARS we are only including waveforms retrieved over ice leads. Within the LARS database, the waveforms are retracked using a simple threshold retracker. Ice lead waveforms are then found to be those with a PP higher than 0.35 for SAR and 0.25 for SARIn, and a stack standard deviation lower than 4 (Armitage and Davidson 2014).

To make a seamless transition between the three satellite missions, the intermission biases were estimated and minimized. In this step a difference from v1 to v2 is that v2 is resampling data directly to monthly instead of diurnal medians. The following steps were completed to handle the intermission biases:

1. Monthly medians were calculated for each mission for the entire region covered by the data set.

2. For overlapping mission pairs (either ERS-2 and Envisat, or Envisat and CryoSat-2), coinciding days were detected and extracted.

3. The trend was removed for each data set containing coinciding monthly medians.

4. For each data set, the median was determined.

5. For each overlapping pair, the median difference was calculated and the data sets were aligned.

6. The data sets were corrected corresponding to the RADS reference (TOPEX/Poseidon).

For CryoSat-2, RADS and LARS data have been adjusted by looking at individual satellite tracks.

The raw but inter-satellite bias corrected satellite data are divided into months filtered and gridded with a resolution of 0.50 x 0.25 (longitude x latitude). For more information, see Rose et al. (2019). A time series showing the monthly median SLA for the entire Arctic region is shown in Figure 4.8.1.

The SLA record was corrected for all geophysical corrections and is referenced to the DTU18MSS (Andersen et al., 2018). This is a change from v1, where we used the DTU15MSS (Andersen et al., 2016). The new MSS is constructed to improve the central Arctic. The ocean tides are from FES2014 (Carrere et al., 2016b). The dynamic atmospheric correction (DAC)

		CCI Sea Level Budget Closure
		ESA/ESRIN contract 4000119910/17/I-NB
		Reference: ESA_SLBC_cci_D4.7
		Version: v1.1
		Date: 14.02.2020
		Page: 55 of 101

applied is the DAC-ERA (Carrere et. al, 2016a) for the ERS-2 and Envisat periods, where MOG2d is used for CryoSat. The DAC can be very large in the Arctic (in the level of the SLA) and very noisy in sea ice covered regions. Therefore, errors in the DAC can introduce large errors in the SLA. There exist two SLA products one with and one without the DAC correction. The SLA without DAC should be used in comparison to tide gauge data.
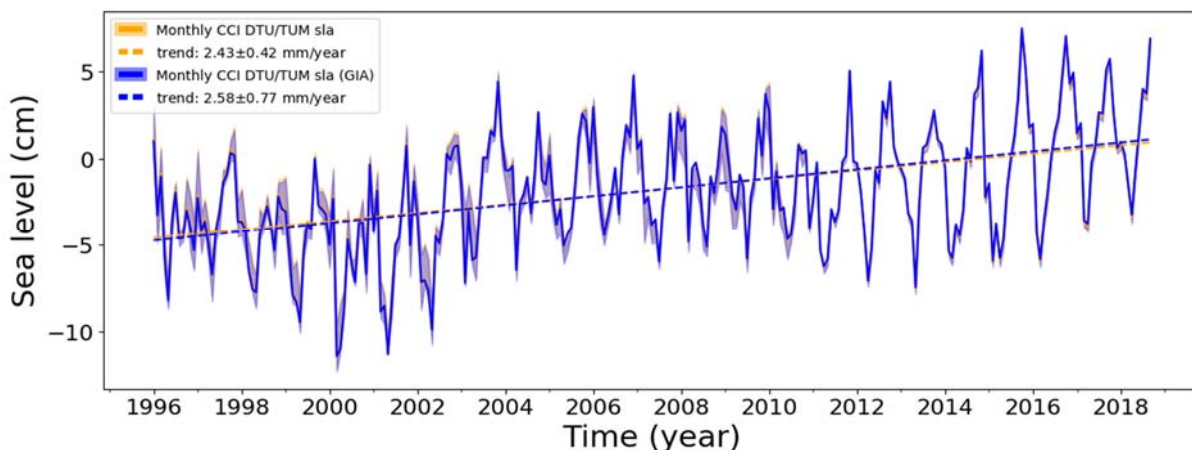
TOPAZ4

Data on both sea level change and steric sea level change are obtained from the TOPAZ4 data assimilation system operated at NERSC. This system represents the Arctic Marine Forecasting Center of the Copernicus Marine Services (http://marine.copernicus.eu/). The system delivers routinely products and information used for analyses, forecast (up to 10 days) and reanalyses.

TOPAZ4 is a coupled ocean and sea ice data assimilation system for the North Atlantic and the Arctic Ocean that is based on the Hybrid Coordinate Ocean Model (HYCOM) and the Ensemble Kalman Filter data assimilation (Sakov et al., 2012). HYCOM is using 28 hybrid z-isopycnal layers at a horizontal resolution varying from 16 km in North Atlantic to 12 km in the Arctic Ocean. The TOPAZ4 system is forced by the ECMWF ERA Interim reanalysis and assimilates along-track altimetry data, sea surface temperatures, sea ice concentrations and sea ice drift derived from satellites along with in-situ temperature and salinity profiles from Argo floats and ice tethered buoys (ITP) and research cruises. For validation results and more details see Sakov et al. (2012) and Xie et al. (2017).

4.8.2 Products

Altimetry

Monthly mean SLA covering the region from 65°N-81-5°N and 180°W-180°E with a resolution of 0.25° in latitudinal direction and 0.5° in longitudinal direction, respectively, are provided for the period January 1996 and October 2018. There are fewer data points from ERS-2 and Envisat compared to CryoSat-2, and for all of the missions, the data coverage is highest during summer/fall.

Figure 4.8.1: Monthly ESA CCI DTU/TUM Arctic sea level anomaly record including GIA_Caron2018.

		CCI Sea Level Budget Closure
		ESA/ESRIN contract 4000119910/17/I-NB
eesa	TECHNISCHE UNIVERSITÄT DRESDEN · Universität Zürich · UNIVERSITY OF LEEDS · LEGOS · Universität Bremen · GOETHE UNIVERSITÄT FRANKFURT AM MAIN · DTU Space National Space Institute · University of Reading · MERCATOR OCEAN INTERNATIONAL	Reference: ESA_SLBC_cci_D4.7
		Version: v1.1
		Date: 14.02.2020
		Page: 56 of 101

TOPAZ4

The products contain gridded sea surface height (meters; relative to geoid), and steric height (meters). The TOPAZ4 covers the Nordic Seas and entire Arctic Oceans bounded by 65°N - 90°N and 180°W to 180°E with a spatial resolution of 0.25°. The temporal coverage is from 2003-2017 at a monthly resolution.

4.8.3 Uncertainty assessment

Altimetry

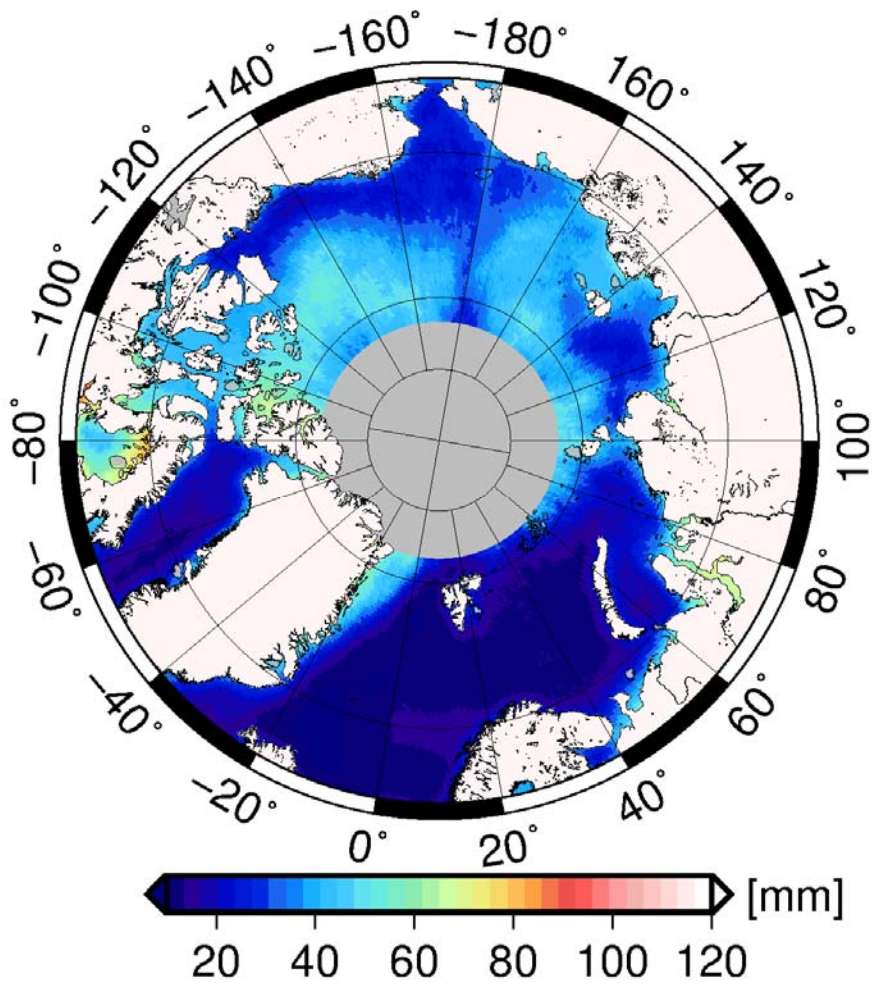When it comes to satellite altimetry in the Arctic Ocean there are multiple error sources:

- Erroneous range estimates caused by highly reflective melt ponds on top of the sea ice, wet ice and refrozen ice/snow (mostly during summer).

- Inaccurate range corrections from atmospheric models – e.g. the dynamic atmospheric correction.

- Inaccurate tide models. The tidal models are based on altimetry, and in an area with less altimetry data, such as sea ice covered regions in the Arctic Ocean, it is to be expected that the tidal model (in this case FES2014) is less accurate.

However, not all of the above listed error sources are directly quantifiable, and those that are, are difficult to keep track of during interpolation. Here, a block bootstrap method by Rose et al. (2019) is used to quantify the uncertainties by determine the confidence interval for each grid cell for every month. Each grid cell is assumed to be uncorrelated. In the bootstrap method data are repeatedly processed 500 times from the first filtering to the final resampled grid point by randomly drawing a new grid cell with replacement from the cells in the original dataset. There can be multiple copies of the cells.

A map of the SLA range difference in the confidence intervals from 2.5% to 97.5% corresponding to a confidence level of 95% is shown in Figure 4.8.2. The gridded monthly data are not normal distributed, hence the standard deviation should be used with care. For more information, see Rose et al. (2019).

TOPAZ4

The sources of error are predominantly arising from deficiency in the TOPAZ4 model system and lack of in-situ data for assimilation within the Arctic Ocean.

		CCI Sea Level Budget Closure
		ESA/ESRIN contract 4000119910/17/I-NB
		Reference: ESA_SLBC_cci_D4.7
		Version: v1.1
		Date: 14.02.2020
		Page: 57 of 101

Figure 4.8.2: The SLA 97% confidence range interval

		CCI Sea Level Budget Closure
		ESA/ESRIN contract 4000119910/17/I-NB
esa	*(university logos)*	Reference: ESA_SLBC_cci_D4.7
		Version: v1.1
		Date: 14.02.2020
		Page: 58 of 101

5. Assessment of budget closure/misclosure

This chapter reports the results of budget assessments. The assessments were conducted in three iterations for three versions v0, v1, and v2 of data products. This report concentrates on the v2 product assessment.

5.1 Ocean mass budget

5.1.1 Data summary

Ocean mass change (see Section 4.3 and Figure 4.3.1)

Ocean mass time-series from the following solutions as described in Section 4.3 were used:

- ITSG-Grace2018 spherical-harmonics based solution, with GIA corrections after A et al. (2013), Peltier et al. (2015) and Caron et al. (2018); globally integrated, buffered and scaled time series.

- CSR-, GFZ- and JPL spherical-harmonics based solution, each with A et al. (2013), Peltier et al. (2015) and Caron et al. (2018) GIA correction; identical method to the 'main product'; globally integrated, buffered and scaled time series.

- One mascon solution by GSFC (Luthcke et al., 2013) dedicated for ocean mass research; globally integrated and scaled geodesic grid product. Used for comparison.

- Chambers' OMC time-series for CSR, GFZ and JPL; spherical-harmonics based, globally integrated, buffered and scaled time series (Johnson and Chambers 2013, updated). Used for comparison.

Mass change over the global ocean were considered. The preferred OMC time series is the one that is based on ITSG-Grace2018 SH solutions and uses the GIA correction after Caron et al. (2018), for the reasons outlined in Section 4.3.

Glacier contribution (see Section 4.4 and Figure 5.1.1)

Integrated mass change time series with monthly resolution based on SLBC_cci v2 gridded data as summarized in Section 4.4. Uncertainties were converted from the originally given 90% confidence interval half width to standard uncertainties by division by 1.645, based on the assumption of a normal distribution of the errors. Trend uncertainties were determined from the uncertainties of the annual mass balances of the years involved in the trend calculation. The root sum square (RSS) of the annual mass balance uncertainties, divided by the length of the time period in question was taken as the trend uncertainty, following the suggestion in Horwath et al. (2019b, Section 5.4.3) that the model errors are spatially and temporally uncorrelated.

		CCI Sea Level Budget Closure
		ESA/ESRIN contract 4000119910/17/I-NB
		Reference: ESA_SLBC_cci_D4.7
		Version: v1.1
		Date: 14.02.2020
		Page: 59 of 101

Ice sheets contribution: Greenland (see Section 4.5 and Figure 5.1.2)

In order to assess mass changes over entire Greenland, we followed two alternative approaches:

- We applied monthly GRACE solutions from the ESA Greenland Ice Sheet CCI project based on CSR GRACE RL06 (GRACE Gravimetric Mass Balance, GMB) (see Section 4.5). This product also includes peripheral glaciers and ice caps not directly joint with the Greenland Ice Sheet.

- We combined the radar-altimetric record over the Greenland Ice Sheet (Section 4.5) with mass change information of the peripheral glaciers (connectivity levels 0 and 1) from the GGM (Section 4.4). The radar-altimetric record is calibrated to ICESat laser altimetry 2003–2009, but is restricted to the ice sheet only. Combining it with the GGM results for peripheral glaciers, the result is consistent with the GRACE GMB approach in assessing all ice mass changes on Greenland.

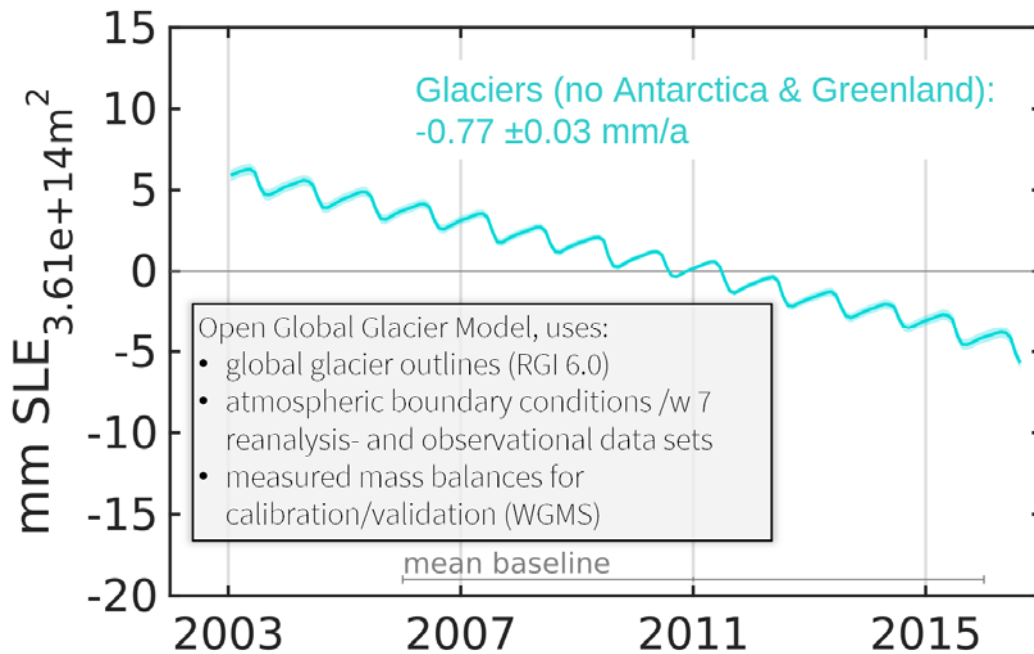*Ice sheets contribution: Antarctica* (see Section 4.6 and Figure 5.1.3)

Similar to Greenland, we followed two approaches in order to determine mass changes of Antarctica over the 2003–2016 period:

- GMB integrated mass change time series for entire from the Antarctic Ice Sheet CCI (see Section 4.6)

- Radar-altimetry record with time-evolving ice-density mask that comprises the entire Antarctic Ice Sheet, including the Antarctic Peninsula (see Section 4.6). Note that discrepancies between altimetry-based and GRACE-based mass change estimates exist for the East Antarctic Ice Sheet. They have been observed previously and are not well understood (see, e.g., Shepherd et al. 2018; Schröder et al. 2019). Possible causes are: errors in the GRACE GIA correction, time-variable penetration effects on radar altimetry; imperfect altimetry inter-mission calibration, imperfect altimetry volume-to-mass conversion.

Land water contribution (see Section 4.7 and Figure 5.1.4)

Net water mass changes on land were considered using the Global Hydrological Model WaterGAP2.2d (WGHM). Our analysis applies an ensemble mean of different model runs with two irrigation scenarios (70% deficit irrigation and optimal irrigation), and two state-of-the-art climate forcings (WFDEI with GPCC and CRU TS 3.23 precipitation bias-correction). Given monthly time stamps were treated as mid-of-month (representing the mass change of each month, respectively). For the land water contribution, no uncertainty assessment is directly available. We have chosen to estimate the uncertainty of the multi-year trend according to the standard deviation of the ensemble-member trends. We use globally averaged total water storage anomalies given as equivalent water heights, rescaled from source area to ocean area.

|		**CCI Sea Level Budget Closure**
		ESA/ESRIN contract 4000119910/17/I-NB
eesa	TECHNISCHE UNIVERSITÄT DRESDEN · Universität Zürich · UNIVERSITY OF LEEDS · LEGOS · Universität Bremen · GOETHE UNIVERSITÄT FRANKFURT AM MAIN · DTU Space National Space Institute · University of Reading · MERCATOR OCEAN INTERNATIONAL	Reference: ESA_SLBC_cci_D4.7
		Version: v1.1
		Date: 14.02.2020
		Page: 60 of 101

Figure 5.1.1: Global glacier mass change and uncertainties with respect to the Jan 2006 to Dec 2015 mean. A negative trend means net mass loss of glaciers, i.e. mass gain for the global ocean. Antarctica and Greenland are excluded.
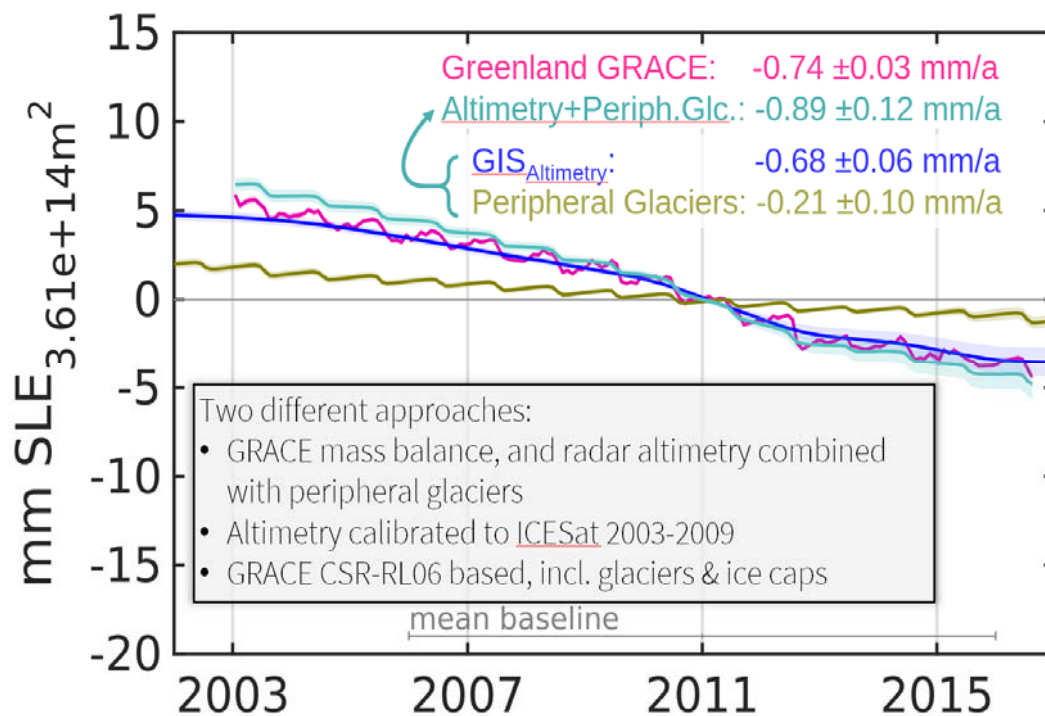
Figure 5.1.2: Greenland Ice Sheet (GIS) mass change from different sources: GRACE gravimetric mass balance (purple), lidar-calibrated radar altimetry (blue) and peripheral glaciers from global glacier model (brown). Altimetry- and glacier-data were combined (green) to be spatially consistent with GRACE data.
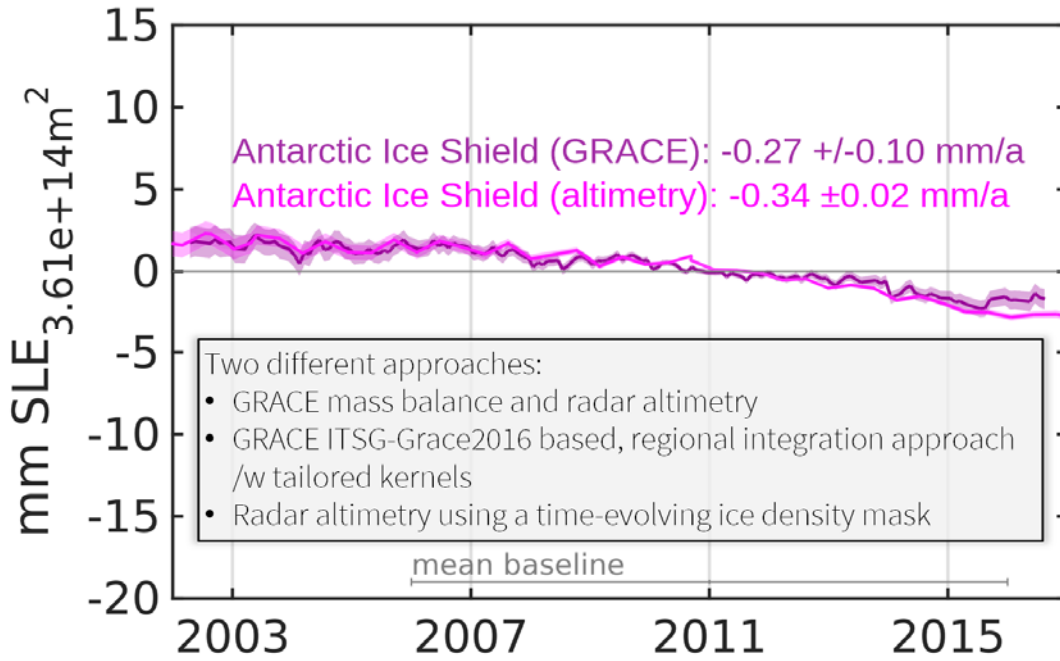
Figure 5.1.3: Antarctic Ice Sheet mass change relative to the Jan 2006 to Dec 2015 mean with 1-sigma uncertainty bands. Negative trends correspond to mass gain in the Global Ocean
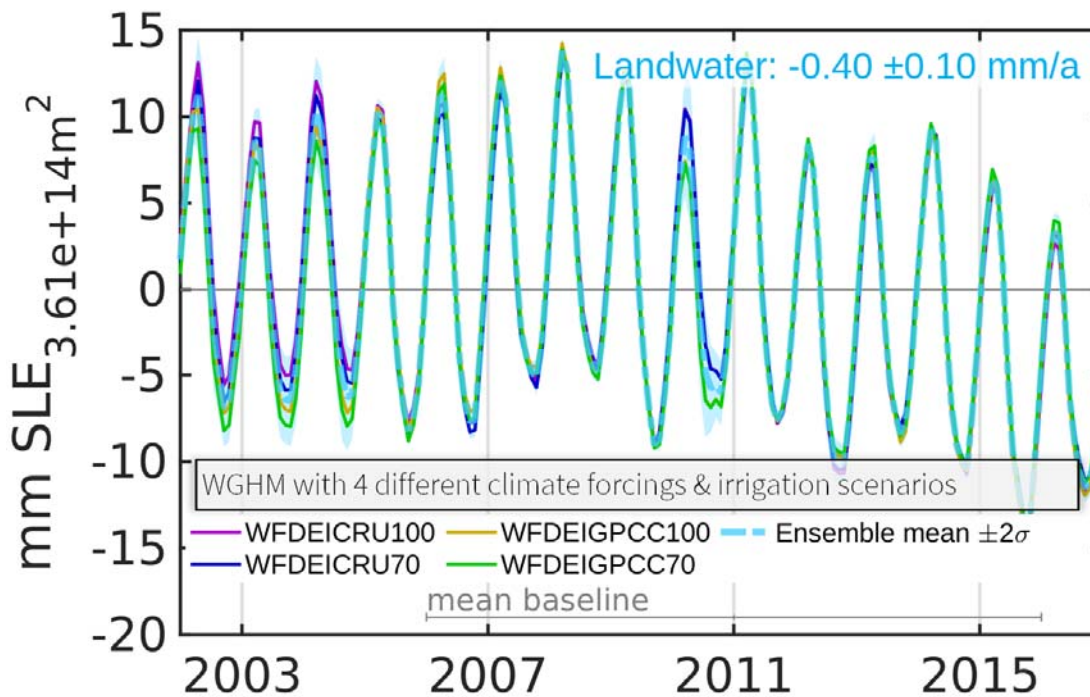
Figure 5.1. 4: Land water storage change with respect to the Jan 2006 to Dec 2015 mean, with negative trends meaning net mass loss off the continents. Note the large seasonal variation in amplitude. The ensemble mean (dashed light blue) is used in the mass budget assessment in this chapter. Also note that multi-annual or decadal oscillations appear to be reflected in the data and may affect trend estimation.

		CCI Sea Level Budget Closure
		ESA/ESRIN contract 4000119910/17/I-NB
		Reference: ESA_SLBC_cci_D4.7
		Version: v1.1
		Date: 14.02.2020
		Page: 62 of 101

5.1.2 Budget assessment

Methods

Time series analysis. The time series of contributing components were considered over a common time interval from 01/2003 to 08/2016. While GRACE data have few single 'missing months' starting from January 2011, the time-series are significantly noisier starting in late 2016 from when only Level-2 data including accelerometer transplants from GRACE-A to the GRACE-B satellite are available. At the time of OMC data processing for this project, GRACE Release 06 data and the corresponding correction products (low degree replacements with that from satellite laser ranging and background GAx models) were only provided for until August 2016. Therefore, we do not provide analyses of the Global Ocean mass budget beyond August 2016 in this assessment.

Version 2 data that were given as gridded mass changes over land were globally integrated and scaled onto a common standard ocean surface area of 3.61e+14 m².

An un-weighted least squares fit of a 6-parameter function (consisting of a constant, a linear component, an annual cosine and sine function and a semi-annual cosine and sine function) was computed for each restricted mass change time-series based on un-interpolated data, respectively. The linear term of this functional fit is treated as the "trend" and is expressed in units of Gt/yr (gigatonnes per year) for the OMC trend and in mm/yr (millimetres per year) for an equivalent sea level change that corresponds to the OMC. This trend is used for assessing the ocean mass budget. A 'de-trended' time series, or one of which the trend has been removed, is the original time series minus the linear term of the fit.

In a similar manner, we subtract the annual and semi-annual components of the fit from the time-series, whenever a seasonal signal is to be removed. Multi-year cycles with smaller wave numbers, e.g. ENSO effects, are thus still included in the remaining signal (residual).

Annual Sine- and Cosine amplitudes derived from the least squares fit to the individual components furthermore serve as input for analyses of seasonal signals. Data with annual temporal resolution were fitted with the same function but without adjusting for annual and semi-annual components.

The Global Ocean mass budget 2003—2016 was derived from the linear components of ocean mass change and the sum of components, namely Glaciers, AIS, GIS and LWS (cf. Equation 2.2). We generated two other sets of time series for purposes of displaying and of analysing the non-linear and non-seasonal components:

- In one set of time series we reduced the annual and semi-annual components.

- In another set of time series we additionally reduced the linear component (trend).

In addition, we then interpolated those time series to a common mid-monthly temporal sampling from 01/2003 to 08/2016. Interpolation is necessary for comparative analyses because of the inhomogeneous time basis of the underlying data products. Based on the

		CCI Sea Level Budget Closure
		ESA/ESRIN contract 4000119910/17/I-NB
		Reference: ESA_SLBC_cci_D4.7
		Version: v1.1
		Date: 14.02.2020
		Page: 63 of 101

common temporal sampling, we calculated the misclosure of the non-linear, non-seasonal components and analysed it statistically, also on a monthly basis. However, the *trends* and analysis of *annual signals* considered throughout this assessment are solely based on original, un-interpolated time series. The same holds true for the evaluation of seasonal amplitudes, which is solely based on analyses of data at original times.

Uncertainties of the trends are taken from D2.4.2. They are considered as standard uncertainties ('one sigma'). Note that these uncertainties exceed the formal uncertainties of the functional fit because their assessment includes systematic effects (e.g. GIA uncertainty, in the case of GRACE-based data products). Uncertainties of sums or differences of the trends from individual contributions are taken as the root sum square of the individual uncertainties. For an assessment on the land water mass trends, we considered the spread between the linear trends obtained from the four land water mass time series that cover the full period 01/2003— 08/2016.

Wherever possible in terms of the provided v2 data, we combine uncertainties in the form

$$\sigma_{total}^2(t) = \sigma_{noise}^2(t) + (\sigma_{trend} \cdot (t-t_o))^2 \qquad (5.1.1)$$

for time series of mass change $m(t)-m(t_o)$ with respect to a reference time t_o. This means, the uncertainty range at the reference time is σ_{noise} and increases in time before and after t_o. Uncertainties of sums or differences of individual budget contributions (such as for the misclosure) are taken as the root sum square of the individual uncertainties. We note that this error propagation neglects any error correlations between the budget elements. Such correlations exist. For example due to conservation of solid Earth mass, errors of the GRACE GIA correction over ocean are anti-correlated with errors of the same correction over land. However, exploring this kind of correlation is left to future work.

Results for linear trends

The linear trends for all considered terms of the ocean mass budget are given in Table 5.1.1. For the time interval 01/2003–08/2016, all considered components show a clear positive trend (with positive meaning mass loss on land):

- The **sum of components** amounts to **2.19 ± 0.15 mm/yr** when GMB results are considered for both ice sheets, and to **2.40 ± 0.16 mm/yr** when (combined) radar altimetry results are considered. The given uncertainty is the root sum square of individual component uncertainties and an LWS ensemble mean is applied.

- The **Greenland** Ice Sheet contributes with **0.74 ± 0.03 mm/yr** from GRACE GMB (comprising entire Greenland) and **0.89 ± 0.12 mm/yr** assessed from radar altimetry and peripheral glaciers combined.

- The **global glaciers** outside Greenland and Antarctica contribute with **0.77 ± 0.03 mm/yr** and thus contribute similarly to OMC as Greenland.

		CCI Sea Level Budget Closure
		ESA/ESRIN contract 4000119910/17/I-NB
eesa	TECHNISCHE UNIVERSITÄT DRESDEN · Universität Zürich · UNIVERSITY OF LEEDS · LEGOS · Universität Bremen · GOETHE UNIVERSITÄT FRANKFURT AM MAIN · DTU Space National Space Institute · University of Reading · MERCATOR OCEAN INTERNATIONAL	Reference: ESA_SLBC_cci_D4.7
		Version: v1.1
		Date: 14.02.2020
		Page: 64 of 101

Table 5.1.1: Mass budget trends 01/2003–08/2016 and their 1-sigma standard uncertainties.

Target	Method	Linear Trend	
Global Glaciers (no Greenland)	GGM	0.77 ± 0.03	
Greenland (GIS & Periph.Glc.)	GRACE	0.74 ± 0.03	
	Radar altimetry / GGM		0.89 ± 0.12
Antarctic Ice Sheet	GRACE	0.27 ± 0.10	
	Radar altimetry		0.34 ± 0.02
Land water	TWS anomalies (WGHM)	0.40 ± 0.10	
Sum of mass contributions		2.19 ± 0.15	2.40 ± 0.16
Ocean mass	GRACE	2.19 ± 0.22	
Misclosure (mass budget)	OMC minus sum mass of contributions	0.00 ± 0.29	-0.21 ± 0.30

- The combined **Antarctic Ice Sheet's** contribution as from GMB is **0.27 ± 0.10 mm/yr**. The corresponding trend derived from altimetry is **0.34 ± 0.02 mm/yr**.

- The trend in **land water storage** for the ensemble of the four considered model variants amounts to **0.40 ± 0.10 mm/yr**.

The OMC trend budget is defined 'closed' when the measured mean ocean mass gain agrees with the sum of mass-losses of contributing components within a reasonable uncertainty range. The trend in mean Global Ocean mass from January 2003 to August 2016 according to our preferred GRACE-based solution (ITSG-Grace2018, Caron's GIA) amounts to +2.19 ± 0.22 mm/a. When GRACE products over the Greenland and Antarctic Ice Shelfs are considered, the sum of mass contributions gives a trend of 2.19 ± 0.15 mm/a; if the altimetry and peripheral glacier products are considered instead, the trend amounts to 2.40 ± 0.16 mm/a (all uncertainties given as 1-σ standard uncertainties).

The corresponding misclosures with combined uncertainties are 0.00 ± 0.29 mm/a (GRACE) and -0.21 ± 0.30 mm/a (altimetry), respectively. It means the mass budget in terms of linear trends is closed within the assessed uncertainty ranges. However, we want to point out that other GIA models (Ice5/6G) may give smaller OMC trends by 0.20 mm/a.

Any closure that is much better than the combined uncertainties may just be a coincidence of trend errors compensating each other.

The observed spread of trends owing to different geodetic and geophysical corrections during the processing of our SLBC_cci v1 and v2 OMC time-series has demonstrated how easily a 'lucky' combination of wrong/insufficient corrections terms and methods may lead to trend values that match the observed sum of components. Table 5.1.1 illustrates this fact by

		CCI Sea Level Budget Closure
		ESA/ESRIN contract 4000119910/17/I-NB
		Reference: ESA_SLBC_cci_D4.7
		Version: v1.1
		Date: 14.02.2020
		Page: 65 of 101

indicating that the choice of the GIA correction or of the GRACE analysis methodology may alter the results independently by more than 0.2 mm/yr.

Analysis of the seasonal mass-change budget

Given the sub-annual temporal data resolution of contributing components and GRACE data, we also investigated the seasonal mass change signal; i.e. the degree of agreement between the annual sine and cosine amplitudes of the assessed mass contributions and the GRACE OMC time series (Figure 5.1.5). Although both time series are almost in phase, we find a small systematic lag: GRACE OMC appears to be approximately 7 days delayed w.r.t. the sum-of-components. Sources of the offset have not been studied conclusively. They might include biases from GAD processing, coastal buffers, leakage effects, water storage modelling or even effects from atmospheric water vapor.

Replacing the land-water ensemble with individual land-water solutions has only marginal effect (on the order of 1 day) on the phase offset. The choice of irrigation scenario is a rather linear effect and has no impact on the phase. Likewise, the choice of the individual RL06 GRACE SH solutions input to our SH-based analysis has no significant effect on the phase. There are, however, significant phase differences with the results of the external GRACE products (GSFC mascons and the Chambers ensemble).
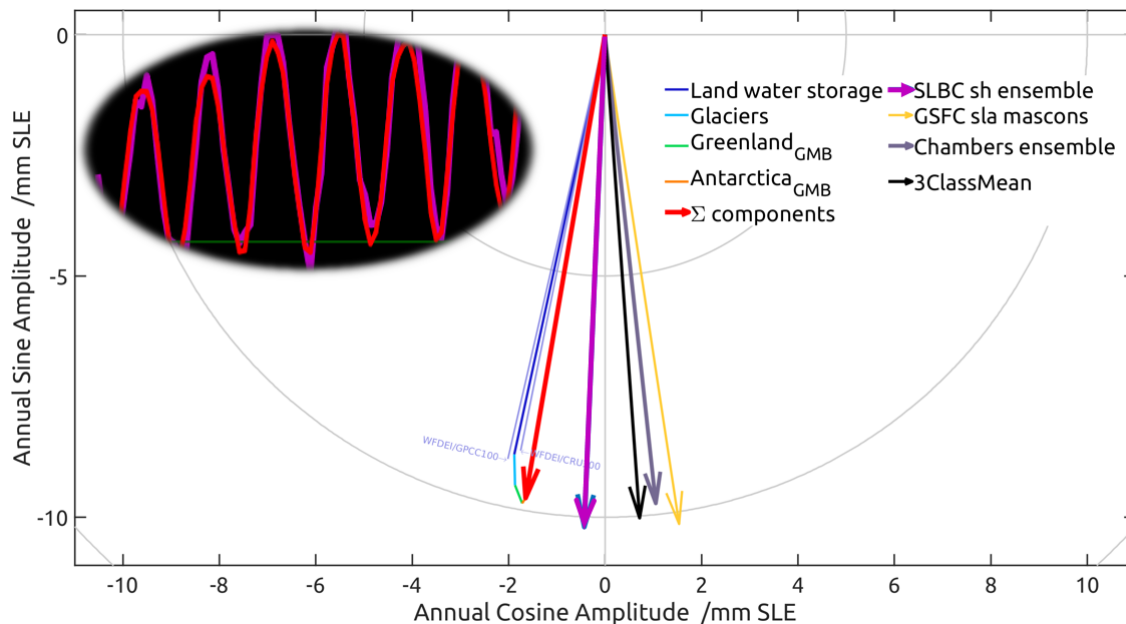
Figure 5.1.5: Phase diagram of annual sine and cosine amplitudes of various GRACE OMC solutions and of the contributing components. The bold red vector shows the sum of contrbiutions, where the individual contributions are shown as coloured blue and green lines. (Dark blue stands for the TWSA ensemble and the faint blue lines depict the WFDEI/CRU and WFDEI/GPCC forcing variants). The purple vector is the ensemble mean of the SH-based OMC solutions generated by SLBC_cci. The individual SH-based OMC solutions forming this ensemble are not distinguishable below the purple vector. Yellow and grey vectors show external GRACE OMC solutions (GSFC mascons, Chambers' ensemble mean). The black vector shows the mean over the three types of GRACE OMC solutions. The phase difference between the red and the purple vector correpends to 7 days.

		CCI Sea Level Budget Closure
		ESA/ESRIN contract 4000119910/17/I-NB
esa	TECHNISCHE UNIVERSITÄT DRESDEN · Universität Zürich · UNIVERSITY OF LEEDS · LEGOS · Universität Bremen · GOETHE UNIVERSITÄT FRANKFURT AM MAIN · DTU Space National Space Institute · University of Reading · MERCATOR OCEAN INTERNATIONAL	Reference: ESA_SLBC_cci_D4.7
		Version: v1.1
		Date: 14.02.2020
		Page: 66 of 101

Analysis of the ocean mass budget misclosure on the level of individual months

In analogy to the trend misclosure described earlier, we further analysed the monthly mass misclosure, which we define as each month's Global Ocean mass (GRACE) minus the sum of contributing components in the same month. Figure 5.1.6 displays the deseasonalized time series of GRACE-based OMC and the sum of mass contributions (GRACE-based for AIS and GIS). The misclosure time series also shown.

The misclosure time series is shown in more detail in Figure 5.1.7 together with the 1-sigma, 2-sigma, and 3-sigma uncertainty ranges. We find that 66.5%, 95.1% and 100% of de-seasonalised monthly misclosure are within 1-sigma, 2-sigma, and 3-sigma. This supports the realism of the uncertainty assessment under assumption of a Gaussian error distribution.

However, it is obvious from Figure 5.1.7 that the misclosure has a temporally correlated, interannual characteristics. The only contribution that exhibits interannual variations of sufficient amplitude is the land water storage. We have calculated a continental mass change (CMC) misclosure by taking the difference between the GRACE based CMC product (see D2.4.2 Product Description Document, Horwath et al. 2019b) and the sum of the LWS and Glacier products. Figure 5.1.8 compares the ocean mass budget misclosure and the CMC misclosure. The close match between the two misclosure time series on interannual scales supports the
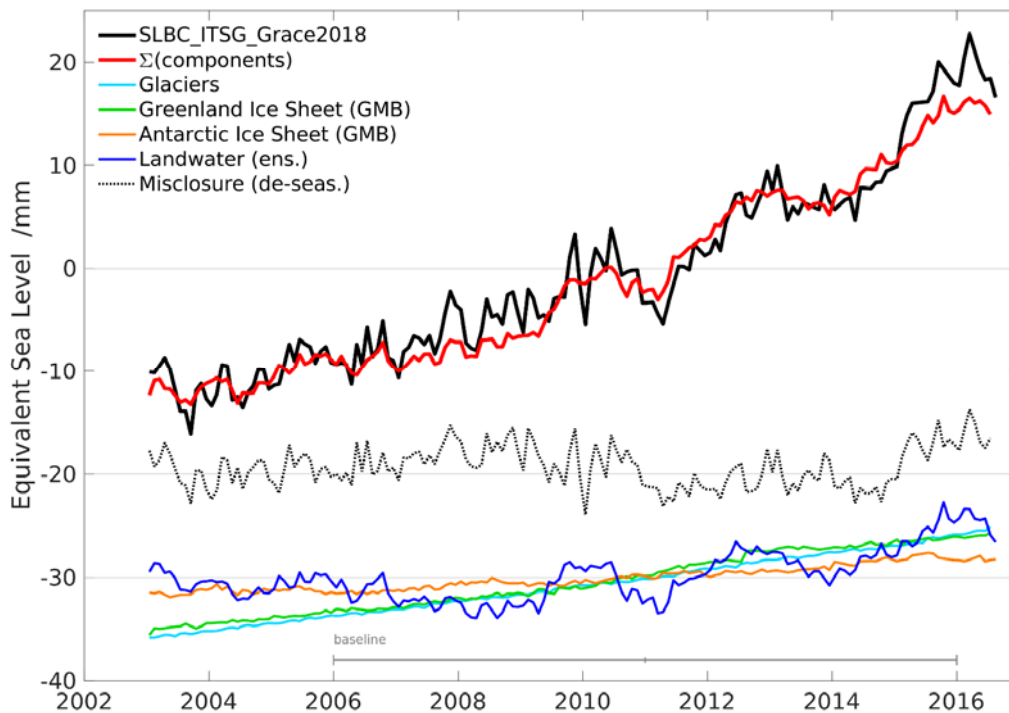

Figure 5.1.6: De-seasonalised contributing components (bottom, shifted by -20 mm) and GRACE Ocean Mass Change (top). The sum of the contributing components is shown in red. GiaC/A/P: OMC solutions ensemble with GIA corrections after Caron et al. (2018), A et al. (2013) and Peltier et al. (2015), respectively. The black curve is the mean ensemble of all five classes. Note that in this figure the ice sheets mass change was derived from GMB products.

		CCI Sea Level Budget Closure
		ESA/ESRIN contract 4000119910/17/I-NB
		Reference: ESA_SLBC_cci_D4.7
		Version: v1.1
		Date: 14.02.2020
		Page: 67 of 101

hypothesis that differences between WGHM results and GRACE results are responsible for the interannual part of the ocean mass budget misclosure.
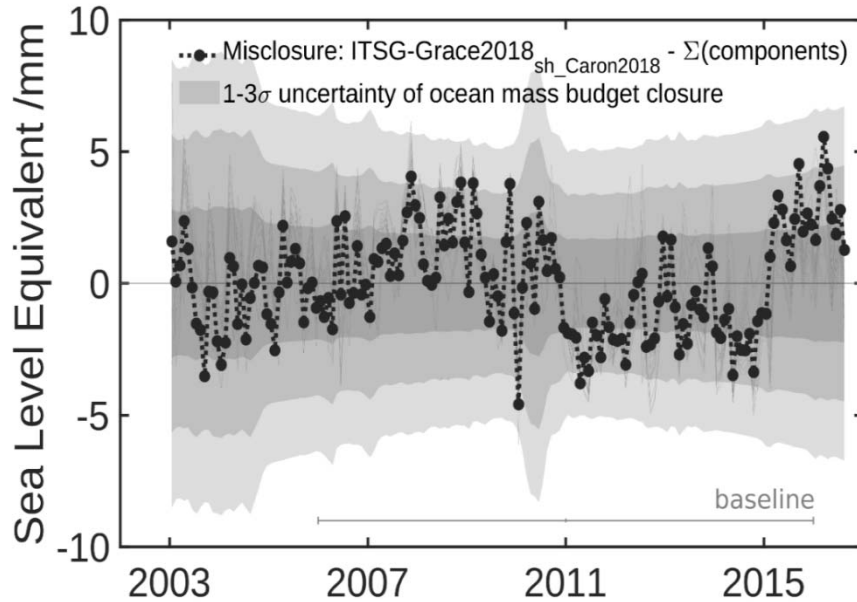
Figure 5.1.7: Monthly ocean mass misclosure (same as grey curve in Figure 5.1.6) plotted on top of the 1—3 σ combined uncertainty. The variety of OMC solutions with different GRACE products and GIA corrections are plotted in the background as faint grey curves.
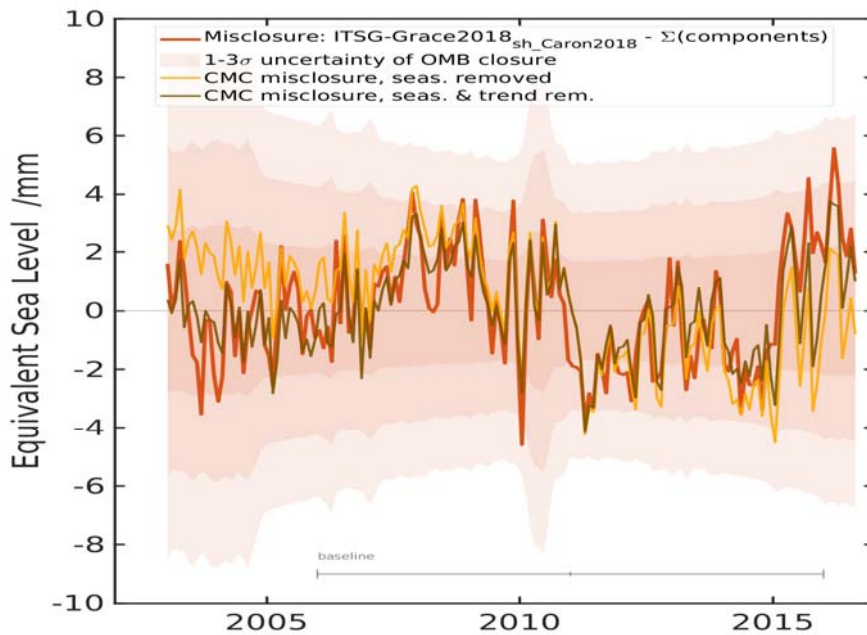
Figure 5.1.8: Red curve and shaded areas: same as in Figure 5.1.7. Yellow curve: Difference between GRACE-based continental mass change and the sum of LWS and glacier mass change, with seasonal signal, or seasonal signal and trend, removed, respectively

		CCI Sea Level Budget Closure
		ESA/ESRIN contract 4000119910/17/I-NB
		Reference: ESA_SLBC_cci_D4.7
		Version: v1.1
		Date: 14.02.2020
		Page: 68 of 101

5.1.3 Discussion and conclusions

The efforts of the SLBC_cci project to analyse data in a common framework have lead to more rigorous results and new kinds of results on the ocean mass budget.

For the linear trend over the 2003-2016 period, the ocean mass budget is closed within the 1σ uncertainties. When using our preferred OMC product (ITSG_2018 with GIA correction according to Caron) and GRACE-based or altimetry-based assessments of ice sheet contributions, the misclosure is 0.00 ± 0.29 mm/yr or -0.21 ± 0.30 mm/yr, respectively. We stress that any closure that is much better than the combined uncertainties may just be a coincidence of trend errors compensating each other.

The closure of the seasonal signal has improved from the v1 assessment to the v2 assessment. The SH-based OMC products are ~7 days late, or the sum of components is ~7 days early. Larger phase differences arise with the external GRACE-based OMC products.

Even on the level of the monthly misclosure time series, the misclosure statistics is in agreement with the assessed uncertainties, where the assessed 1-sigma uncertainty is on the order of 2 mm.

The misclosure contains residual interannual signal. Analysis of the continental mass budget indicates that this is due to differences between the land water storage variations as simulated by WGHM and as derived by our SH-based GRACE analysis.

5.2 Global sea level budget

The sea level budget closure assessment was performed using two approaches: (1) comparison of observed sea level with sum of individual components from SLBC_cci v2, and (2) with SLBC_cci v2 GRACE-based ocean mass for the mass components. Two-time periods were considered:

Period 1 (P(1)): the entire altimetry era, 1993-2016, where the sea level budget closure was investigated by comparing observed rate of sea level rise with the sum of contributions estimated independently.

Period 2 (P(2)): over the Argo/GRACE era, 2003-2016, where the sea level budget closure was investigated by comparing observed rate of sea level first with the sum of contributions as in P(1) and then with the sum of steric and GRACE based ocean mass.

5.2.1 Data summary

Observed altimetry sea level data (see Section 4.1, Figure 4.1.1 and Figure 5.2.1)

The v2 altimetry based GMSL was used as described in Section 4.1. Uncertainties from Ablain et al. (2019) were converted from 90% confidence interval half-width to standard uncertainties by division by 1.645.

		CCI Sea Level Budget Closure
	TECHNISCHE UNIVERSITÄT DRESDEN · Universität Zürich · UNIVERSITY OF LEEDS · LEGOS · Universität Bremen · GOETHE UNIVERSITÄT FRANKFURT AM MAIN · DTU Space National Space Institute · University of Reading · MERCATOR OCEAN INTERNATIONAL	**ESA/ESRIN contract 4000119910/17/I-NB**
		Reference: ESA_SLBC_cci_D4.7
		Version: v1.1
		Date: 14.02.2020
		Page: 69 of 101

Glacier contribution (see Section 4.4, Figure 5.2.2)

Integrated glacier mass changes were used as specified in Section 5.1.1. Glacier trend uncertainty for budget assessment is estimated by taking the mean of the uncertainty of glacier mass loss rate over the periods of interest (P1 and P2).

Ice sheets contribution: Greenland (see Section 4.5, Figure 5.2.2*)*

Time series from the two alternative approaches as described in Section 5.1.1 were used.

The v2 GMB solution is not corrected for GIA. We apply the GIA contribution for Greenland mentioned to be -5.4 Gt/yr in the D2.4.2 Document (Horwath et al. 2019b, Section 6.4.2) which is based on A et al. (2013).

Ice sheets contribution: Antarctica (see Section 4.6, Figure 5.2.2)

Time series from the two alternative approaches as described in Section 5.1.1 were used.

The altimetry-based product at 140 days resolution is used and has been linearly interpolated at monthly time scale to correspond to other sea level component time scale. The trend uncertainty was computed as the gradient of cumulative uncertainty over the period of interest (cumulative year divided by number of years of interest).

The trend uncertainty over the Antarctica Ice sheet from GRACE is 38 Gt/yr (Horwath et al. 2019b, as an update of Nagler et al. 2018b).
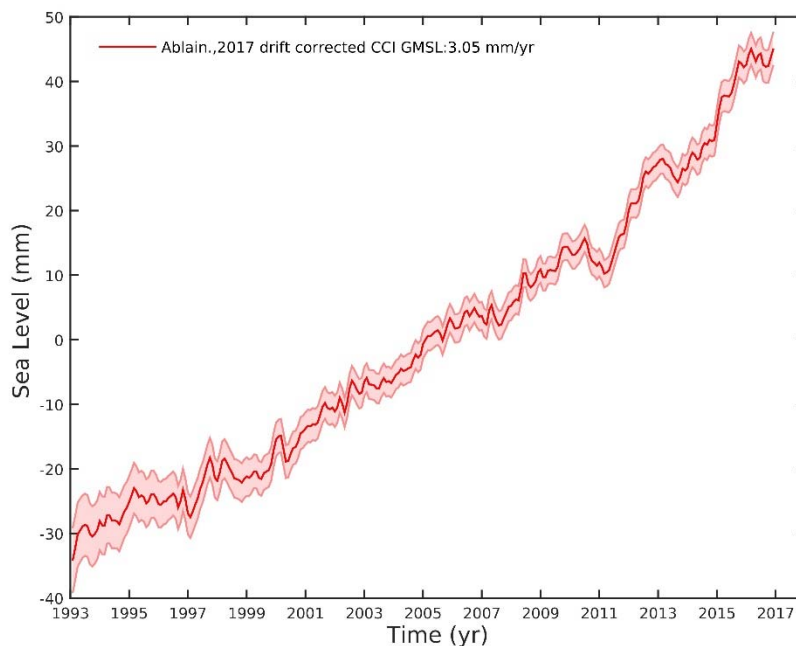
Figure 5.2.1: CCI based GMSL averaged over 65°N and 65°S latitudes, TOPEX A drift correction over Jan. 1993-Feb. 1999 applied

		CCI Sea Level Budget Closure
		ESA/ESRIN contract 4000119910/17/I-NB
		Reference: ESA_SLBC_cci_D4.7
		Version: v1.1
		Date: 14.02.2020
		Page: 70 of 101

Land water contribution (see Section 4.7, Figure 5.2.2)

As in Section 5.1.1, net water mass changes on land were considered using the Global Hydrological Model WaterGAP2.2d (WGHM). Our analysis applies an ensemble mean of different model runs with two irrigation scenarios (70% deficit irrigation and optimal irrigation), and two state-of-the-art climate forcings (WFDEI with GPCC and CRU TS 3.23 precipitation bias-correction).

The uncertainty over each time step is estimated as the RMS of the four data sets from the ensemble mean. The trend uncertainty is the standard deviation of the trend of the individual data sets over the two periods of interest (P1 and P2).

Figure 5.2.2 displays the individual SLBC_cci_v2 mass components time series over 1993-2016.

Ocean mass change from GRACE (see Section 4.3, Figure 5.2.3)

Ocean mass changes products from the sources as described in Section 5.1.1 were used. Different from the ocean mass budget assessment in Section 5.1, here the ocean mass change was considered over the latitude range restricted to 65°S - 65°N, except for the Chambers time series where such a latitude restriction was not available.

Figure 5.2.3 displays the GRACE based ocean mass time series over 2003-July 2016 from various processing groups with the three different GIA corrections applied.
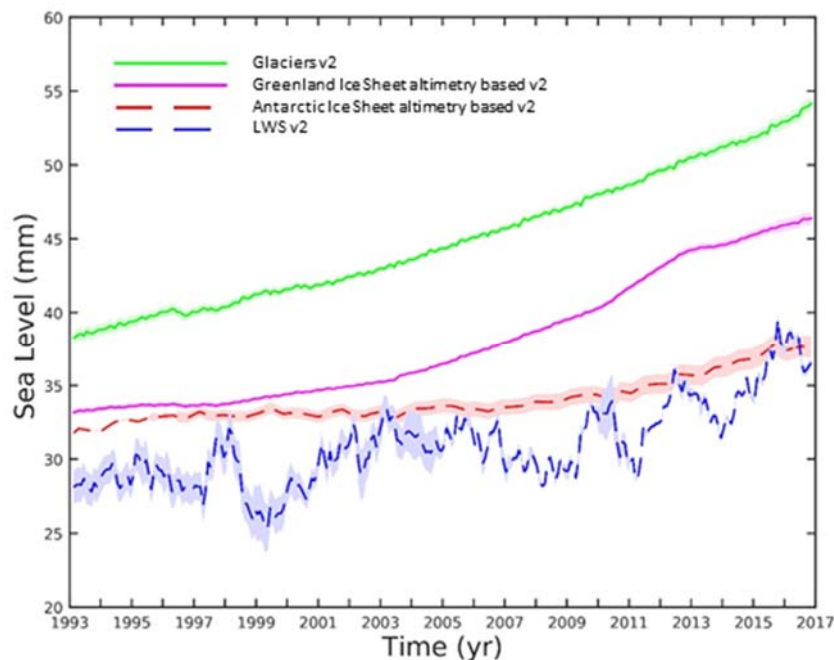
Figure 5.2.2: SLBC_cci v2 mass components in equivalent sea level (mm) contributing to total sea level over 1993-2016

		CCI Sea Level Budget Closure
		ESA/ESRIN contract 4000119910/17/I-NB
		Reference: ESA_SLBC_cci_D4.7
		Version: v1.1
		Date: 14.02.2020
		Page: 71 of 101

Steric sea level component

The SLBC_cci v2 steric product consists of globally averaged and gridded 5°x5° time series over of monthly mean Steric Sea Level Anomaly (SSLA) based on XBT and XCTD and Argo profiles over 2003-2016 as described in Section 4.2. The SLBC_cci v2 steric data covers only until the depth of 2000m. Therefore deep ocean steric trend contribution of 0.1 ± 0.1 mm/yr based on Purkey and Johnson (2010) is considered in the budget assessment along with the contribution until 2000m depth.

Uncertainty estimates are provided at each time step. Trend uncertainty is estimated as the root sum square of the gradient of time step uncertainty over the period of interest and the deep ocean contribution uncertainty of 0.1 mm/yr.

Since the steric SLBC_cci v2 product is available only from 2003, it is therefore used for P(2) budget assessment whereas over the P(1) period, steric data from Dieng et al., 2017 at monthly time scale and thermosteric sea level data from WCRP Global Sea level Budget group (2018) at annual time scale have been used (Figure 5.2.4a). Comparison of SLBC_cci v2 steric data with WCRP Global Sea level Budget group (2018) is in Figure 5.2.4b.

The thermosteric time series estimated until the depth of 2000 m from WCRP (2018) is an ensemble mean from 11 different processing groups that have used XBTs and CTDs during the
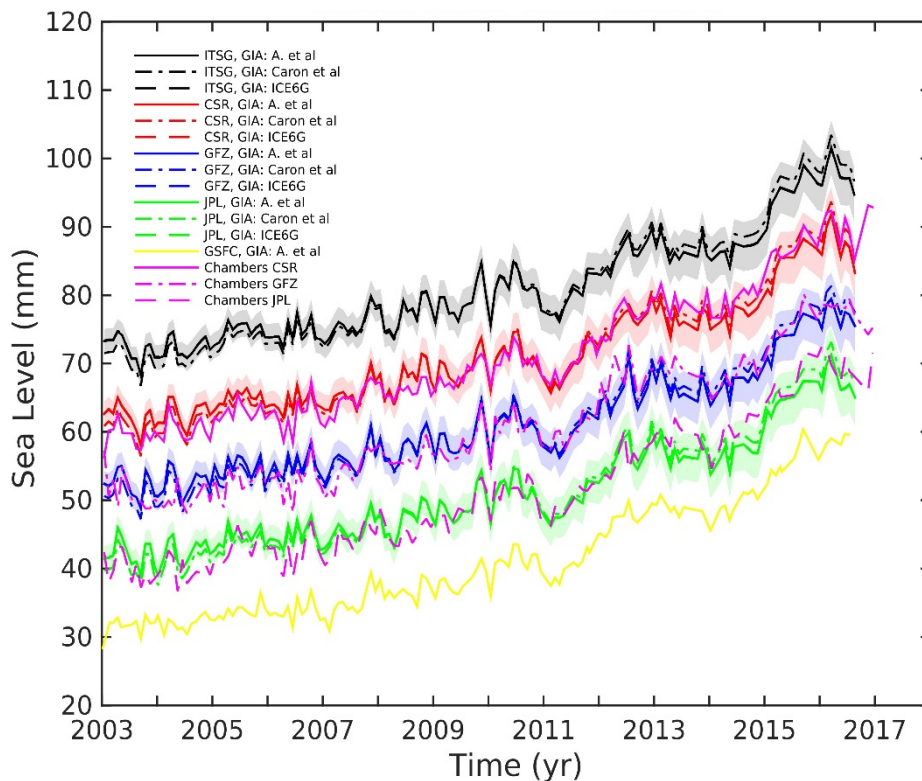
Figure 5.2.3: GRACE based ocean mass contribution in mm from various processing groups with three different GIA corrections over 2003-2016. The main SLBC_cci v2 product is ITSG (in black) while all others shown correspond to supplementary GRACE products.

		CCI Sea Level Budget Closure
		ESA/ESRIN contract 4000119910/17/I-NB
		Reference: ESA_SLBC_cci_D4.7
		Version: v1.1
		Date: 14.02.2020
		Page: 72 of 101

pre-Argo era (i.e. from 1993 until 2003/2005), followed by Argo floats data until 2015. Deep ocean contribution of 0.1 mm/yr has also been included in this data set. The ensemble mean steric time series from Dieng et al. (2017) comprises the following three data sets for the period 1993-2004: the updated versions of Ishii and Kimoto (2009), NOAA data set (Levitus et al., 2012) and EN4 data set (Good et al., 2013). Over the recent years, these data sets integrate Argo data from IPRC, JAMSTEC and SCRIPPS. Deep ocean contribution has also been included.
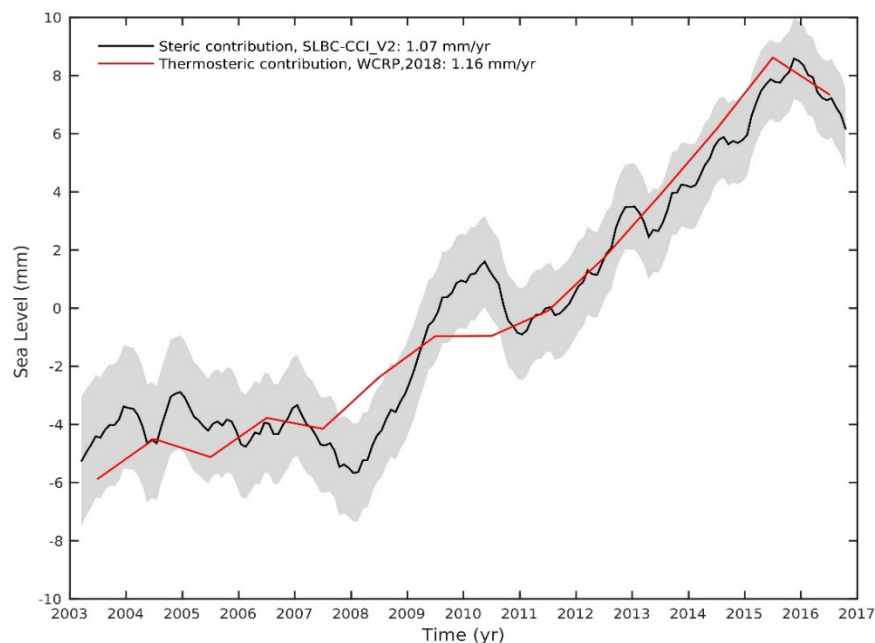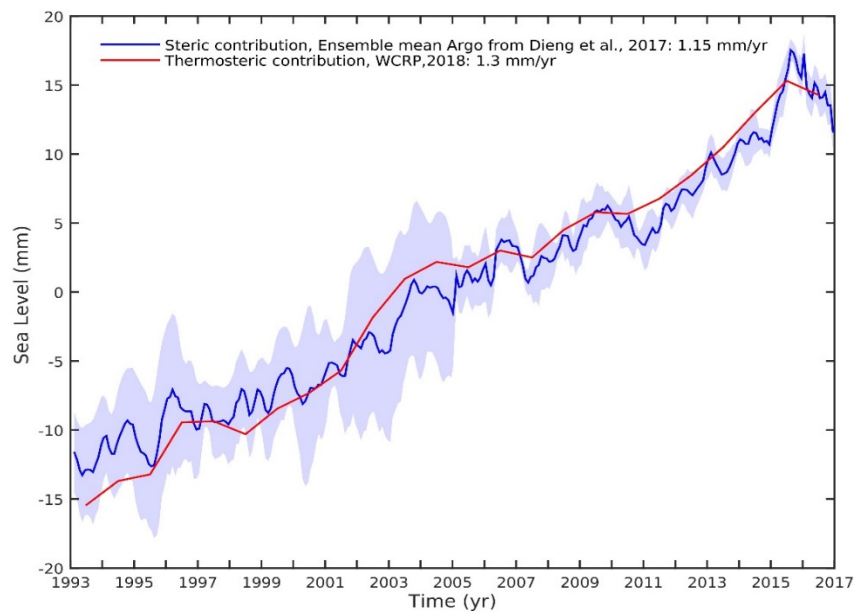
5.2.4: a (top): Dieng et al., 2017 steric (in blue) and WCRP, 2018 thermosteric (in red) sea level time series over 1993-2016. **b (bottom):** SLBC_cci v2 steric (in black) and WCRP, 2018 thermosteric (in red) time series over 2003-2016.

		CCI Sea Level Budget Closure
		ESA/ESRIN contract 4000119910/17/I-NB
eesa		Reference: ESA_SLBC_cci_D4.7
		Version: v1.1
		Date: 14.02.2020
		Page: 73 of 101

5.2.2 Budget assessment

Methods

The annual and semi-annual cycles were removed in all sea level components time series through a least-squares fit of 12-month and 6-month period sinusoids. No interpolation was performed to fill any existing data gaps in the time series. Linear trends were then estimated using the least squares fit methodology on the un-interpolated data without annual and semi-annual cycles.

For the products whose mass components and associated errors are provided in gigatons (Gt) per year, we converted them into mm of sea level equivalent (SLE) by dividing by a factor of 361 (assuming that 361 Gt of ice mass would raise globally the mean sea level by 1 mm approximately). All results below are expressed in mm SLE.

Period P1: the altimetry era (1993-2016)

The global mean sea level budget was estimated by comparing the GMSL observed by satellite altimetry with the sum of the SLBC_cci v2 components except for the steric sea level component over 1993-2016, where steric data from Dieng et al. (2017) was used. Since the thermosteric data from WCRP, 2018 is at annual time resolution, it is used only for annual sea level budget assessment.

Figure 5.2.5 displays the global mean sea level change estimated as the sum of individual SLBC_cci v2 components superimposed to the altimetry-based GMSL. Individual components are also displayed. The global mean sea level trend (Table 5.2.1) obtained as the sum of individual SLBC_cci v2 components over 1993-2016 accounts to 2.91±0.22 mm/yr, whereas observed GMSL trend value accounts to 3.05±0.24 mm/yr leaving a residual of 0.14±0.3 mm/yr. In terms of interannual variability, the GMSL obtained from the sum of components corresponds well with observed altimetry-based CCI GMSL, except in the beginning years. This is expected, as the TOPEX A drift correction between 1993 and 1998 is not yet precise. In addition to this, we can also observe the high uncertainty range in the sum of components time series initially until 2005. This high range of uncertainty is mainly due to the steric component (which also exhibits high uncertainty range between 1993 and 2003) as it is based on XBT data over 1993-2003/2005 and therefore suffers from sparse coverage both geographically and at depth (below 700 m). The RMS of the residual time series over 1993-2016 amounts to 2.2 mm.

		CCI Sea Level Budget Closure
		ESA/ESRIN contract 4000119910/17/I-NB
		Reference: ESA_SLBC_cci_D4.7
		Version: v1.1
		Date: 14.02.2020
		Page: 74 of 101

Table 5.2.1: Observed GMSL trend compared with sum of components trend over 1993-2016

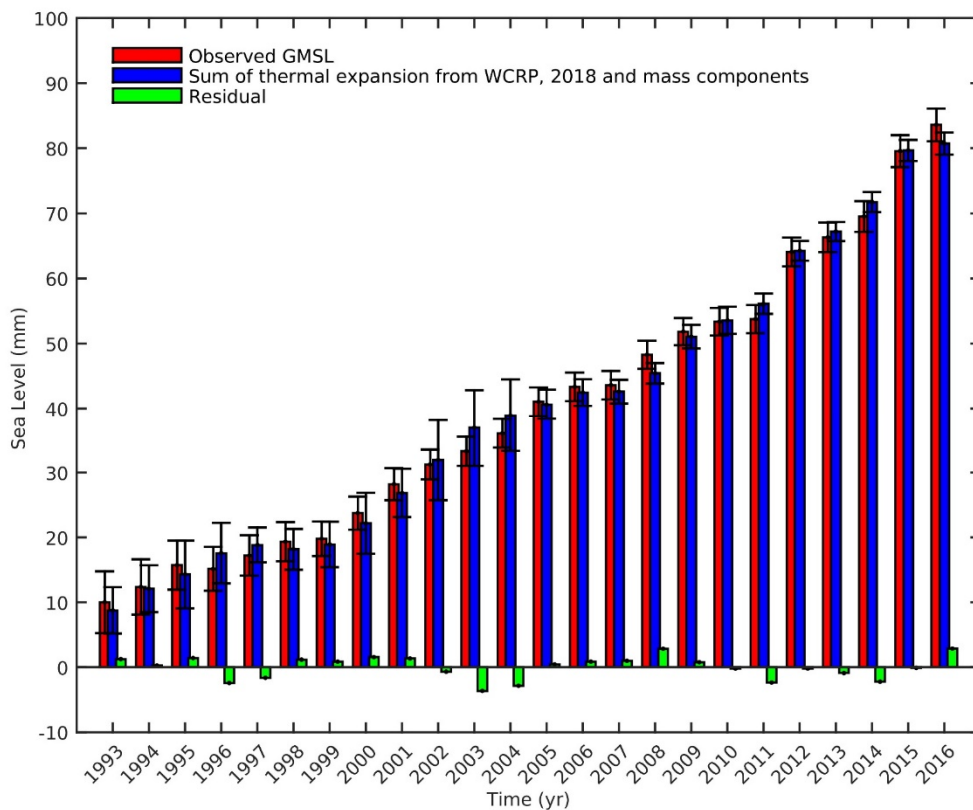|	1993-2016	
Budget	Trend (mm/yr)	Uncertainty (mm/yr)
Observed Altimetry GMSL	**3.05**	**0.24**
Steric, Dieng et al.,2017	1.15	0.12
Glaciers	0.64	0.13
Greenland Ice Sheet	0.43	0.038
Greenland Peripheral Glacier	0.17	0.08
Antarctica Ice Sheet	0.2	0.027
Land Water	0.32	0.1
Sum of components	**2.91**	**0.22**
Residual	0.14	0.3
RMS	2.2 mm	
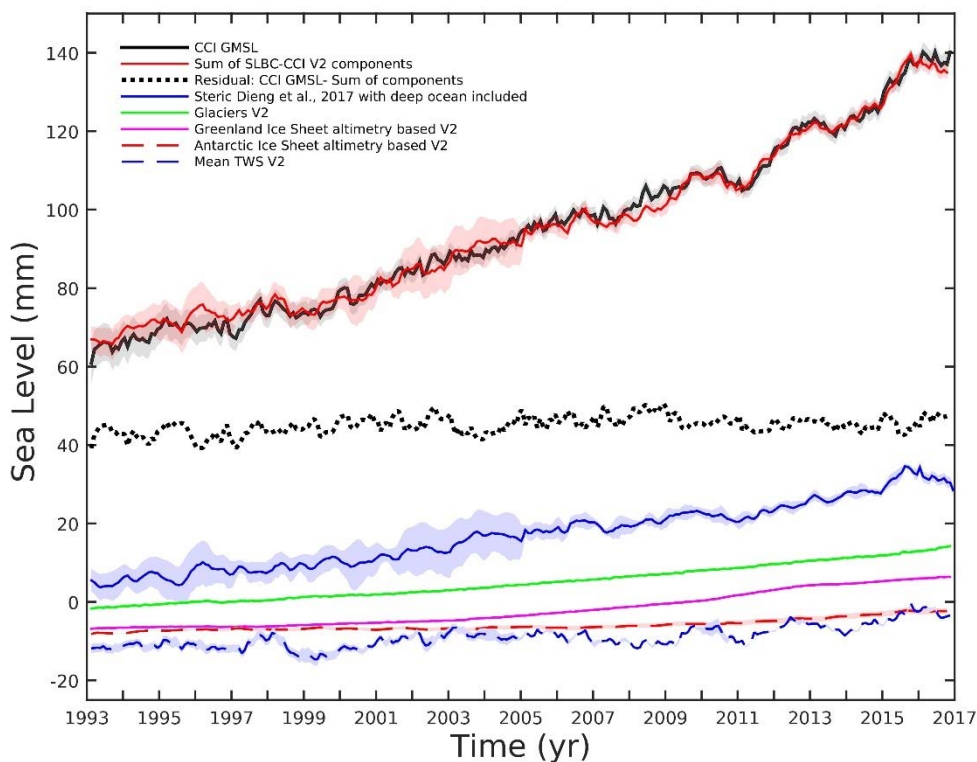
Figure 5.2.5: Observed CCI GMSL (black) superimposed with the GMSL estimated from the sum of SLBC_cci v2 sea level components (in red) over 1993-2016.The residual time series (i.e. CCI GMSL- sum of components) is shown as dotted black time series. The individual components, steric (in blue), glaciers (in green), Greenland (in magenta, altimetry-based), Antarctica (dashed red, altimetry-based) and TWS (dashed blue) are also displayed.

		CCI Sea Level Budget Closure
		ESA/ESRIN contract 4000119910/17/I-NB
		Reference: ESA_SLBC_cci_D4.7
		Version: v1.1
		Date: 14.02.2020
		Page: 75 of 101

In addition to the time series and trend based sea level budget assessment, annual sea level budget was also assessed. Figure 5.2.6 displays the annual sea level budget based on SLBC_cci v2 mass components and WCRP, 2018 thermosteric component and compared with the observed altimetry sea level. We can notice that for most of the years between 1993 and 2016, the annual budget remains closed. Certain years show a small range of residual signal which is within the combined uncertainties. Performing the same assessment using Dieng et al. (2017) steric data instead of the WCRP Global Sea level Budget group (2018) also yields similar results, and hence is not shown.

Period P2: the Argo/GRACE era (2003-2015)

For this time period, the sea level budget closure was investigated by comparing observed GMSL first with the sum of individual SLBC_cci v2 sea level components as in P(1) (explained in the previous section) and then with the sum of steric and GRACE based ocean mass. Table 5.2.2 summarizes the trend value of observed CCI GMSL and sum of each SLBC_cci v2 components contributing to sea level variations over 2003-2016. For the 2003-2016 period, the steric data from this project has been used. Sea level budget assessment over this time period was performed using two different sets of AIS and GIS data: (1) altimetry based, over 2003-2016 complete years (2) GRACE based AIS and GIS contribution over 2003-August2016. In Table 5.2.2, the GRACE based contributions and henceforth the corresponding sea level
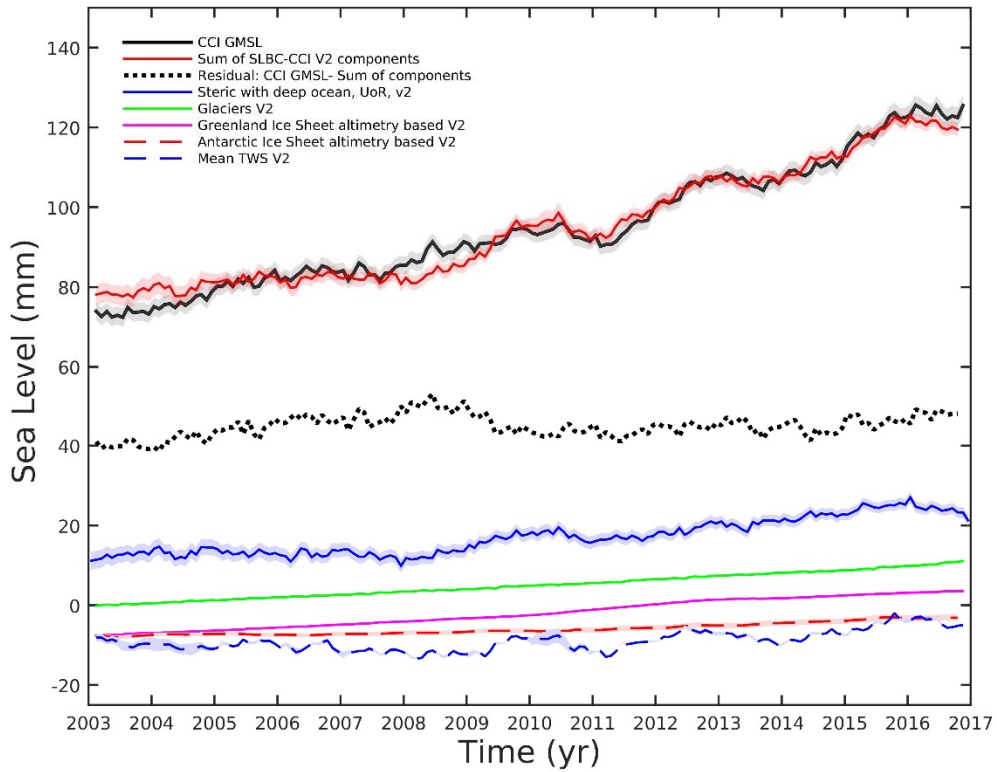

Figure 5.2.6: Annual sea level budget analysis over 1993-2016 using SLBC_cci v2 sea level components

Table 5.2.2: Observed CCI GMSL trend compared with sum of components trend over 2003-2016. GRACE based AIS and GIS contributions and their corresponding budget trend values are in italic.
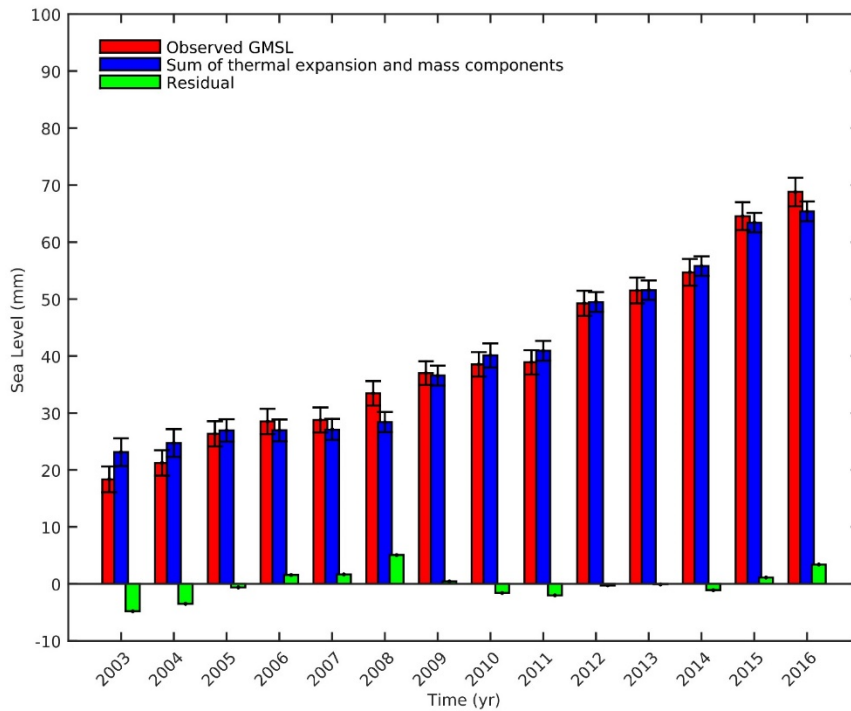
	2003-2016/*2003-July 2016*	
Budget	Trend (mm/yr)	Uncertainty (mm/yr)
Observed Altimetry GMSL	3.66/*3.64*	0.24
Steric UoR v2	1.07/*1.09*	0.1
Glaciers	0.77	0.13
Radar GIS including peripheral/ *GRACE GIS*	0.88/*0.77*	0.11/*0.02*
Radar AIS/ *GRACE AIS*	0.35/*0.28*	0.02/*0.1*
Land Water	0.42/0.41	0.1
Sum of components	3.49/*3.32*	0.22/*0.2*
Residual	0.17/*0.32*	0.32/*0.31*
RMS	2.78 mm/*3.1 mm*	

budget are shown in italic. From the table, we can observe that the sum of components based on altimetry AIS/GIS contributions is 3.49±0.22 mm/yr and whereas the sum based on GRACE AIS/GIS contributions is 3.32±0.2 mm/yr, respectively, thereby leaving a residual of 0.17±0.32mm/yr and 0.32±0.31 mm/yr respectively. The slightly higher trend residual in the case of GRACE AIS/GIS based budget could be attributed to trend estimation over time period when the complete end year is not accounted for. To verify this, sea level budget assessment was performed over August 2003-August 2016, and the residual trend as a result decreased to 0.24±0.3 mm/yr (instead of 0.32±0.31 mm/yr over 2003-July 2016). Figure 5.2.7 displays the global mean sea level budget estimated as the sum of individual SLBC_cci v2 sea level components (in red) superimposed to the CCI observed altimetry based global mean sea level time series (in black) over 2003-2015 and its corresponding residual (dotted black line). The individual components are also displayed in the same figure. Altimetry based AIS and GIS time series are depicted in Figure 5.2.7. (GRACE based time series are also similar and henceforth not shown here).

In addition to trend based sea level budget assessment, annual sea level budget was also assessed. Figure 5.2.8 displays the annual sea level budget based on SLBC_cci v2 sea level components (altimetry based in the case of AIS and GIS) compared with the observed altimetry sea level. We can notice that the annual sea level budget residual is higher in the initial years after which the residuals are lower.

		CCI Sea Level Budget Closure
		ESA/ESRIN contract 4000119910/17/I-NB
		Reference: ESA_SLBC_cci_D4.7
		Version: v1.1
		Date: 14.02.2020
		Page: 77 of 101

Figure 5.2.7: Same as in Figure 5.2.5 but over 2003-2016

**Figure 5.2.8:** Annual sea level budget analysis over 2003-2016 using SLBC_cci v2 sea level components

		CCI Sea Level Budget Closure
		ESA/ESRIN contract 4000119910/17/I-NB
		Reference: ESA_SLBC_cci_D4.7
		Version: v1.1
		Date: 14.02.2020
		Page: 78 of 101

Sea level budget residual analysis in terms of interannual variability

In Figure 5.2.7., taking a closer look at the residual curve (dotted black line), we can observe the amplitude of the residual to be slightly higher over 2005-2009. To study this further, we superimposed detrend altimetry based observed GMSL time series with the detrended sum of components time series as shown in Figure 5.2.9. The residual time series has also been detrended and shown. By detrending the time series, we can obtain time series that contain only its interannual variability. In Figure 5.2.9, we can observe that there is no correlation between the detrended observed GMSL and detrended sum of components time series between 2003 and 2011 after which both detrended time series are well correlated (>0.8). This non-correlation explains the sea level budget residual being higher during over 2003-2011 than the rest of the period of interest.

In order to identify the sea level component responsible for the sea level budget non correlation in terms of interannual variability over 2003-2011, we adopted the methodology by Dieng et al. (2015). We compared the detrended time series of each sea level component with the inverse (i.e. multiplied by -1) of the detrended residual time series. The two main components that contribute to the interannual variability in global mean sea level are the steric and land water components. The rest of the sea level components: glaciers, AIS and GIS do not contribute to total sea level in terms of interannual variability.

Figure 5.2.10 shows the comparison of the inverse detrended sea level budget residual time series with detrended steric (Figure 5.2.10a) and detrended land water (Figure 5.2.10b) components. High correlation (>0.8) between the detrended steric and inverse detrended residual between 2003 and 2010 (visible in Figure 5.2.10a) shows that it is the steric
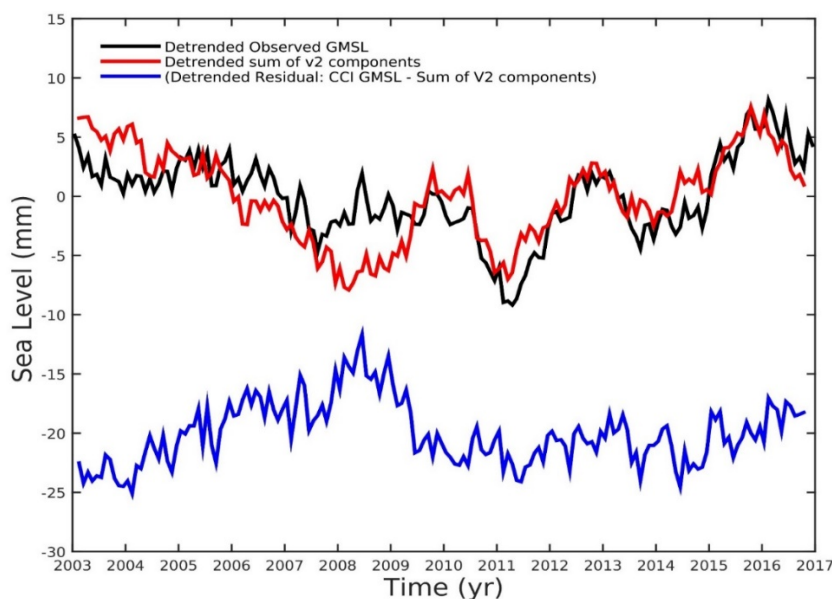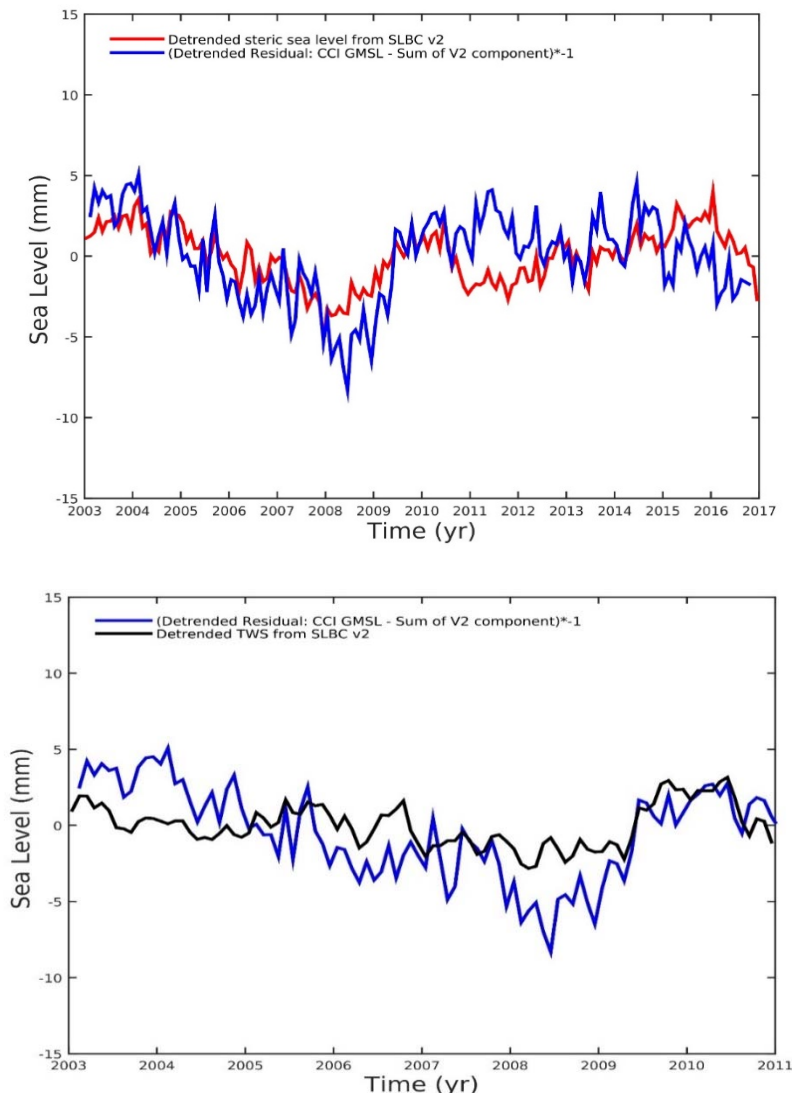

Figure 5.2.9: Comparison of detrended observed sea level (in black) with detrended sum of components (red). The detrended residual is also displayed (in blue)

		CCI Sea Level Budget Closure
		ESA/ESRIN contract 4000119910/17/I-NB
		Reference: ESA_SLBC_cci_D4.7
		Version: v1.1
		Date: 14.02.2020
		Page: 79 of 101

component that contributes to the sea level budget mis-closure in terms of interannual variability over this period. Similarly, high correlation (>0.8) between detrended land water and inverse detrended residual time series over 2010-2011 (and not before) shows that the land water component contributes to the mis-closure in terms of interannual variability over 2010-2011 (Figure 5.2.10b).

Sea level budget using GRACE ocean mass

Over 2003-2016 time period corresponding to the Argo/GRACE era, the individual mass components (glaciers, AIS, GIS, TWS) can be replaced by ocean mass directly observed by GRACE. Therefore, over this time period the sea level budget was also performed using the main and supplementary SLBC_cci v2 GRACE ocean mass products over Jan.2003-Aug.2016. Table 5.2.3 summarizes their corresponding trend values, residual trends and RMS.

Figure 5.2.10 a (top): Comparison of detrended steric sea level time series with inverse (i.e. multiplied by -1) detrended sea level budget residual. **b (bottom):** Comparison of detrended land water time series with inverse (i.e. multiplied by -1) detrended sea level budget residual

		CCI Sea Level Budget Closure
	TECHNISCHE UNIVERSITÄT DRESDEN — Universität Zürich — UNIVERSITY OF LEEDS — LEGOS — Universität Bremen — GOETHE UNIVERSITÄT FRANKFURT AM MAIN — DTU Space National Space Institute — University of Reading — MERCATOR OCEAN INTERNATIONAL	**ESA/ESRIN contract 4000119910/17/I-NB**
esa		Reference: ESA_SLBC_cci_D4.7
		Version: v1.1
		Date: 14.02.2020
		Page: 80 of 101

Table 5.2.3: Observed CCI GMSL trend over Jan. 2003 - Aug. 2016 compared to the sum of components, where the mass component is based on GRACE. Individual columns correspond to different GRACE solutions.

| Trend (mm/yr)	Jan. 2003-August 2016				
	ITSG A et al.,2013	ITSG Caron et al., 2018	ITSG ICE6G	GSFC Mascon	Mean Chambers (Global)
Observed GMSL	3.58±0.24	3.58±0.24	3.58±0.24	3.58±0.24	3.58±0.24
Steric v2	1.07±0.1	1.07±0.1	1.07±0.1	1.07±0.1	1.07±0.1
GRACE	1.89±0.25	2.18±0.25	1.87±0.25	2.11	2.17
Sum	2.96±0.27	3.25±0.27	2.94±0.27	3.18	3.24
Residual	0.62±0.36	0.33±0.36	0.64±0.36	0.4	0.34
RMS (mm)	3.67	2.94	3.7	3.08	2.94

In terms of sea level budget residual trend values, the ITSG GRACE ocean mass based with Caron et al., 2018 GIA correction produces the least residual trend of 0.33±0.36 mm/yr and RMS of 2.94 mm. Figure 5.2.11 displays the sea level budget analysis performed using the ITSG Caron et al., 2018 GRACE ocean and SLBC_cci v2 steric component. If we consider full years for the trend estimation, i.e., between August 2003 (instead of Jan. 2003) and August 2016, the residual trend slightly decreases to 0.27±0.36 mm/yr with a RMS of 2.7 mm. The steric + GRACE and the residual trend uncertainties are estimated as the RSS of the steric and GRACE uncertainties.
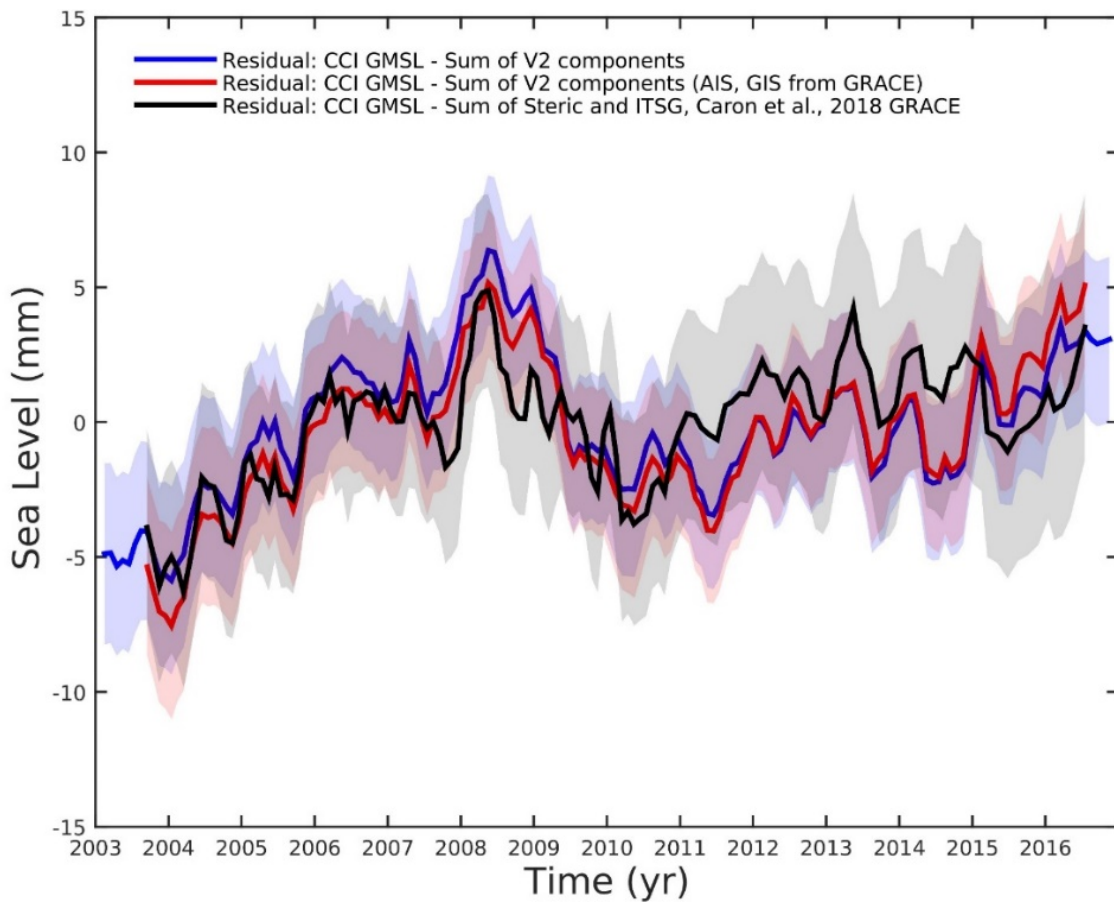
5.2.3 Discussion and conclusions

In terms of trend estimation, SLBC_cci v2 products have brought the global sea level budget mis-closure over P(1) closer to zero, as compared to the v1 products. The inclusion of peripheral glaciers in Greenland has contributed to this improvement. For 1993-2016, the residual trend and the RMS of the residuals amount to 0.14±0.3 mm/yr and 2.2 mm, respectively. For 2003-2016, the residual trend amounts to 0.17±0.3 mm/yr and 0.33±0.36 mm/yr using the sum of mass components and GRACE ocean mass respectively.

Over 2003-2016, the sea level budget residual time series are well within the uncertainty estimates contributed by all sea level components. Figure 5.2.12 displays the sea level budget residual time series estimated using (a) sum of all v2 components with AIS and GIS based on radar altimetry, (b) sum of v2 components with AIS and GIS from GRACE, (c) sum of steric and GRACE ocean mass. The corresponding uncertainties are also displayed. The residual uncertainties are estimated as the RSS of the GMSL and sea level components uncertainties. We can observe that the residual budget time series are well within their uncertainty range.

		CCI Sea Level Budget Closure
		ESA/ESRIN contract 4000119910/17/I-NB
		Reference: ESA_SLBC_cci_D4.7
		Version: v1.1
		Date: 14.02.2020
		Page: 81 of 101

In terms of interannual variability, important sea level budget residuals still remain between 2003 and 2011 and have been attributed to steric and land water components. Efforts are needed to understand the cause of their roles in the sea level budget mis-closure in terms of interannual variability in the future.
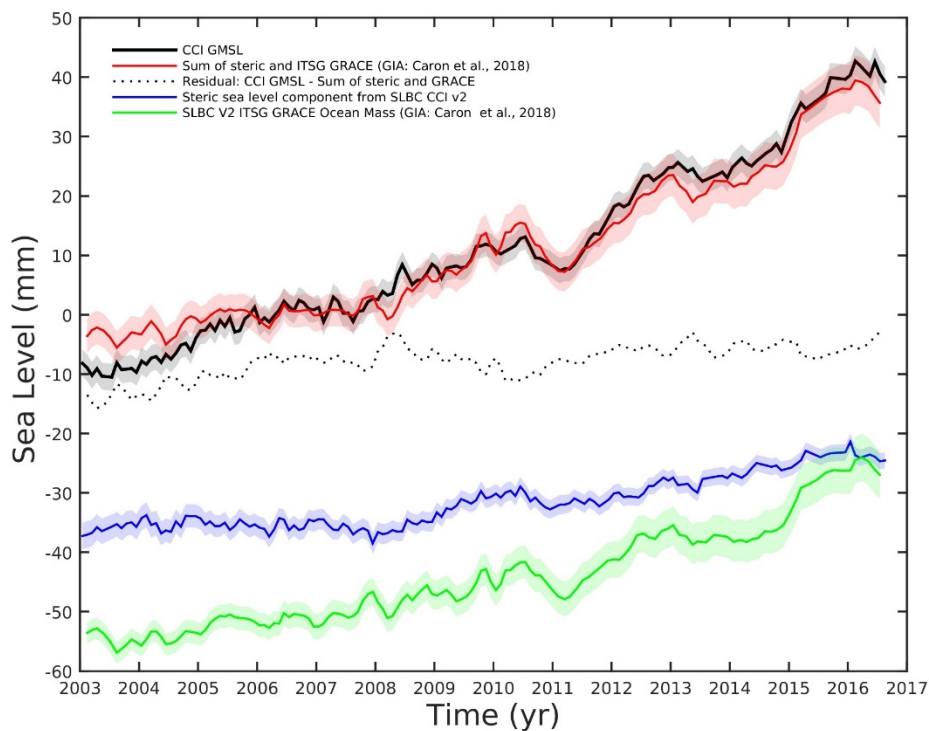
Figure 5.2.11: Sea level budget analysis using ITSG Caron et al., 2018 GRACE (green) ocean mass and SLBC_cci v2 steric component (blue). The observed GMSL is in black, sum of GRACE and steric in red and residual time series in black dotted lines.

		CCI Sea Level Budget Closure
		ESA/ESRIN contract 4000119910/17/I-NB
		Reference: ESA_SLBC_cci_D4.7
		Version: v1.1
		Date: 14.02.2020
		Page: 82 of 101

Figure 5.2.12: Sea level budget residual time series estimated using (a) sum of all v2 components with AIS and GIS based on radar altimetry (in blue), (b) sum of v2 components with AIS and GIS from GRACE (in red), (c) sum of steric and GRACE ocean mass (in black)

		CCI Sea Level Budget Closure
		ESA/ESRIN contract 4000119910/17/I-NB
		Reference: ESA_SLBC_cci_D4.7
		Version: v1.1
		Date: 14.02.2020
		Page: 83 of 101

5.3 Arctic sea level budget

5.3.1 Data summary

The DTU Arctic altimeter data. The spatial distribution of data coverage of the altimeter data in the Arctic Ocean is shown in Figure 5.3.1. It is clear that distinct areas inside the Arctic Ocean only have data availability less than 25%. As this is also seasonally dependent it can be concluded that large part of the Arctic Ocean offers limited altimeter-based estimates of sea surface height (SSH), in particular during winter. In turn, the time series and associated trends of altimeter-based SSH estimates are inflicted with uncertainties.

A reduction in the overall trend in the Arctic sea level is noted during the past 14 years (2003-2016; 1.2 mm/yr) compared to the full time period (1993-2016; 2.4 mm/yr), see Figure 5.3.2. There is also a distinct evidence of sea level decline on the Siberian shelf during the latter period.

GRACE Ocean mass data: SH solution and mascons are the two main solutions of GRACE ocean mass data. Examples of 3 SH-Solutions estimated in the SLB_cci project is shown in Figure 5.3.3. The SH solutions cannot include areas close to the coast (~300km), as they would include signal that leaks in from the continents. Hence, the total spatial coverage in the Arctic is rather poor, leading to non-preferred SH solutions in the Arctic Ocean.
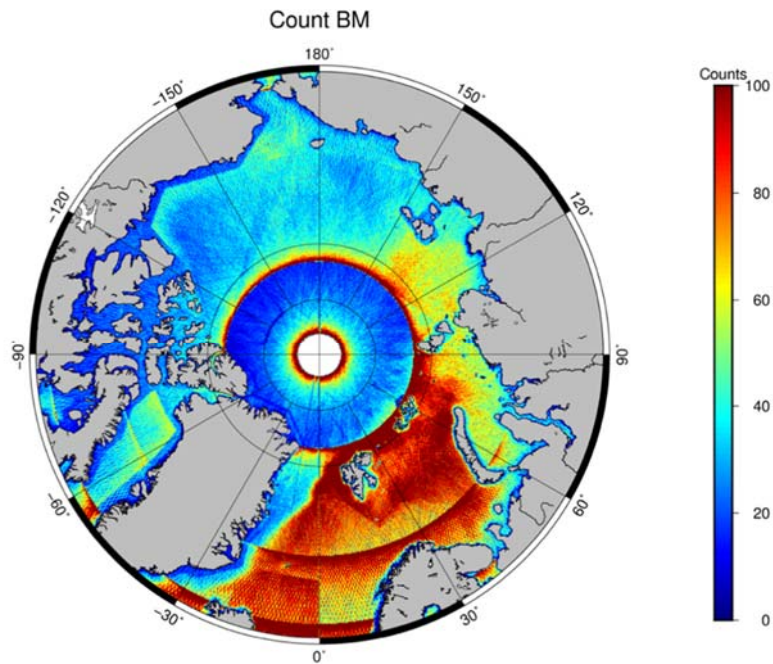
In contrast, the mascons are not just representing gravity measurements, they also include localised pre-assumptions and a-priori information. In this project, two mascons products, one from JPL and one from GSFC, for the period 2003-2016 are used to examine the ocean mass change in the Arctic Ocean (Figure 5.3.4).

Our analysis reveals that the trend in ocean mass change for the time period 2003-2016 (Figure 5.3.4) is much higher in the GSFC mascon product (4.9 mm/yr) compared to the JPL data (2.0 mm/yr).

Additional datasets used for the sea level budget assessment include:

- EN4, version 4 of the Met Office Hadley Centre "EN" series of global quality-controlled ocean temperature and salinity profiles (T&S) for the time period 2003-2016.
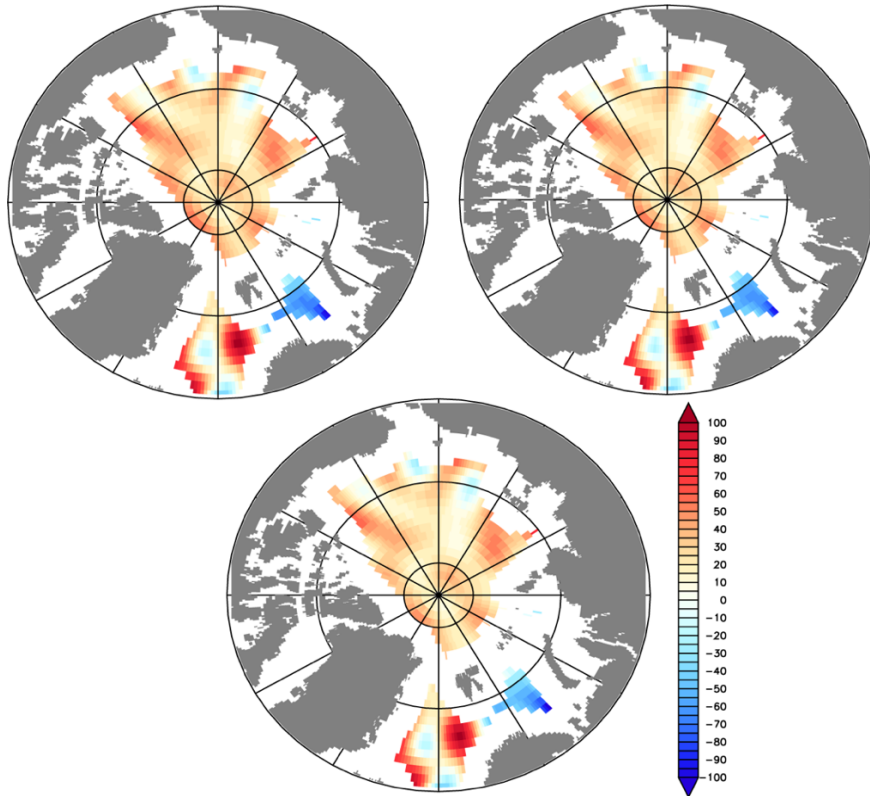- Monthly gridded NERSC TOPAZ4 reanalyses data for the period 2003-2016.

		CCI Sea Level Budget Closure
		ESA/ESRIN contract 4000119910/17/I-NB
		Reference: ESA_SLBC_cci_D4.7
		Version: v1.1
		Date: 14.02.2020
		Page: 84 of 101

Count BM

Figure 5.3.1: Illustration of the altimeter-based data coverage for the Arctic Ocean for the year 2015.
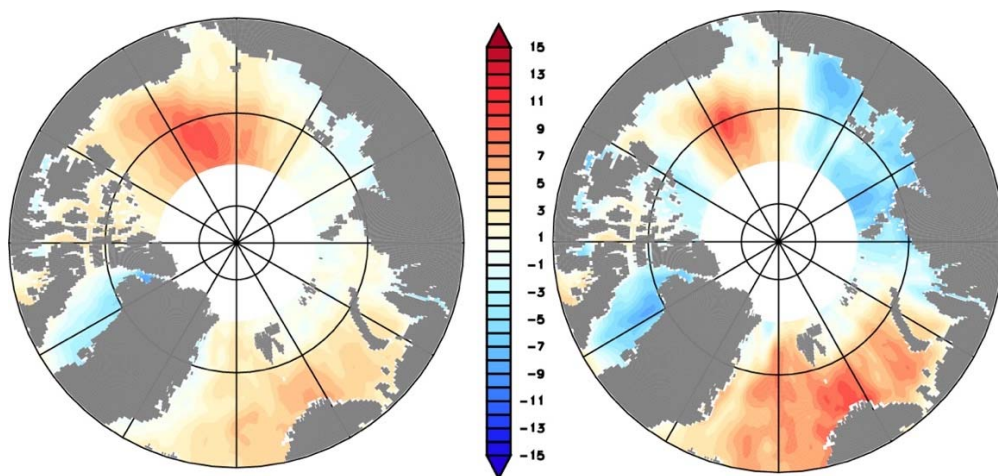
Figure 5.3.2: Sea level trend for the two time periods: 1993-2016 (left; mean **2.4 mm/yr**) and 2003-2016 (right; mean **1.2 mm/yr**)

	CCI Sea Level Budget Closure
	ESA/ESRIN contract 4000119910/17/I-NB
	Reference: ESA_SLBC_cci_D4.7
	Version: v1.1
	Date: 14.02.2020
	Page: 85 of 101

Figure 5.3.3: Ocean mass change gridded products (April 2011; kg/m²) based on ITSG2018 using three different GIA models, A2013-Ice5Gv2 (upper left), Ice-6Gv5a (upper right), CaronIvins2018 (lower)
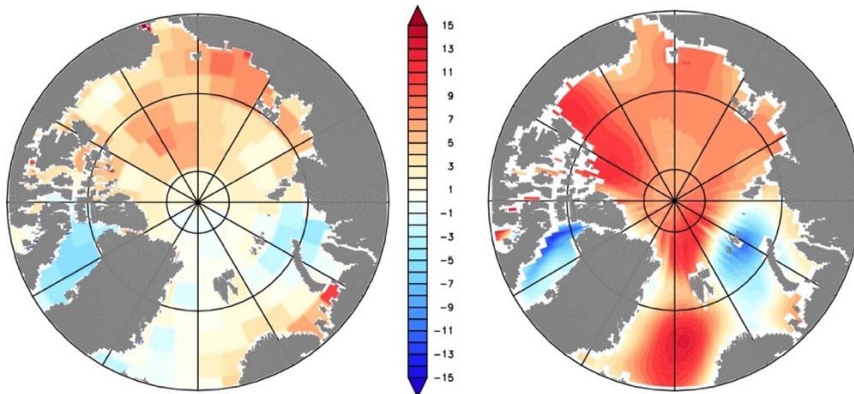
Figure 5.3.4: Trend in ocean mass change for the time period 1993-2016: (left) JPL (mean **2.0 mm/yr**); (right) GSFC (mean **4.9 mm/yr**)

		CCI Sea Level Budget Closure
		ESA/ESRIN contract 4000119910/17/I-NB
		Reference: ESA_SLBC_cci_D4.7
		Version: v1.1
		Date: 14.02.2020
		Page: 86 of 101

5.3.2 Budget assessment

The Arctic sea level budget from observations is shown in Figure 5.3.5. In this assessment the coverage for the Arctic region is the entire ocean area north of 65°N. The sum of the ocean mass change (mean 2.0 mm/yr) and steric height (mean 1.4 mm/yr) trend in the Arctic Ocean is found to be higher than the trend in Arctic Sea level (mean 1.2 mm/yr). The residual is found to be bipolar, being positive in the Nordic Seas- Barents Sea region and negative over the rest of the Arctic, especially in the Beaufort Gyre and in parts of the Siberian Shelf. A positive signature in the residual indicates that the trend in sea level is higher compared to the sum of the trend in ocean mass change and steric height.

The TOPAZ sea level budget assessment is shown in Figure 5.3.6 and is compared to the observation-based budget assessment of the same quantities shown in Figure 5.3.5. The total SSH trend is clearly different being almost 3-times larger in the TOPAZ4 simulations (mean 3.5 mm/yr) compared to the altimeter-based observations (mean 1.2 mm/yr). The steric components, on the other hand, are comparable (mean 2.0 mm/yr for TOPAZ4 versus mean 1.4 mm/yr for EN4). This is somewhat expected as TOPAZ4 is assimilating the EN4 data set. However, several distinct regional differences are noticed, such as in the Beaufort Gyre and the Lofoten Basin within the Norwegian Sea. Regarding the trends in the mass change components it should be noted that they are not comparable. First, the TOPAZ4 value is simply emerging from the total SSH minus the steric component and is not properly accounting for the ice sheet melting and change of the geoid. Second, the GRACE values are representing one of the two mascon products, none of which have been adequately validated for the high latitude and Arctic Ocean.
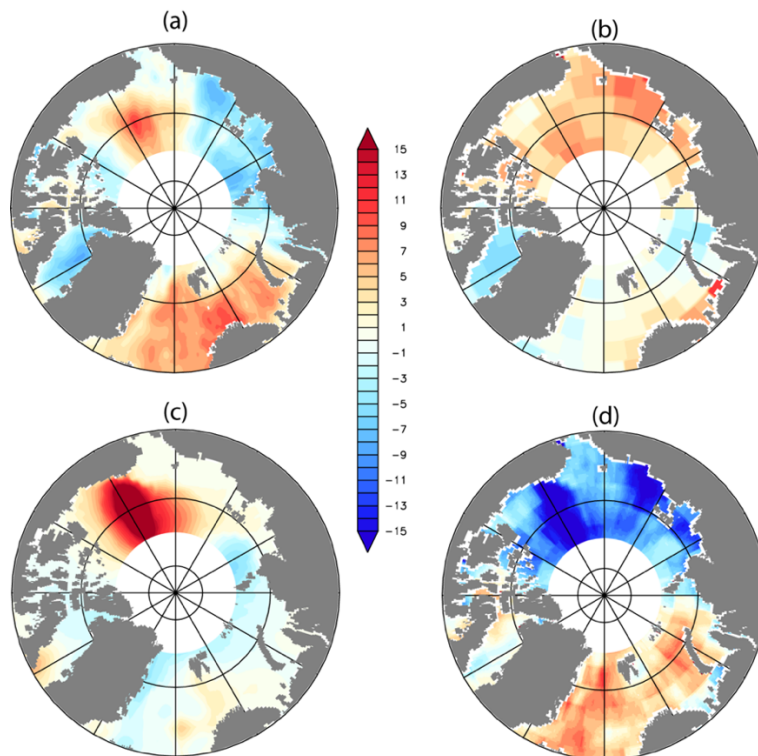
5.3.3 Discussion and conclusions

The sea level trend in the high latitude seas and Arctic Ocean (Figure 5.3.5a) shows that there are two distinct regions with increasing trend (Nordic Seas-Barents Sea and Beaufort Sea) and two regions with decreasing trend (Canadian Archipelago and Siberian Shelf) in sea level. This is an indication of the complexity of the Arctic region, where distinct local differences are prominent due to the presence of sea ice as well as the large range in water depths and differences in water masses.

In order to further assess these results, the time series and corresponding mean linear trend estimates are compared in Figure 5.3.7. This comparison includes the SSH from altimetry, the mass changes derived from GRACE and the ocean steric contribution derived from the EN4 in-situ climatology of temperature and salinity.

Inter-comparison of the time series of the sea level change and ocean mass change over the Arctic region reveals two distinct time periods during which the two time-series are either in-phase or out-of-phase. During the 7-year time-period (2003-2009) the time series are in-phase, while during the next 6 years, 2010-2015, they are out-of-phase. Moreover, the steric height variability is in phase with the ocean mass change over the entire time period. This result

		CCI Sea Level Budget Closure
		ESA/ESRIN contract 4000119910/17/I-NB
		Reference: ESA_SLBC_cci_D4.7
		Version: v1.1
		Date: 14.02.2020
		Page: 87 of 101

Figure 5.3.5: Trend in (a) sea level; mean **1.2 mm/yr**, (b) ocean mass change; mean **2.0 mm/yr**, and (c) steric height; mean **1.4 mm/yr** for the time period 1993-2016. (d) The residual trend (ssh-ocean mass+steric); mean -**2.2 mm/yr**.
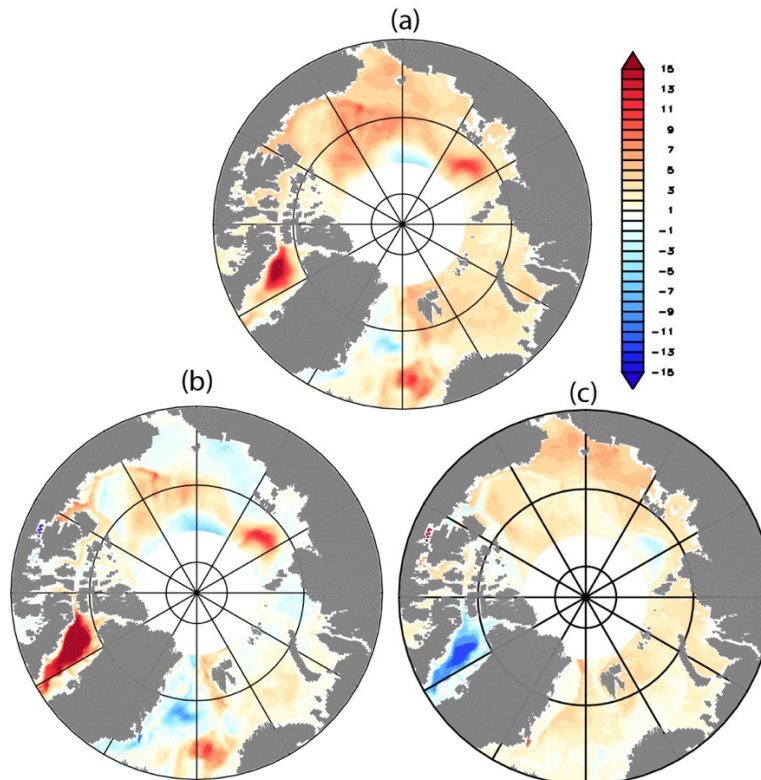

Figure 5.3.6: Trend in TOPAZ sea level (**3.5 mm/yr**), steric height (**2.0 mm/yr**) and ocean mass change (**1.5 mm/yr**) for the time period 1993-2016.

		CCI Sea Level Budget Closure
		ESA/ESRIN contract 4000119910/17/I-NB
·eesa	TECHNISCHE UNIVERSITÄT DRESDEN · Universität Zürich · UNIVERSITY OF LEEDS · LEGOS · Universität Bremen · GOETHE UNIVERSITÄT FRANKFURT AM MAIN · DTU Space National Space Institute · University of Reading · MERCATOR OCEAN INTERNATIONAL	Reference: ESA_SLBC_cci_D4.7
		Version: v1.1
		Date: 14.02.2020
		Page: 88 of 101

is yet another example of the complexity and challenges associated with the sea level budget study of the high latitude seas and Arctic Ocean.

All in all, these results suggest that:

- It is highly necessary to:
    - Improve the geographical and seasonal altimeter coverage and reduce polar gap;
    - Improve estimation of the steric component through more in-situ hydrographic observations with better coverage;
    - Data within sea ice do not have sea state bias information. This component has significant contribution in the Arctic Ocean and should be included through, for instance, the use of the SAMOSA+ retracker for Cryosat which is available in the ESA GPOD SARvatore for Cryosat-2 online processing service (https://gpod.eo.esa.int/services/CRYOSAT_SAR)." In addition newer satellites like ICESAT-2 and Sentinel- should be introduced;
    - Significant uncertainty can be subscribed to 3 the shift of altimetry sensor from LRM to SAR in the middle of the time series;
    - Create long time series from multiple altimeter satellites whereby biases connected with different corrections and processing methods are reliably removed;
- Closing of the regional sea level budget for the Arctic Ocean and neighboring seas at annual and possibly seasonal time scales will depend on reliable estimates with uncertainties of the individual components, notably:
    - proper estimates of seasonal bias in data coverage, especially with respect to sea ice;
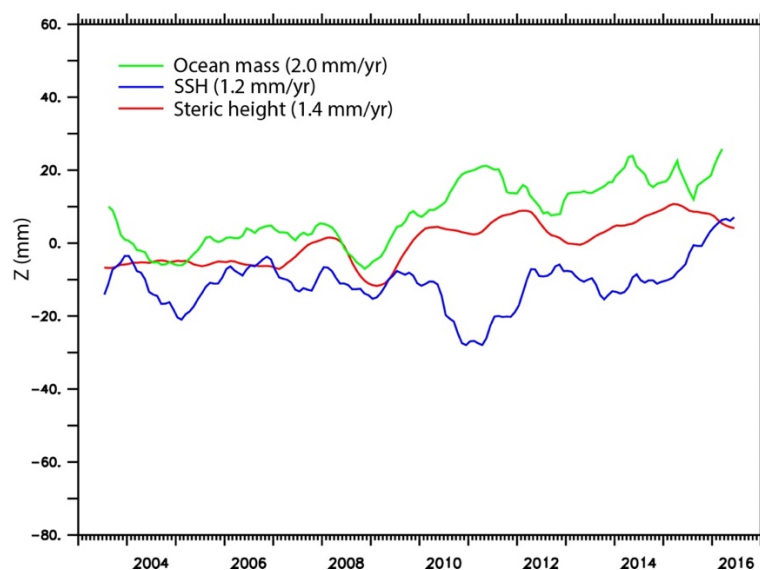
Figure 5.3.7: Time series (1 year running mean) and corresponding mean linear trend estimates (in parenthesis) of the sea surface height (SSH) from altimetry (blue), mass changes from ice sheet melting converted to ssh from GRACE (green), and ocean steric contribution (red) for the time period 2003 to 2016. Area corresponds to the entire Arctic region outside the polar gap.

		CCI Sea Level Budget Closure
		ESA/ESRIN contract 4000119910/17/I-NB
		Reference: ESA_SLBC_cci_D4.7
		Version: v1.1
		Date: 14.02.2020
		Page: 89 of 101

- better estimate of leakage of signals in the GRACE data due to coarse spatial resolutions;
- including trend assessment for sub-regions, in addition to the entire region north of 66°N.

- Future perspectives include:
    - Correction of LRM altimeter data (e.g., water level from sea ice covered oceans) using ALES+ ocean re-tracker; and including Cryosat-2 in this computation to have identically processed data throughout the time series to avoid retracker bias.
    - A new Global tailored-kernel solution (similar to mascons) of the GRACE ocean mass data based on SH. Also extending the time series with GRACE-FO
    - Assimilation of SMOS salinity in TOPAZ model (an initiative funded by ESA under the Arctic + Salinity project).
    - Doubling the resolution of the TOPAZ model (funded by the Copernicus Marine Services).

		CCI Sea Level Budget Closure
		ESA/ESRIN contract 4000119910/17/I-NB
		Reference: ESA_SLBC_cci_D4.7
		Version: v1.1
		Date: 14.02.2020
		Page: 90 of 101

6. Conclusions

6.1 SLBC_cci achievements

The SLBC_cci project has put forward developments to improve, in a coordinated way, data products on every element of the sea level budget and ocean mass budget. Major achievements for the individual budget elements were the following:

Global mean se level (Section 4.1): A major achievement under the SLBC_cci project using GMSL time series from the ESA CCI 2.0 gridded sea level data averaged is the incorporation into our analysis of the uncertainty estimate over each GMSL time step from Ablain et al. (2019). Three major sources of errors were considered in performing variance-co variance matrix to obtain GMSL uncertainty. In terms of trend uncertainty, Ablain et al. (2019) estimates the GMSL trend uncertainty to be ± 0.4 mm/yr (90% confidence level, after correcting the TOPEX A drift) which means that at 1 sigma the uncertainty is ± 0.24 mm/yr. As altimetry record increases in length in future, the uncertainty estimate is expected to improve and change.

Steric sea level change (Section 4.2): We developed a formal uncertainty framework around the estimation of steric height from Argo profiles, including propagation to gridded and time series products. The framework includes simple models to estimate each uncertainty source and their error covariance structures. Inclusion of sea surface temperature from SST-cci at the surface and in the mixed layer, including uncertainties, constrains estimates of steric change in the upper ocean and improves coverage early in the Argo record.

Ocean mass change (Section 4.3): Implementation of, and advances in, methodology to infer OMC from GRACE SH solutions. Application of the methodology to the most recent GRACE solution releases. Elaboration of comprehensive insights into the sensitivity to ccoices of input data and to methodological choices, such as details of the treatment of background models.

Glacier contribution (Section 4.4): The introduction of an ensemble approach to reconstruct glacier mass change and the systematic multi-objective optimization of the global model parameters lead to results that generally confirm the previous estimates, and which also agree well with methods based on observations only (Zemp et al., 2019). However, the increased model performance (higher correlation with observations on individual glaciers, better representation of the observed variance of mass balance) increases the confidence in the results.

Ice sheet contribution – Greenland (Section 4.5): We devised an empirical and effective way to convert the radar altimetry elevation changes into mass changes. The resulting time series has been independently tested against the GRACE derived time series and it has shown very high compatibility. Moreover we gained deeper insight into the uncertainty assessment for the Greenland mass balance for both the GRACE and the altimetry-based estimates.

		CCI Sea Level Budget Closure
		ESA/ESRIN contract 4000119910/17/I-NB
eesa	(university logos)	Reference: ESA_SLBC_cci_D4.7
		Version: v1.1
		Date: 14.02.2020
		Page: 91 of 101

Thanks to the coherent and homogenized datasets of this project, we could compute the sea level fingerprint for all the present-day contribution to the sea level rise. Most importantly we found that such sea level fingerprint could be a potential source of a small but systematic error in the sea level measured by altimetry.

Ice sheet contribution – Antarctica (Section 4.6): The new time series of Antarctica mass change from satellite radar altimetry is the result of an improved processing chain and a better characterization of uncertainties. With a time-evolving ice and snow density mask and a new method for interpolating surface elevation change in areas located beyond the latitudinal limit of satellite radar altimeters and in between satellite tracks, we have provided an updated time series of Antarctica mass change from 1992 to 2017 revealing that ice losses at Pine Island and Thwaites Glaciers basins are about 6 times greater than at the start of our survey.

Land water contribution (Section 4.7): Enhancement of reservoir operation algorithm implemented in model by including commissioning year for individual reservoirs. Implementation of regional model parameterizations to improve simulation of GWD trends. Acquisition of comprehensive insights into the model sensitivity to choices of irrigation water use assumption and climate input data. Development of a non-standard model version that includes the effect of glacier water storage variations on the continental water cycle.

Arctic Ocean focus for all components (Section 4.8): Despite the fact that the Arctic Ocean is notoriously difficult for altimeter-based sea level observations important progress have been made to understand and consolidate sea level budget closure for the Arctic. Sea level budget closure is highly dependent on i.e. the products used (i.e. GRACE solution). Closure found on the mm/year level was consequently considered successful. Significant regional variability revealed the complexity of the changes observed in the Arctic Ocean with distinct contributions from in and outflow and local pressure variations.

Significant efforts have been made by the multidisciplinary consortium to converge to a **unified framework** for their data products and uncertainty characterisation to allow for their consistent combination in sea level budget and ocean mass budget analyses. This framework addressed aspects like

- the definition of common temporal intervals (with the core intervals being the altimetry era 1993-2016 and the GRACE/Argo era 2003-2016)
- the definition of a baseline state (the mean state over the 10-year interval 2006-2015) as the reference for time series of changes of sea level and its contribution
- uncertainties expressed for the changes w.r.t. this reference state. Account for temporal correlation in the uncertainty characterisation

The ocean mass budget and the sea level budget assessments were performed by pursuing the realization of the common framework. New aspects of budget assessments were explored:

		CCI Sea Level Budget Closure
		ESA/ESRIN contract 4000119910/17/I-NB
		Reference: ESA_SLBC_cci_D4.7
		Version: v1.1
		Date: 14.02.2020
		Page: 92 of 101

- statistics of ocean mass budget misclosure on a monthly level compared to monthly uncertainties
- preliminary analyses on the the seasonal components of the ocean mass budget
- investigations into causes of misclosure from a joint analysis of total sea level budget and ocean mass budget.

For the long-term trends over the two periods 1993-2016 (the altimetry period) and 2003-2016 (the GRACE / Argo period), the budget of the global sea level and of the ocean mass is closed within uncertainties on the order of 0.3 mm/yr (1 sigma). Moreover, the budgets are also closed within uncertainties for interannual variations.

We stress that any closure that is much better than the combined uncertainties of the involved elements may just be a coincidence of errors compensating each other. While SLBC_cci has worked on improving the uncertainty assessments for the involved elements, some systematic uncertainties involved could not be reduced within the project (such as GIA and Degree-1 uncertainties for GRACE-based ocean mass change). Ironically (but in agreement with expectations) the rigorous uncertainty assessment increased the stated uncertainties in some cases (compare the results for GMSL in Figure 4.1.1).

The **sea level budget analysis for the Arctic Ocean** (the region north of 65°N) underlined the complexity of sea-level related processes and their assessment in the Arctic. For example, the interannual evolution of SSH seems to be out of phase with both ocean mass and steric height over 2010-2016.

The results of the two-year SLBC_cci project clearly leave room for improvement. Points of improvement on many levels were identified together with ideas of extending the scope of work. Those were reported in a roadmap towards follow-on activities. It is summarized in the next subsection.

6.2 A roadmap towards follow-on activities

The SLBC_cci project (04/2017–03/2019) exercised sea-level budget analyses by taking advantage of the improved quality of related EO datasets produced within the CCI programme. The focus of SLBC_cci was on the GMSL budget. It wass supplemented by a regional case study for the Arctic Ocean. Large efforts have been invested in generating consistent datasets of the individual budget elements and characterising their uncertainties in a well-defined consistent way. It is specific to SLBC_cci to concentrate on datasets generated by the consortium members so that they have first-hand insights into their genesis and uncertainty characteristics. The uncertainty characterisation was propagated through the budget closure assessment and its interpretation, which required methodological developments for this budget closure assessment. This project approach is complementary to projects like the WCRP initiative described above, to which it contributed essentially.

		CCI Sea Level Budget Closure
		ESA/ESRIN contract 4000119910/17/I-NB
		Reference: ESA_SLBC_cci_D4.7
		Version: v1.1
		Date: 14.02.2020
		Page: 93 of 101

From its design, SLBC_cci was intended to prepare the way for continuing efforts of extended and possibly more operational sea-level budget assessments.

Obvious needs of further development include the extension of the considered time series and methodological improvements for assessing the elements of the sea-level budgets and their uncertainties as well as for the budget assessment itself. A closer investigation of budget elements with high uncertainty, as revealed by SLBC_cci, is also required. Moreover the sea-level budget assessment efforts need to keep pace with the development of the CCI programme, by exploring the links and synergies with new ECVs not included so far and by interacting with the Climate Modelling User Group (CMUG).

More fundamentally, the focus needs to be extended to regional sea level. While GMSL is an important global indicator, it is indispensable to monitor and understand the geographic patterns of sea-level change, called regional sea level. Regional sea level reflects the different processes causing sea-level change, which may be hidden in GMSL. Understanding and projecting these processes, with implications down to coastal impact research, is the ultimate goal.

The causes of regional sea-level changes are well identified (e.g. Stammer et al. 2013):

- Changes in ocean dynamics induced by changes in freshwater and heat fluxes and by atmospheric forcing lead to non-uniform temperature and salinity changes with associated regional halosteric effects, and also lead to dynamically induced changes in ocean mass distribution.

- Ongoing global ice and water mass redistribution as well as the solid Earth's glacial isostatic adjustment (GIA) to past mass redistributions induce deformations of ocean basins and changes in the gravity field. This in turn leads to a passive (or 'static', as opposed to ocean-dynamic) redistribution of ocean water. The passive reaction to ongoing land ice and land water mass changes is termed sea-level fingerprint.

Hence, processes causing GMSL rise and regional changes are not the same, even though they are related. For example, melting of land ice acts on regional sea level via the passive reaction and changes in salinity. While salinity has no effect on the global mean sea level, it plays an important role at regional scale, depending on the region. It is important to determine which factor dominates depending on the region. For example, in the Arctic, salinity effects are mostly responsible for the observed regional sea-level patterns, whereas in the tropical Pacific, it is the thermal expansion.

Another important issue is to study the role of natural climate modes as main drivers of the regional patterns and their temporal variability.

Moreover, at a regional scale, the problem of detection and attribution remains an unsolved problem and is worth to be considered. Open questions include:

		CCI Sea Level Budget Closure
		ESA/ESRIN contract 4000119910/17/I-NB
		Reference: ESA_SLBC_cci_D4.7
		Version: v1.1
		Date: 14.02.2020
		Page: 94 of 101

- Are regional trend patterns in sea level still dominated by natural climate modes, i.e., internal climate variability?

- Is the forced (anthropogenic) signal already emerging, and where? What length of regional sea-level record is needed for the emergence of anthropogenic signal?

- Can we already detect the 'static' fingerprint in the regional sea-level trends corrected for steric effects? Are the data accurate enough for that purpose?

Thereby, a complication arises from the fact that climate variations in a given ocean basin can significantly modulate the variability in other ocean basins. This evidence is supported by several recent studies with observational and model data, and is consistent with current understanding of remote mechanisms of influence. In examining sea-level variability and changes at interannual to decadal time scales, individual basins cannot be considered separately. Thus, regional sea-level changes should be studied within a global perspective. That is, even if for practical purpose, regional analyses may be conducted in parallel, they need to be combined and discussed with a synergetic view at the end.

A Sea-Level Budget Follow-On project is proposed to build on the capacity developed by the SLBC_cci consortium. The project should continue the approach of SLBC_cci to focus on the use of EO data (with a strong legacy from the ongoing CCI programme) and modelling data that the consortium partners understand very well, including their uncertainty characterisation. The project should continue and extend the previous activities according to the scientific requirements outlined above. A new and timely aspect should consist in developing the global view on regional sea-level patterns, and thereby in developments towards detection and attribution of regional patterns of sea-level change.

The objectives can be categorized as follows:

a. Extension in time, and update where necessary, of the core GMSL budget elements and of the GMSL budget assessment.

b. Improvements of the estimation of budget components and their uncertainty assessments. Inclusion of new satellite missions and new sensors where available.

c. Methodological improvements and extension for the budget assessments.

d. Assessment, in a global perspective, of regional sea-level change and the regional sea-level budget. That is, assessment of our understanding of the origin of regional sea-level changes and their underlying processes.

The roadmap is specified in more detail by Horwath et al. (2019a).

		CCI Sea Level Budget Closure
		ESA/ESRIN contract 4000119910/17/I-NB
		Reference: ESA_SLBC_cci_D4.7
		Version: v1.1
		Date: 14.02.2020
		Page: 95 of 101

7. References

A, G., Wahr, J., and Zhong, S. (2013): Computations of the viscoelastic response of a 3-D compressible Earth to surface loading: an application to Glacial Isostatic Adjustment in Antarctica and Canada, *Geophys. J. Int.,* 192, 557–572, doi: 10.1093/gji/ggs030.

Ablain, M., et al. (2015): Improved sea level record over the satellite altimetry era (1993–2010) from the climate change Initiative project, *Ocean Sci.,* 11, 67–82, doi:10.5194/os-11-67-2015.

Ablain M., R. Jugier, L. Zawadki, and N. Taburet (2017a): The TOPEX-A Drift and Impacts on GMSL Time Series. *AVISO Website.* October 2017. https://meetings.aviso.altimetry.fr/fileadmin/user_upload/tx_ausyclsseminar/files/Poster_OSTST17_GMSL_Drift_TOPEX-A.pdf.

Ablain, M., J. F. Legeais, P. Prandi, M. Marcos, L. Fenoglio-Marc, H. B. Dieng, J. Benveniste, and A. Cazenave (2017b): Altimetry-based sea level at global and regional scales, *Surv. Geophys.,* 38, 7–31, doi: 10.1007/s10712-016-9389-8.

Ablain, M., Meyssignac, B., Zawadzki, L., Jugier, R., Ribes, A., Spada, G., ... & Picot, N. (2019). Uncertainty in satellite estimates of global mean sea-level changes, trend and acceleration. Earth System Science Data, 11(3), 1189-1202.

Andersen, O., Knudsen, P., and Stenseng, L. (2018): A New DTU18 MSS Mean Sea Surface – Improvement fromSAR Altimetry. 172. Abstract from 25 years of progress in radar altimetry symposium, Portugal.

Andersen, O. B., Stenseng, L., Piccioni, G., and Knudsen, P. (2016): The DTU15 MSS (Mean Sea Surface) and DTU15LAT (Lowest Astronomical Tide) reference surface. Abstract from ESA Living Planet Symposium 2016, Prague, Czech Republic.

Armitage, T. W. K., and M. W. J. Davidson (2014): Using the Interferometric Capabilities of the ESA CryoSat-2 Mission to Improve the Accuracy of Sea Ice Freeboard Retrievals, IEEE Transactions on Geoscience and Remote Sensing, vol. 52, no. 1, pp. 529-536, Jan. 2014. doi: 10.1109/TGRS.2013.2242082

Barletta, V. R., Sørensen, L. S., and Forsberg, R. (2013): Scatter of mass changes estimates at basin scale for Greenland and Antarctica. *The Cryosphere*, 7(5), 1411–1432

Bergmann-Wolf, I., Zhang, L. & Dobslaw, H. (2014). Global Eustatic Sea-Level Variations for the Approximation of Geocenter Motion from Grace. *Journal of Geodetic Science*, 4(1), doi:10.2478/jogs-2014-0006

Blazquez, A., Meyssignac, B., Lemoine, J. M., Berthier, E., Ribes, A., & Cazenave, A. (2018). Exploring the uncertainty in GRACE estimates of the mass redistributions at the Earth surface: implications for the global water and sea level budgets. *Geophysical Journal International*, 215(1), 415-430.

Brown, G.S. (1977): The average impulse response of a rough surface and its applications. IEEE Trans. Antennas Propag. 25, 67–74. http://dx.doi.org/10.1109/TAP.1977.1141536.

Caron, L., Ivins, E. R., Larour, E., Adhikari, S., Nilsson, J., and Blewitt, G. (2018): GIA model statistics for GRACE hydrology, cryosphere, and ocean science. *Geophysical Research Letters*, 45, 2203–2212. doi: 10.1002/2017GL076644.

Carrere, L., Faugère, Y., and Ablain, M. (2016a): Major improvement of altimetry sea level estimations using pressure-derived corrections based on ERA-Interim atmospheric reanalysis. *Ocean Science*, *12*(3), 825–842. doi: 10.5194/os-12-825-2016.

Carrere L., F. Lyard, M. Cancet, A. Guillot, and N. Picot (2016b): FES 2014, a new tidal model – Validation results and perspectives for improvements: Presentation to ESA Living Planet Conference, Prague 2016.

Cazenave, A., Dominh, K., Guinehut, S., Berthier, E., Llovel, W., Ramillien, G., . . . Larnicol, G. (2009). Sea level budget over 2003-2008: A reevaluation from GRACE space gravimetry, satellite altimetry and Argo. Global and Planetary Change. doi:https://doi.org/10.1016/j.gloplacha.2008.10.004

Cazenave A. and Le Cozannet G. (2014): Sea level rise and coastal impacts, Earth's Future, vol2, issue2, 15-34, doi :10.1002/2013EF000188.

Chambers, D. P. (2009): Calculating trends from GRACE in the presence of large changes in continental ice storage and ocean mass, *Geophysical Journal International*, 176(2), 415–419. doi: 10.1111/j.1365-246X.2008.04012.x.

CCI Sea Level Budget Closure
ESA/ESRIN contract 4000119910/17/I-NB
Reference: ESA_SLBC_cci_D4.7
Version: v1.1
Date: 14.02.2020
Page: 96 of 101

Chambers D., Wahr J., Tamisiea M., and Nerem, R. (2010): Ocean mass from GRACE and glacial isostatic adjustment. Journal of Geophysical Research: Solid Earth (1978–2012), 115(B11).

Chambers, D. P., and J. A. Bonin (2012): Evaluation of Release-05 GRACE time-variable gravity coefficients over the ocean, *Ocean Sci.*, 8, 859–868, doi: 10.5194/os-8–859-2012.

Chambers D.P., Cazenave A., Champollion N., Dieng H., Llovel, W., Forsberg R., von Schuckmann, K., and Wada Y. (2017). Evaluation of the global mean sea level budget between 1993 and 2014. Surveys in Geophysics, 38(1), 309-327, doi: 10.1007/s10712-016-9381-3.

Chen, X., Zhang, X., Church, J. A., Watson, C. S., King, M. A., Monselesan, D., Legresy, B., and Harig, C. (2017): The increasing rate of global mean sea-level rise during 1993-2014. Nature Climate Change, vol. 7, pages 492–495, doi:10.1038/nclimate3325.

Cheng, M.K., B. D. Tapley, and J. C. Ries (2013): Deceleration in the Earth's oblateness, *Jour. Geophys. Res.*,V118, 1-8, doi: 10.1002/jgrb.50058, 2013.

Church, J.A., P.U. Clark, A. Cazenave, J.M. Gregory, S. Jevrejeva, A. Levermann, M.A. Merrifield, G.A. Milne, R.S. Nerem, P.D. Nunn, A.J. Payne, W.T. Pfeffer, D. Stammer and A.S. Unnikrishnan (2013): Sea Level Change. In: Climate Change 2013: The Physical Science Basis. Contribution of Working Group I to the Fifth Assessment Report of the Intergovernmental Panel on Climate Change. Cambridge University Press, Cambridge, United Kingdom and New York, NY, USA.

Cornford, S. L., Martin, D. F., Graves, D. T., Ranken, D. F., Le Brocq, A. M., Gladstone, R. M., Payne, A. J., Ng, E. G and Lipscomb, W. H. (2013): Adaptive mesh, finite volume modeling of marine ice sheets. *Journal of Computational Physics*, 232(1), 529-549. doi:10.1016/j.jcp.2012.08.037.

Dieng, H. B., Cazenave, A., von Schuckmann, K., Ablain, M., & Meyssignac, B. (2015). Sea level budget over 2005-2013: missing contributions and data errors. Ocean Science, 11(5).

Dieng, H.B, A. Cazenave, B. Meyssignac, and M. Ablain (2017): New estimate of the current rate of sea level rise from a sea level budget approach, *Geophysical Research Letters*, 44, doi:10.1002/2017GL073308.

Dobslaw, H., Bergmann-Wolf, I., Dill, R., Forootan, E., Klemann, V., Kusche, J., and Sasgen, I. (2015): The updated ESA Earth System Model for future gravity mission simulation studies, *Journal of Geodesy*, 89, 5, 505–513, doi: 10.1007/s00190-014-0787-8.

Dobslaw, H., Flechtner, F., Bergmann-Wolf, I., Dahle, C., Dill, R., Esselborn, S., ... , and Thomas, M. (2013): Simulating high-frequency atmosphere-ocean mass variability for dealiasing of satellite gravity observations: AOD1B RL05. *Journal of Geophysical Research: Oceans*, 118(7), 3704-3711. doi: 10.1002/jgrc.20271.

Döll, P., Fiedler, K., & Zhang, J. (2009). Global-scale analysis of river flow alterations due to water withdrawals and reservoirs. Hydrology and Earth System Sciences, 13(12), 2413.

Döll, Petra; Müller Schmied, Hannes; Schuh, Carina; Portmann, Felix T.; Eicker, Annette (2014): Global-scale assessment of groundwater depletion and related groundwater ab-stractions. Combining hydrological modeling with information from well observations and GRACE satellites. *Water Resour. Res.* 50 (7), pp. 5698–5720. DOI: 10.1002/2014WR015595.

Flechtner, F., Dobslaw, H., and Fagiolini, E. (2014): *AOD1B product description document for product release 05 (Rev. 4.2, May 20, 2014).* Technical Note, GFZ German Research Centre for Geosciences Department, 1.

Forsberg, R., L. Sørensen, et al. (2013): *Comprehensive Error Characterisation Report for the Ice_Sheets_cci project of ESA's Climate Change Initiative*, version 1.2, 06 June 2013.

Good, S. A., M. J. Martin, and N. A. Rayner (2013): EN4: Quality controlled ocean temperature and salinity profiles and monthly objective analyses with uncertainty estimates, *J. Geophys. Res. Oceans*, 118, 6704–6716, doi:10.1002/2013JC009067.

Groh, A.; Horwath, M.; Gutknecht, B.D.; Hogg, A.; Shepherd, A. (2019): Improved estimates of Antarctic mass balance from updated GRACE solution series. Poster presented at ESA Living Planet Symposium 2019, Milano

Haeberli, W. and Linsbauer, A. (2013): Brief communication: Global glacier volumes and sea level – small but systematic effects of ice below the surface of the ocean and of new local lakes on land, *The Cryosphere*, 7, 817-821.

Harris, I. P. D. J., Jones, P. D., Osborn, T. J., and Lister, D. H. (2014): Updated high-resolution grids of monthly climatic observations–the CRU TS3. 10 Dataset. *International Journal of Climatology*, 34(3), 623-642.

Hayne, G.S. (1980): Radar altimeter mean return waveforms from near-normal-incidence ocean surface scattering. *IEEE Trans. Antennas Propag.* 28, 687–692. doi: 10.1109/TAP.1980.1142398.

	CCI Sea Level Budget Closure
	ESA/ESRIN contract 4000119910/17/I-NB
	Reference: ESA_SLBC_cci_D4.7
	Version: v1.1
	Date: 14.02.2020
	Page: 97 of 101

Henry O, Ablain M, Meyssignac B, Cazenave A, Masters D, Nerem S, Leuliette E, and Garric G (2014): Investigating and reducing differences between the satellite altimetry-based global mean sea level time series provided by different processing groups. *J Geod* 88:351–361. doi: 10.1007/s00190-013-0687-3.

Hirahara, S., Ishii, M., & Fukuda, Y. (2014). Centennial-Scale Sea Surface Temperature Analysis and Its Uncertainty. Journal of Climate, 27. doi:10.1175/JCLI-D-12-00837.1

Horwath, M., and Groh, A. (2016): The GRACE mass change estimators developed for ESA's CCI ice sheet mass balance products. *Proc. GRACE Science Team Meeting 2016*, Potsdam, 5-7 November 2016. http://www.gfz-potsdam.de/en/section/global-geomonitoring-and-gravity-field/topics/development-operation-and-analysis-of-gravity-field-satellite-missions/grace/gstm/gstm-2016/proceedings/.

Horwath, M.; Novotny, K.; Cazenave, A.; Palanisamy, H.; Marzeion, B.; Paul, F.; Döll, P.; Cáceres, D.; Hogg, A.; Otosaka, I.; Shepherd, A.; Barletta, V.R.; Forsberg, R.; Andersen, O.B.; Ranndal, H.; Johannessen, J.; Gutknecht, B.D.; Merchant, Ch.J.; von Schuckmann, K. (2019a): ESA Climate Change Initiative (CCI) Sea Level Budget Closure (SLBC_cci) Roadmap towards a SLB_cci follow-on activity. Version 1.0, 08.03.2019.

Horwath, M.; Novotny, K.; Cazenave, A.; Palanisamy, H.; Marzeion, B.; Paul, F.; Döll, P.; Cáceres, D.; Hogg, A.; Shepherd, A.; Otosaka, I.; Forsberg, R.; Barletta, V.R.; Simonsen, S.; Andersen, O.B.; Rose, S.K.;Ranndal, H.; Johannessen, J.A.; Raj, R.P.; Gutknecht, B.D.; Merchant, Ch.J.; von Schuckmann, K. (2019b): *ESA Climate Change Initiative (CCI) Sea Level Budget Closure (SLBC_cci). Product Description Document D2.4.2: Version 2 data sets and uncertainty assessments.* Version 1.2, 18 Jun. 2019.

Horwath, M.; Novotny, K.; Cazenave, A.; Palanisamy, H.; Marzeion, B.; J.-H. Malles; Paul, F.; Döll, P.; Cáceres, D.; Hogg, A.; Shepherd, A.; Otosaka, I.; Forsberg, R.; Barletta, V.R.; Andersen, O.B.; Ranndal, H.; Johannessen, J.; Nilsen, J.E.; Gutknecht, B.D.; Merchant, Ch.J.; von Schuckmann, K. (2019c): ESA Climate Change Initiative (CCI) Sea Level Budget Closure (SLBC_cci) Document D3.2: SLBC Assessment Report 2 based on version 1 data. Version 1.1, 08 March 2019.

Horwath, M.; Novotny, K.; Cazenave, A.; Palanisamy, H.; Marzeion, B.; Paul, F.; Döll, P.; Cáceres, D.; Hogg, A.; Otosaka, I.; Shepherd, A.; Forsberg, R.; Barletta, V.R.; Andersen, O.B.; Rose, S.K.; H.; Johannessen, J.; Raj, R.P.; Gutknecht, B.D.; Merchant, Ch.J.; MacIntosh, C.R.; von Schuckmann, K. (2019d): ESA Climate Change Initiative (CCI) Sea Level Budget Closure (SLBC_cci). SLBC Assessment Report 3 based on version 2 data (D3.3). Version 1.1, 15 November 2019.

Ishii, M., & Kimoto, M. (2009). Reevaluation of historical ocean heat content variations with time-varying XBT and MBT depth bias corrections. Journal of Oceanography. doi:10.1007/s10872-009-0027-7

Ishii, M., Fukuda, Y., Hirahara, S., Yasui, S., Suzuki, T., & Sato, K. (2017). Accuracy of global upper ocean heat content estimation expected from present observational data sets. Sola, 13, 163-167.

Ivins E., James T., Wahr J., Schrama E., Landerer F., and Simon K. (2013): Antarctic contribution to sea level rise observed by GRACE with improved GIA correction. *J. Geophys. Res.: Solid Earth*, 118(6), 3126-3141, doe doi.org/10.1002/jgrb.50208.

JCGM (2008). Evaluation of measurement data—Guide to the expression of uncertainty in measurement. Int. Organ. Stand. Geneva, available under https://www.bipm.org/utils/common/documents/jcgm/JCGM_100_2008_E.pdf

Johnson, G. C., and D. P. Chambers (2013): Ocean bottom pressure seasonal cycles and decadal trends from GRACE Release-05: Ocean circulation implications, *J. Geophys. Res. Oceans*, 118, 4228–4240, doi: 10.1002/jgrc.20307.

Khvorostovsky, et al. (2016): Algorithm Theoretical Baseline Document (ATBD) for the Greenland_Ice_Sheet_cci project of ESA's Climate Change Initiative, version 3.1 (ST-DTU-ESAGISCCI-ATBD-001), 09 Sep 2016.

Khvorostovsky, K. et al. (2018). Algorithm Theoretical Baseline Document (ATBD) for the Greenland Ice Sheet CCI project of ESA's Climate Change Initiative, version 3.2, 28 Jun 2018. Available from: http://www.esa-icesheets-cci.or

Klinger, B., Mayer-Gürr, T., Behzadpour, S., Ellmer, M., Kvas, A., and Zehentner, N. (2016): The new ITSG-Grace2016 release. *Geophys. Res. Abstr.*, 18, EGU2016–11547.

	CCI Sea Level Budget Closure
	ESA/ESRIN contract 4000119910/17/I-NB
	Reference: ESA_SLBC_cci_D4.7
	Version: v1.1
	Date: 14.02.2020
	Page: 98 of 101

Kusche, J., Uebbing, B., Rietbroek, R., Shum, C. K., and Khan, Z. H. (2016): Sea level budget in the Bay of Bengal (2002–2014) from GRACE and altimetry. *Journal of Geophysical Research: Oceans*, 121, 1194–1217, doi: 10.1002/2015JC011471.

Legeais J.F., Ablain M., Zawadzki L., Zuo H., Johannessen J.A., Scharffenberg M.G., Fenoglio-Marc L., Fernandes J., Andersen O.B., Rudenko S., Cipollini P., Quartly G.D., Passaro M., Cazenave A., and Benveniste J. (2018): An improved and homogeneous altimeter sea level record from the ESA Climate Change Initiative, *Earth Syst. Sci. Data*, 10, 281-301, doi: 10.5194/essd-10-281-2018.

Leuliette, E., & Miller, L. (2009). Closing the sea level rise budget with altimetry, Argo, and GRACE. *Geophysical Research Letters*, 36(4). doi:10.1029/2008GL036010

Levitus S., et al. (2012): World ocean heat content and thermosteric sea level change (0–2000 m), 1955–2010. *Geophys. Res. Lett.*, 39, L10603. doi: 10.1029/2012GL051106.

Luthcke, S. B., Sabaka, T. J., Loomis, B. D., Arendt, A. A., McCarthy, J. J., and Camp, J. (2013): Antarctica, Greenland and Gulf of Alaska land-ice evolution from an iterated GRACE global mascon solution. *J. Glac.*, 59(216), 613–631. doi: 10.3189/2013JoG12J147.

Marzeion, B., Jarosch, A. H., and Hofer, M. (2012): Past and future sealevel change from the surface mass balance of glaciers, *The Cryosphere*, 6, 1295–1322, doi: 10.5194/tc-6-1295-2012.

Masters D, Nerem RS, Choe C, Leuliette E, Beckley B, White N, and Ablain M (2012): Comparison of global mean sea level time series from TOPEX/Poseidon, Jason-1, and Jason-2. *Mar Geod* 35:20–41, doi: 10.1080/01490419.2012.717862.

Mayer-Gürr, T., Behzadpour, S., Ellmer, M., Klinger, B., Kvas, A., Strasser, S., & Zehentner, N. (2018a). ITSG-Grace2018: The new GRACE time series from TU Graz. *Abstract from GRACE / GRACE-FO Science Team Meeting 2018*, Potsdam, Germany.

Mayer-Gürr, T., Behzadpour, S., Ellmer, M., Kvas, A., Klinger, B., and Zehentner, N. (2016): ITSG-Grace2016 - Monthly and Daily Gravity Field Solutions from GRACE. *GFZ Data Services*. doi: 10.5880/icgem.2016.007.

Mayer-Gürr, Torsten; Behzadpur, Saniya; Ellmer, Matthias; Kvas, Andreas; Klinger, Beate; Strasser, Sebastian; Zehentner, Norbert (2018b): ITSG-Grace2018 - Monthly, Daily and Static Gravity Field Solutions from GRACE. *GFZ Data Services.* http://doi.org/10.5880/ICGEM.2018.003

McMillan, M., Shepherd , A., Sundal, A., Briggs, K.,Muir, A., Ridout, A., Hogg, A., Wingham, D. (2014): Increased ice losses from Antarctica detected by CryoSat-2. *Geophysical Research Letters* 41(11), doi: 10.1002/2014GL060111.

Müller Schmied, H.; Eisner, S.; Franz, D.; Wattenbach, M.; Portmann, F. T.; Flörke, M.; Döll, P. (2014): Sensitivity of simulated global-scale freshwater fluxes and storages to input data, hydrological model structure, human water use and calibration. *Hydrol. Earth Syst. Sci.* 18 (9), pp. 3511–3538. DOI: 10.5194/hess-18-3511-2014.

Nagler, T., D. Floricioiu, A. Groh, M. Horwath, A. Kusk, A. Muir, J. Wuite (2018a): Algorithm Theoretical Basis Document (ATBD) for the Antarctic_Ice_Sheet_cci project of ESA's Climate Change Initiative, version 2.1, 05 July 2018. Available from: http://www.esa-icesheets-antarctica-cci.org/.

Nagler, T., et al. (2018b): Comprehensive Error Characterisation Report (CECR). Antarctic_Ice_Sheet_cci project, ESA's Climate Change Initiative, version 2.1, 05 July 2018. Available from: http://www.esa-icesheets-antarctica-cci.org/.

Nagler, T. et al. (2018c). Product User Guide(PUG) for the Greenland_Ice_Sheet_cci project of ESA's Climate Change Initiative, version 2.2, 27 June 2018. Available from: http://www.esa-icesheets-greenland-cci.org/

Nagler, T. et al. (2018d). Product User Guide(PUG) for the Greenland_Ice_Sheet_cci project of ESA's Climate Change Initiative, version 2.2, 27 June 2018. Available from: http://www.esa-icesheets-greenland-cci.org/

Nerem, R. S., Beckley, B. D., Fasullo, J. T., Hamlington, B. D., Masters, D., and Mitchum, G. T. (2018): Climate-change–driven accelerated sea-level rise detected in the altimeter era. PNAS Proceedings of the National Academy of Sciences, 115 (9) 2022-2025; doi: 10.1073/pnas.1717312115

Nilsson, J., Vallelonga, P., Simonsen, S.B. , Sørensen, L.S., Forsberg, R., Dahl-Jensen, D., Hirabayashi, M. (2015): Greenland 2012 Melt Event Effects on CryoSat-2 Radar Altimetry. *Geophysical Research Letters* 42 (10): 3919–26. doi:10.1002/2015GL063296.

CCI Sea Level Budget Closure
ESA/ESRIN contract 4000119910/17/I-NB
Reference: ESA_SLBC_cci_D4.7
Version: v1.1
Date: 14.02.2020
Page: 99 of 101

Novotny, K.; Horwath, M.; Cazenave, A.; Palanisamy, H.; Marzeion, B.; Paul, F.; Le Bris, R.; Döll, P.; Caceres, D.; Hogg, A.; Shepherd, A.; Forsberg, R.; Sørensen, L.; Andersen, O.B.; Johannessen, J.; Nilsen, J.E.; Gutknecht, B.D.; Merchant, Ch.J.; Macintosh, C.R. (2017a): ESA Climate Change Initiative (CCI) Sea Level Budget Closure (SLBC_cci). Science Requirements Document D1.1, Report at initial point of project. Version 1.2, 25 August 2017

Novotny, K.; Horwath, M.; Cazenave, A.; Palanisamy, H.; Marzeion, B.; Paul, F.; Döll, P.; Cáceres, D.; Hogg, A.; Shepherd, A.; Forsberg, R.; Sørensen, L.; Barletta, V.R.; Andersen, O.B.; Ranndal, H.; Johannessen, J.; Nilsen, J.E.; Gutknecht, B.D.; Merchant, Ch.J.; MacIntosh, C.R.; Old, Ch.; von Schuckmann, K. (2018a): ESA Climate Change Initiative (CCI) Sea Level Budget Closure (SLBC_cci) Science Requirements Updated and Preliminary Thoughts on Roadmap. Version 1.0, 05.06.2018.

Novotny, K.; Horwath, M.; Cazenave, A.; Palanisamy, H.; Marzeion, B.; Paul, F.; Le Bris, R.; Döll, P.; Caceres, D.; Hogg, A.; Shepherd, A.; Forsberg, R.; Sørensen, L.; Andersen, O.B.; Johannessen, J.; Nilsen, J.E.; Gutknecht, B.D.; Merchant, Ch.J.; Macintosh, C.R. (2017b): ESA Climate Change Initiative (CCI) Sea Level Budget Closure (SLBC_cci). Product Description Document D2.1.2: Version 0 data sets and uncertainty assessments. Version 1.2, 27 Sept 2017.

Novotny, K.; Horwath, M.; Cazenave, A.; Palanisamy, H.; Marzeion, B.; Paul, F.; Döll, P.; Cáceres, D.; Hogg, A.; Shepherd, A.; Otosaka, I.; Forsberg, R.; Barletta, V.R.; Andersen, O.B.; Ranndal, H.; Johannessen, J.; Nilsen, J.E.; Gutknecht, B.D.; Merchant, Ch.J.; MacIntosh, C.R.; Old, Ch.; von Schuckmann, K. (2018b): ESA Climate Change Initiative (CCI) Sea Level Budget Closure (SLBC_cci). Product Description Document D2.3.2: Version 1 data sets and uncertainty assessments. Version 1.2, 22 Nov 2018.

Novotny, K.; Horwath, M.; Cazenave, A.; Palanisamy, H.; Marzeion, B.; Paul, F.; Döll, P.; Cáceres, D.; Hogg, A.; Shepherd, A.; Forsberg, R.; Sørensen, L.; Barletta, V.R.; Andersen, O.B.; Ranndal, H.; Johannessen, J.; Nilsen, J.E.; Gutknecht, B.D.; Merchant, Ch.J.; MacIntosh, C.R., von Schuckmann, K. (2018c): ESA Climate Change Initiative (CCI) Sea Level Budget Closure (SLBC_cci) Sea Level Budget Closure Assessment Report D3.1. Version 1.1, 07.05.2018.

Passaro, M., Cipollini, P., Vignudelli, S., Quartly, G., and Snaith, H. (2014): ALES: A multimission subwaveform retracker for coastal and open ocean altimetry. *Remote Sens. Environ.* 145, 173–189. doi: 10.1016/j.rse.2014.02.008.

Passaro, M., S. K. Rose, O. B. Andersen, E. Boergens, F. M. Calafat, D. Dettmering, and J. Benveniste (2018): ALES+: Adapting a homogenous ocean retracker for satellite altimetry to sea ice leads, coastal and inland waters. *Remote Sens. Environ.*, 211, 456-471. doi: 10.1016/j.rse.2018.02.074.

Peltier W.R. (2004): Global glacial isostasy and the surface of the ice-age Earth: the ICE-5G (VM2) model and GRACE, *Annual Review of Earth and Planetary Sciences* 32:111.

Peltier, W. R., Argus, D. F., and Drummond, R. (2015): Space geodesy constrains ice age terminal deglaciation: The global ICE-6G_C (VM5a) model: Global Glacial Isostatic Adjustment. *J. Geophys. Res. Solid Earth*, 120(1), 450–487. doi: 10.1002/2014JB011176.

Pfeffer, W. T., Arendt, A. A., Bliss, A., Bolch, T., Cogley, J. G., Gardner, A. S., … and Miles, E. S. (2014). The Randolph Glacier Inventory: a globally complete inventory of glaciers. *Journal of Glaciology*, 60(221), 537-552.

Purkey, S. and Johnson, G. C.: Warming of global abyssal and deep southern ocean waters between the 1990s and 2000s: Contributions to global heat and sea level rise budget, J. Climate, 23, 6336–6351, https://doi.org/10.1175/2010JCLI3682.1, 2010.

Quartly G.D., Legeais J.F., Ablain M., Zawadzki L., Fernandes J., Rudenko S., Carrère L., García P.N., Cipollini P., Andersen O.B., Poisson J.C., Sabrina Mbajon Njiche S.M., Cazenave A., and Benveniste J. (2017): A new phase in the production of quality-controlled sea level data, *Earth Syst. Sci. Data,* 9, 557–572, doi: 10.5194/essd-9-557-2017.

Quinn, K.J, and Ponte, R.M. (2010): Uncertainty in ocean mass trends from GRACE. *Geophys J In*, 181 (2): 762-768. doi: 10.1111/j.1365-246X.2010.04508.x.

Reager J. T., Gardner A. S., Famiglietti J. S., Wiese D. N., Eicker,A., and Lo M. H. (2016): A decade of sea level rise slowed by climate-driven hydrology. Science, 351(6274), 699-703. doi: 10.1126/science.aad8386.

		CCI Sea Level Budget Closure
		ESA/ESRIN contract 4000119910/17/I-NB
.esa	TECHNISCHE UNIVERSITÄT DRESDEN · Universität Zürich · UNIVERSITY OF LEEDS · LEGOS · Universität Bremen · GOETHE UNIVERSITÄT FRANKFURT AM MAIN · DTU Space National Space Institute · University of Reading · MERCATOR OCEAN INTERNATIONAL	Reference: ESA_SLBC_cci_D4.7
		Version: v1.1
		Date: 14.02.2020
		Page: 100 of 101

Rietbroek, R, Brunnabend, S-E, Kusche, J, Schröter, J, and Dahle,C (2016):-Revisiting the contemporary sea-level budget on global and regional scales. *PNAS* 2016 113 (6) 1504-1509, doi: 10.1073/pnas.1519132113.

Robson, J., Sutton, R. T., Archibald, A., Cooper, , F., Christensen, M., Gray, L. J., Holliday, N. P.,, & Macintosh, C., McMillan, M., Moat, B., Russo, M., . (2018). Recent multivariate changes in the North Atlantic climate system, with a focus on 2005-2016. International Journal of Climatology. doi:https://doi.org/10.1002/joc.5815

Rose, S.K., Andersen, O.B., Passaro, M., Ludwigsen, C.A., Schwatke, C. (2019): Arctic Ocean Sea Level Record from the Complete Radar Altimetry Era: 1991–2018. Remote Sensing, 11(14), 1672, doi: 10.3390/rs11141672

Sakov, P., F. Counillon, L. Bertino, K. A. Lisæter, P. R. Oke, and A. Korablev (2012): TOPAZ4: an ocean-sea ice data assimilation system for the North Atlantic and Arctic. *Ocean Science*, 8:633-656, doi:10.5194/os-8-633-2012.

Scharroo, R., Leuliette, E. W., Lillibridge, J. L., Byrne, D., Naeije, M. C., and Mitchum, G. T. (2013): RADS: Consistent multi-mission products, Proceedings of the Symposium on 20 Years of Progress in Radar Altimetry, Venice: ESA Spec. Publ., ESA SP-710, 4.

Schneider, U.; Becker, A.; Finger, P.; Meyer-Christoffer, A.; Rudolf, B.; and Ziese, M. (2015): GPCC Full Data Reanalysis Version 7.0 at 0.5°: Monthly Land-Surface Precipitation from Rain-Gauges built on GTS-based and Historic Data. R*esearch Data Archive at the National Center for Atmospheric Research, Computational and Information Systems Laboratory, Boulder, Colo.* (Updated irregularly.). DOI: 10.5676/DWD_GPCC/FD_M_V7_050.

Schröder, L., Horwath, M., Dietrich, R., Helm, V., Broeke, M. R., & Ligtenberg, S. R. (2019). Four decades of Antarctic surface elevation changes from multi-mission satellite altimetry. The Cryosphere, 13(2), 427-449.

Shepherd, A., Ivins, E., Rignot, E., Smith, B., van den Broeke, M., Velicogna, I., ..., Groh, A., ..., Horwath, M, ..., Schröder, L., et al. (2018). Mass balance of the Antarctic Ice Sheet from 1992 to 2017. Nature, 556, pages 219-222.

Shepherd, A., Gilbert, L., Muir, A. S., Konrad, H., McMillan, M., Slater, T., ... & Engdahl, M. (2019). Trends in Antarctic Ice Sheet Elevation and Mass. Geophysical Research Letters.

Simonsen, S. B., and Sørensen, L.S: (2017): Implications of Changing Scattering Properties on Greenland Ice Sheet Volume Change from Cryosat-2 Altimetry. *Remote Sensing of Environment* 190 (March). Elsevier Inc.: 207–16. doi:10.1016/j.rse.2016.12.012.

Sørensen L.S., et al. (2017): *Product Specification Document (PSD) for the Greenland_Ice_Sheet_cci project of ESA's Climate Change Initiative*, version 2.3 (ST-DTU-ESA-GISCCI-PSD-001), 20 March 2017.

Sørensen, L. S., Simonsen, S. B., Nielsen, K., Lucas-Picher, P., Spada, G., Adalgeirsdóttir, G., ... Hvidberg, C. S. (2011): Mass balance of the Greenland ice sheet (2003-2008) from ICESat data - the impact of interpolation, sampling and firn density. *The Cryosphere*, 5(1), 173–186. http://doi.org/10.5194/tc-5-173-2011.

Sørensen L. S., Simonsen, S.B., Forsberg, R., Khvorostovsky, K., Meister, R., and Engdahl, M. E.. (2018): 25 Years of Elevation Changes of the Greenland Ice Sheet from ERS, Envisat, and CryoSat-2 Radar Altimetry. *Earth and Planetary Science Letters* 495. Elsevier B.V.: 234–41. doi:10.1016/j.epsl.2018.05.015.

Stammer D., Cazenave A., Ponte R., and Tamisiea M. (2013): Contemporary regional sea level changes, *Annual Review of Marine Sciences*, 5, 21–46, doi: 10.1146/annurev-marine-121211-172406.

Stenseng, L. (2011): *Polar Remote Sensing by CryoSat-type Radar Altimetry*. Ph.D. thesis. National Space Institute, Technical University of Denmark.

Swenson S., Chambers D., and Wahr J. (2008): Estimating geocenter variations from a combination of GRACE and ocean model output. *Journal of Geophysical Research: Solid Earth*, 113(B8), doi: 10.1029/2007JB005338.

Tamisiea M. (2011): Ongoing glacial isostatic contributions to observations of sea level change. Geophysical Journal International, 186(3), 1036-1044.

Thorvaldsen, A. et al. (2018) Product User Guide (PUG) for the Antarctic_Ice_Sheet_cci project of ESA's Climate Change Initiative, version 1.4, 26 June 2018. Available from: http://esa-icesheets-antarctica-cci.org/

		CCI Sea Level Budget Closure
		ESA/ESRIN contract 4000119910/17/I-NB
esa		Reference: ESA_SLBC_cci_D4.7
		Version: v1.1
		Date: 14.02.2020
		Page: 101 of 101

Uebbing, B., Kusche, J., Rietbroek, R., & Landerer, F. W. (2019). Processing choices affect ocean mass estimates from GRACE. Journal of Geophysical Research: Oceans, 124(2), 1029-1044.

von Schuckmann K, and Le Traon P-Y (2011): How well can we derive Global Ocean Indicators from Argo data? *Ocean Sci.,* 7:783-791, doi: 10.5194/os-7-783-2011.

von Schuckmann, K., Gaillard, F., & Le Traon, P.-Y. (2009). Global hydrographic variability patterns during 2003–2008. Journal of Geophysical Research: Oceans, 119(C9). doi:10.1029/2008JC005237

von Schuckmann, K., Salee, J.-B., Chambers, D., Le Traon, P.-Y., Cabanes, C., Gaillard, F., . . . Hamon, M. (2014). Consistency of the current global ocean observing systems from an Argo perspective. Ocean Science. doi:10.5194/os-10-547-2014

von Schuckmann K., Palmer M.D., Trenberth K.E., Cazenave A., Chambers D., Champollion N., et al. (2016): Earth's energy imbalance: an imperative for monitoring, Nature Climate Change, 26, 138-144.

WCRP Global Sea Level Budget Group (the) (2018): Global sea level budget, 1993-present, *Earth System Science Data*, 10, 1551-1590, doi: 10.5194/essd-10-1551-2018.

Weedon, G. P.; Balsamo, G.; Bellouin, N.; Gomes, S.; Best, M. J.; and Viterbo, P. (2014): The WFDEI meteorological forcing data set. WATCH Forcing Data methodology applied to ERA-Interim reanalysis data. *Water Resour. Res.* 50 (9), pp. 7505–7514. DOI: 10.1002/2014WR015638.

WGMS (2016): *Fluctuations of Glaciers Database.* World Glacier Monitoring Service, Zurich, Switzerland. doi: 10.5904/wgms-fog-2016-08.

Willis, J., Chambers, D., & Nerem, R. (2008). Assessing the globally averaged sea level budget on seasonal tointerannual timescales. Journal of Geophysial Research, 113, C06015. doi:10.1029/2007JC004517

Xie, J., L. Bertino , F. Counillon, K. A. Lisæter, and P. Sakov (2017): Quality assessment of the TOPAZ4 reanalysis in the Arctic over the period 1991-2013, *Ocean Sci.*, 13(1), pp. 123-144, doi:10.5194/os-2016-38, 2016 doi:10.5194/os-13-123-2017.

Zemp, M., Huss, M., Thibert, E., Eckert, N., McNabb, R., Huber, J., Barandun, M., Machguth, H., Nussbaumer, S.U., Gärtner-Roer, I., Thomson, L., Paul, F., Maussion, F., Kutuzov, S., Cogley, J.G. (2019): Global glacier mass changes and their contributions to sea-level rise from 1961 to 2016. Nature 568, 382–386, doi: 10.1038/s41586-019-1071-0

Zwally, H. J., M. B. Giovinetto, M. A. Beckley, J. L. Saba (2012): *Antarctic and Greenland Drainage Systems*, GSFC Cryospheric Sciences Laboratory, at http://icesat4.gsfc.nasa.gov/cryo_data/ant_grn_drainage_systems.php.